Section 2: Chapter 6

The Role of Glutamate Receptors and Phosphorylation in Molecular Models of Learning and Memory

Long Term Potentiation: A Molecular Scale Model for Memory Formation

In Chapter 1, we described the neurons of the brain as being biological wires and synapses as being connections between these wires. This, like any model of the brain, begs the question: How do we learn? At some level, learning must entail the creation of new wires and new connections between wires. This concept is formalized by the term synaptic plasticity. It is a model for the formation of memories at the cellular level that describes the formation of these new synaptic connections and the alteration of existing synaptic connections. One form of synaptic plasticity, known as long term potentiation (LTP), has emerged as the preeminent conceptual framework for investigating the molecular basis of memory.[1] LTP is characterized by a long-lasting increase in synaptic strength that is caused by a brief period of coordinated neuronal activity. As one can see in the example recording shown in Figure 1, a larger post-synaptic current is observed in the recording electrode (compare point 2 to point 1) after 1 s of 100 Hz stimulation. While actually correlating these electrophysiological events with an abstraction like memory formation is extremely difficult, synaptic reinforcement through LTP certainly has the hallmarks that intuitively seem necessary to form memories.[2] In a sense, a memory is a change in the way we think. LTP is a readily characterizeable change in the way we think: one part of the brain begins to communicate more strongly with another part of the brain.

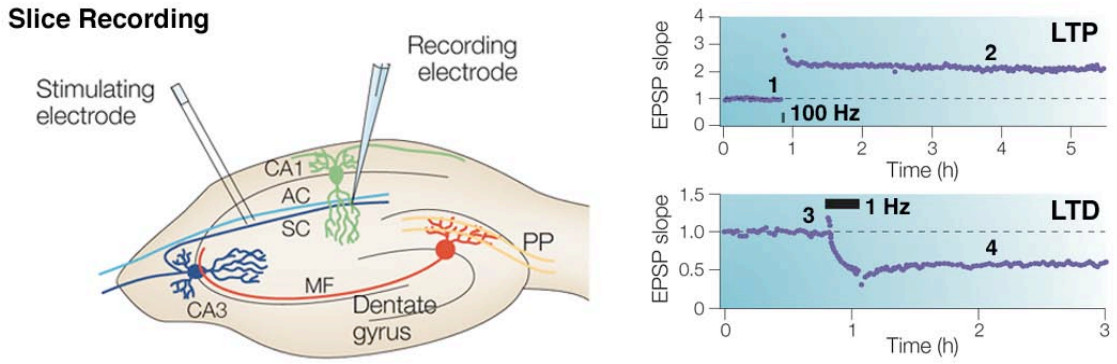

Figure 1. LTP and LTD. Left: A schematic diagram of the rodent hippocampal slice preparation, showing the main excitatory pathways of the brain (AC = associational/ commissural, MF = mossy fibre, PP = perforant path, SC = Schaeffer collateral). Typical electrode placements for studying synaptic plasticity at Schaeffer collateral-commisural synapses are shown. Right: Time-course plots showing the slopes of field excitatory postsynaptic potentials (EPSPs) against time during LTP (1s, 100 Hz stimulation) and LTD (15 min., 1 Hz stimulation). The black bars represent the time of the stimulus and the numbers denote reference points for comparing synaptic strength. Adapted from Collingridge, 2004.[1]

Of course, to modify the way the brain thinks, it must sometimes be necessary to weaken the connection between two neurons as well. There is an electrophysiological manifestation of this process as well, called long term depression (LTD). A low frequency stimulus over a relatively long period of time can lead to LTD of synaptic transmission. For example, in Figure 1, a smaller post-synaptic current is observed in the recording electrode (compare points 3 and 4) after 15 minutes of 1 Hz stimulation. Bidirectional and reversible alterations in synaptic efficiency make possible the storage of information in the brain.[3]

Glutamate Receptors And Their Role in Synaptic Plasticity

While the nAChR, which we have focused on to this point, is important in communication in the nervous system, it is not the primary locus of learning and memory.[4] Glutamate receptors (GluRs) and GABA (γ-aminobutyric acid) receptors (GABARs), both ionotropic and metabotropic in nature, mediate most synaptic transmission in the vertebrate central nervous system (CNS).[1] Here, we will focus on the role of ionotropic GluRs. Glutamate (Glu) activates three main classes of ionotropic glutamate receptor, named after the selective agonists AMPA (α-amino-3-hydroxy-5-methyl-4-isoxazole-propionic acid), NMDA (*N*-methyl-D-aspartate) and kainite. Each GluR comprises a heterotetrameric cation channel. The AMPA and NMDA subtypes thus far appear to be more important to LTP and LTD.[1] The AMPA receptor (AMPAR) is a sodium channel composed of combinations of GluR1, 2, 3, and 4 subunits (~ 850 amino acids each). The NMDA receptor (NMDAR) is composed of combinations of NR1, 2A, 2B, 2C, and 2D subunits (~ 1500 amino acids each) and passes both Na^+ and Ca^{2+}. Both the AMPAR and the NMDAR gate in response to Glu, but NMDARs also require glycine (Gly) or D-serine (D-Ser) as a coagonist. (Scheme 1) AMPAR and NMDAR channel subunits have an extracellular ligand binding domain and three transmembrane domains (See Chapter 8 for images of the NMDAR subunit toplogy). The NMDAR has a long intracellular C-terminus that allows it to interact with numerous scaffolding proteins.

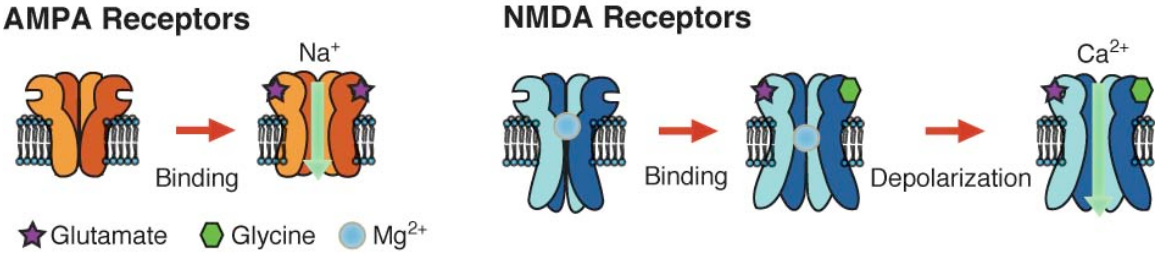

Scheme 1. AMPAR and NMDAR Gating.

Changes to AMPARs are responsible for most of the changes in postsynaptic currents that are commonly studied during LTP and LTD experiments.[5] AMPAR modulation during synaptic plasticity involves alteration of the function of channels already present at the synapse as well as the trafficking of AMPARs in and out of the synapse. A single type of amino acid modification, phosphorylation, is an important regulatory element in both of these processes.[5] This is a posttranslational modification carried out on Ser, Thr, and Tyr residues. The phosphate group is applied by kinases and removed by phosphatases (PPases).[6] Chapter 7 describes our attempts to devise a biochemical method to establish precise temporal control over phosphorylation with photolabile caging groups.

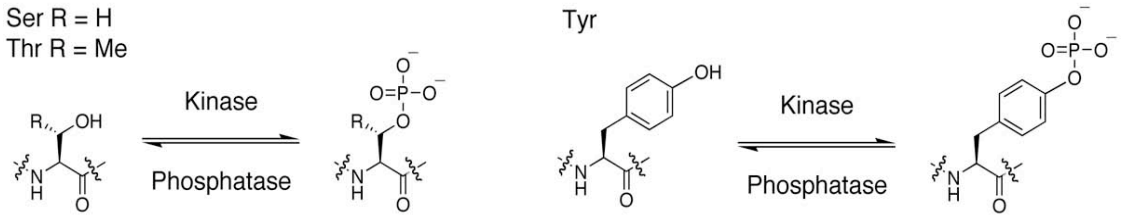

Scheme 2. Ser, Thr, and Tyr Phosphorylation.

While AMPAR modifications give rise to the postsynaptic current changes of LTP and LTP, it is NMDA receptors that are the triggers for these processes.[7] NMDARs govern LTP and LTD induction through their role as coincidence detectors, a kind of molecular "and" gate. Not only do NMDARs require Glu and Gly to gate, but the membrane must also be depolarized by the opening of other receptors.[8] In the resting state, the NMDAR pore is blocked by a Mg^{2+} ion. Membrane depolarization allows the ion to leave so that Ca^{2+} can flow through the NMDAR pore. (Scheme 1) This is an extremely subtle chemical phenomenon, which may have a cation-π interaction at its heart.[9] It is the subject of our investigation in Chapter 8. The Ca^{2+} which enters the cell activates a number of processes which are important to LTP, involving modifications to both the NMDARs themselves and to AMPARs.[3] Among these modifications is phosphoryaltion of tyrosines in the C-terminal tail of the NMDAR.[10]

Before we begin a discussion of the molecular mechanisms of LTP as a lead-in to Chapters 7 and 8, a few comments on what will not be discussed in this chapter are in order. Gouaux and coworkers have expressed a soluble protein comprising the extracellular ligand binding domain of the AMPAR, and crystallography of this species has produced detailed insights into Glu binding and channel activation.[11] They have performed similar studies with the NMDAR NR1A Gly-binding region.[12] However, we will not comment on these structures here, as our interests are in NMDAR Mg^{2+} blockade and GluR phosphorylation, which are events that occur in the transmembrane and intracellular regions, respectively.

An Overview of Long Term Potentiation

During LTP, AMPARs tend to move more than NMDARs, so for simplicity's sake, we will begin with an overview that assumes static NMDARs as triggers of LTP involving dynamic AMPARs, and then discuss the trafficking of NMDARs. This is meant to give a conceptual overview of LTP, and simplifies many of the details of the process. Under basal conditions (A in Fig. 2), AMPARs are the primary loci of transmission at glutamatergic synapses.[3] They are not static even in the absence of LTP, they tend to be trafficked constitutively.[1] Receptor trafficking involves the intracellular movement of receptors from sites of synthesis to the plasma membrane, where they function, and then to sites of degradation. The receptors are inserted into and removed from the plasma membrane by exocytosis and endocytosis respectively, and diffuse laterally within the plasma membrane.

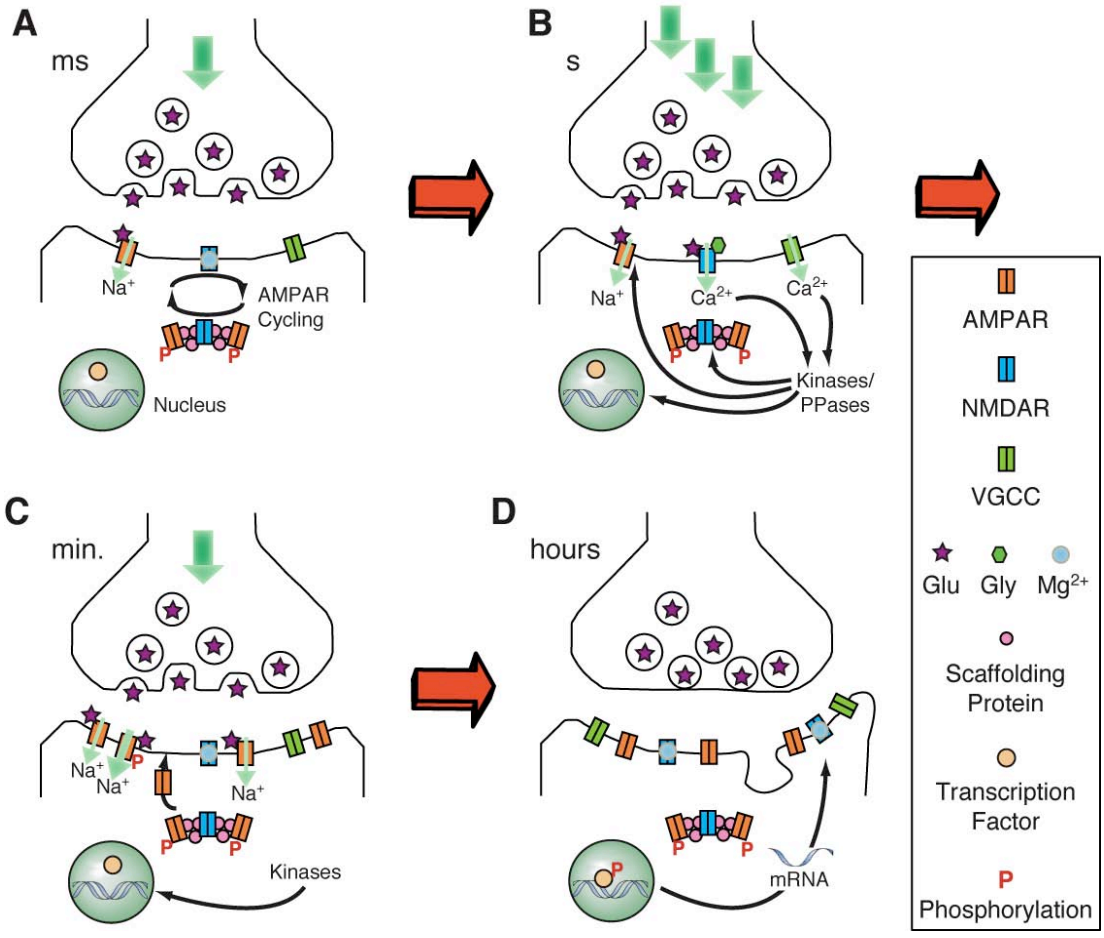

Figure 2. Molecular Mechanisms Involved in the Initiation and Maintenance of Synaptic Plasticity. A. The basal state: a presynaptic action potential causes release of Glu and activation of postsynaptic AMPAR currents. B. Repetitive activity at the presynaptic terminus causes postsynaptic membrane depolarization through AMPAR opening. Voltage-gated calcium channels (VGCCs) and NMDARs open to allow Ca^{2+} influx (Gly is always present at saturating concentrations). Ca^{2+} influx causes activation of kinases. C. Phosphorylation of AMPARs causes changes in their single-channel and trafficking behavior, strengthening the synapse to give the electrophysiological phenomenon of LTP. D. Kinase phosphorylation of transcription factors turns on the production of mRNAs which will lead to the growth of new synapses.

When a coordinated series of inputs arrives at the presynaptic terminus, the AMPAR currents are sufficient to depolarize the membrane, which opens voltage-gated calcium channels (VGCCs) and NMDARs. (Fig. 2B) Gly and D-Ser are always present in the synapse at sufficient concentrations to open NMDARs, so it is the membrane depolarization that meets the final requirement for their opening.[3] The Ca^{2+} influx from the NMDARs and VGCCs causes activation of kinases like calcium/ calmodulin-dependent protein kinase II (CaMKII).[3] These kinases phosphorylate AMPARs, NMDARs, and scaffolding proteins, causing changes in both channel function (a change in the current passed by the channel) and channel trafficking (a change in their distribution). Both of these types of changes are shown in Figure 2C. Addition of channels and potentiation of their function gives rise to the increase in post-synaptic currents seen in Figure 1. Finally, on a much longer timescale, activation of other kinases, such as those in the p42/44 mitogen-activated protein kinase (MAPK) pathway, can lead to upregulation of transcription factors. This means the production of new mRNAs to manufacture new proteins and create new synaptic connections, a process known as synaptic morphogenesis (Fig. 2D).[3]

These complex modifications and motions of GluRs do not occur by molecules randomly diffusing in solution to reach their targets. All of the LTP processes described above are controlled by protein-protein interactions, both between receptors and kinases themselves, and among scaffolding proteins.[13] These scaffolding proteins establish high local concentrations of the active proteins and link them to the cytoskeleton for transport to and from the membrane. A cartoon depicting a hypothetical assemblage of an AMPAR, NMDAR, and mGluR with associated scaffolding proteins is shown in Figure 3A. Scaffolded complexes of this sort can be seen in electron micrographs of the synapse.[13]

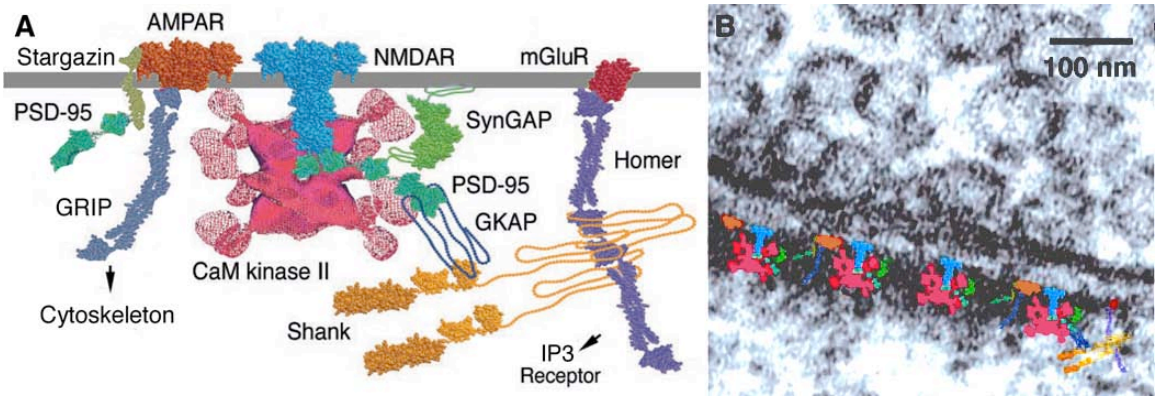

Figure 3. Scaffolding of GluRs. A. Cartoon showing a signaling complex. Glutamate receptor-interacting protein (GRIP), post-synaptic density protein 95 (PSD-95), G-kinase anchoring proteins (GKAP), synaptic GTP-ase activating protein (SynGAP), inositol triphosphate (IP3) receptor. Sizes and shapes of molecules based on crystal structures or electron microscopy data where available. B. The components of A are shown overlayed on the postsynaptic density in an electron micrograph of a synapse. Docked vesicles can be seen on the presynaptic side. Adapted from Kennedy, 2000.[13]

The LTP Trigger: NMDAR Mg^{2+} Block

Despite the complexity of the downstream events, there is no doubt that the lynchpin which triggers LTP is the removal of the Mg^{2+} ion from the pore of the NMDAR. NMDAR calcium influx is responsible for LTP, VGCC activation is not sufficient. When NMDA (which does not activate AMPA receptors) is applied to neurons with an electrophysiologically-applied depolarization, events that resemble LTP can be induced.[1] We wish to study the precise chemical nature of the Mg^{2+} blockade in order to understand this crucial ion channel process. Several studies using conventional mutagenesis have implied key roles for Trp residues in the pore of the NMDAR in binding magnesium.[14, 15] They have hypothesized that a cation-π interaction may be responsible for Mg^{2+} block of NR2B-containing receptors.[15] These studies were performed in oocytes, so we should be able to translate their techniques directly to our unnatural amino acid mutagenesis studies. Furthermore, our familiarity with Trp and the cation-π interaction makes study of Mg^{2+} binding an excellent point of entry into this exciting field. This is the subject of Chapter 8.

AMPAR Modulation by Phosphorylation

As noted above, many of the AMPAR modifications are controlled by phosphorylation. Phosphorylation can affect both the function of single receptors and their surface expression levels. These effects can arise either from the phosphorylation of associated proteins or of the receptors themselves. We will focus on the direct phosphorylation of the receptors as this is what we will eventually probe with the unnatural amino acids developed in Chapter 7. Studies using site-directed mutagenesis have shown that AMPARs are phosphorylated on at least 12 distinct sites.[5] Various protein kinases have been implicated in the induction of NMDAR-dependent LTP. These include protein kinase C (PKC), CaMKII, protein kinase A (PKA), MAPK, and phosphatidylinositol 3-kinase (PI3K).[1] As one might expect, PPases have been implicated in NMDAR-dependent LTD, in particular, protein phosphatases 1 (PP1) and 2B (PP2B).[1] We will give two examples highlighting the two types of effect that phosphorylation can have.

Sites 831 and 847, which have homologs on the other AMPAR subunits, are the major sites of phosphorylation on the GluR1 subunit.[5] PKC and CaMKII phosphorylate S831 and PKA phosphorylates S847.[5] Recordings in HEK 293 cells have shown that exogenous application of these kinases can result in potentiation of the AMPA-induced currents.[16] (Fig. 4) The site-specificty of the phosphorylation events was established by mutation of these residues to Ala, which reduced potentiation.[16] (Fig. 4) However, this seemingly straightforward study revealed some of the complexities of AMPAR phosphorylation. The phosphorylation rates at S831 appear to be dependent on the phosphorylation state of S847 and visa-versa.[5] The timecourses of phosphorylation of the

two sites are similar, so deconvoluting data on functional effects is difficult. Moreover, there are no highly selective phosphatases for either site, so one cannot examine the specific effects of dephosphorylation on channel currents.[5] A method for site-specific biochemical control of the rates of phosphorylation and dephosphorylation such as the one we describe in Chapter 7 would be extremely useful to studying these processes. These sorts of effects can easily be studied in oocytes, an expression system with which we have demonstrated the utility of unnatural amino acid mutagenesis repeatedly.

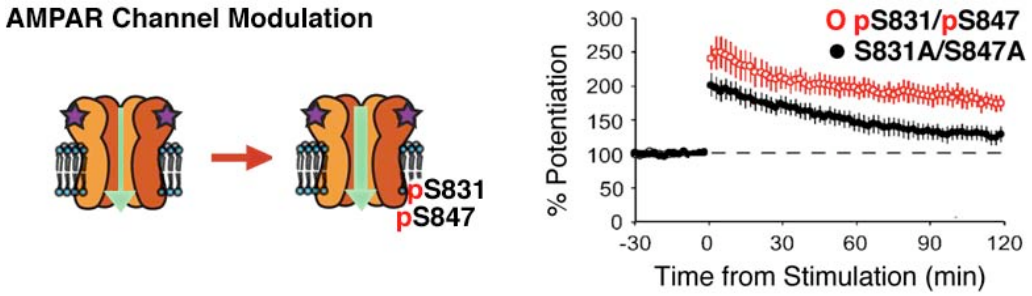

Figure 4. AMPAR Channel Modulation by Phosphorylation. Mouse brain slice responses to AMPA application from wild type and double mutant mice under phosphorylating conditions. Adapted from Lee *et al.*, 2003.[16]

What about the effects of phosphorylation on AMPAR trafficking? Oocyte systems will not be suitable for studying this, as trafficking in oocytes is not sufficiently relevant to the mammalian systems, which are our primary concern. We have recently demonstrated that we can perform unnatural amino acid experiments in mammalian cells by recapitulating elements of the cation-π study of ACh binding described in Chapter 2.[17] These experiments were performed in CHO and HEK cells. Importantly, we have also shown that we can make mammalian unnatural amino acid methodology work with a GluR, the NMDA receptor. (Fig. 5)

Figure 5. Expression of the NMDA receptor in CHO-K1 cells. Both traces involve wild type NR1 plus NR2A with a TAG codon at position 606. WT Recovery: tRNA with Trp attached gives strong current. "Read Through": tRNA with no amino acid attached gives negligible current.

We found that we obtain significant currents when we rescue wild type behavior by delivering the appropriate aminoacyl tRNA. (i.e. a Trp to a W606 to TAG mutation) Readthrough (current from nonacylated tRNA) is negligible, indicating that the phenotype we observe will come from our unnatural amino acid only and not from background. It will be valuable to use mammalian cell expression to verify findings from oocyte experiments as well as in mammalian-specific experiments, because scaffolding protein interactions are know to vary between oocytes and mammalian cells.

Trafficking experiments depend on one's ability to visualize the receptor in space and cannot be conducted purely with electrophysiology. Several approaches have been used by other labs to visualize AMPARs.[1] One approach uses antibodies that recognize extracellular AMPAR subunit epitopes in conjunction with protocols that induce NMDAR-dependent LTP and LTD.[18] AMPAR distributions were monitored using fluorescently conjugated secondary antibodies. One can see from Figure 6 that the number of labeled AMPARs increases after LTP is induced. (Fig. 6, Top) This an example of receptor insertion in the first phase of LTP. In another study using GluR2 subunits conjugated to green fluorescent protein (GFP), one can see that they are introduced into a newly budding synapse.[19] (Fig. 6, Bottom) This is an example of synaptic morphogenesis, a later stage of LTP (Fig. 2D)

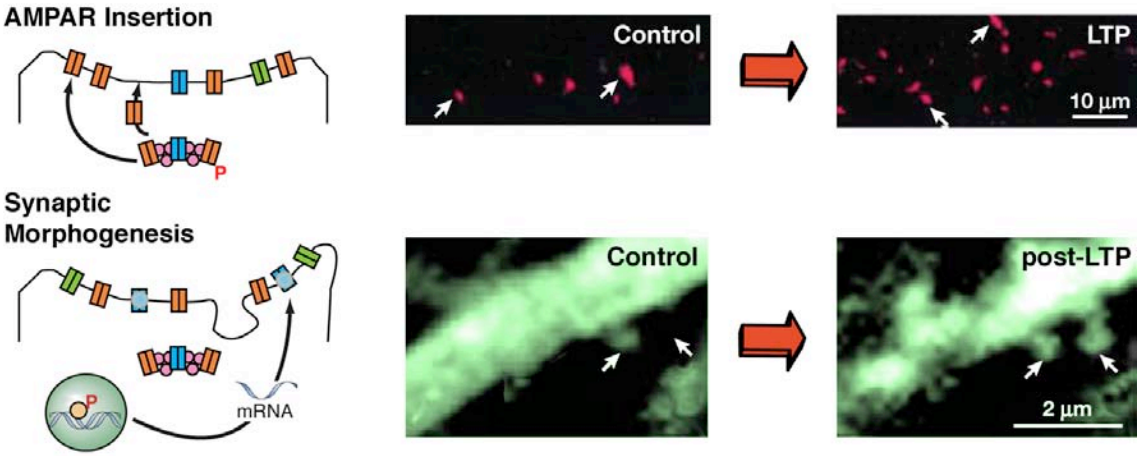

Figure 6. AMPAR Trafficking. Top: LTP induction causes trafficking of GluR1-containing receptors to the cell surface. Imaged with N-terminal GluR1 primary antibody. Bottom: GluR1-GFP fusions are targeted to previously empty dendritic spines by LTP induction. Images from Collingridge *et al.*, 2004.[1]

Many proteins (i.e. scaffolding and cytoskeletal proteins, see Fig. 3) are involved in governing these processes, and phosphorylation plays a very prominent role in regulating association with other proteins. It is likely that the insertion and removal of AMPARs involves many kinases and phosphatases, and that some of these are involved in aspects of LTP and LTD other than AMPAR trafficking. The best characterized example of

phosphorylation-dependent trafficking involves phosphorylation of GluR2 S880 which inhibits AMPAR binding to GRIP, so that the AMPARs are released from subsynaptic pools and surface expression is decreased.[1]

NMDA Receptors

NMDARs are also affected by phosphorylation both in terms of single channel effects and receptor trafficking. In contrast to AMPARs, which are primarily phosphorylated on Ser, NMDARs are phosphorylated on a series of Tyr residues contained in their large, intracellular, C-terminal tails. For example, the NR2B subunit has 30 tyrosines in its C-terminal tail, at least 3 of which are phosphorylated.[10] Many interacting proteins also cling to these tails, so that the machinery for regulating phosphorylation is also present. Specifically, the Src family of kinases co-precipitate with NMDARs in immunoprecipitation experiments and activation of Src activity increases NMDAR single-channel opening rates and potentiates synaptic currents.[10] (Fig. 7) This can be reversed by treatment with recombinant striatal-enriched tyrosine phosphatase (STEP).[10] (Fig. 7) Although it is known that direct NMDAR phosphorylation is responsible for these changes, it is not clear whether phosphorylation of a single one of the 30 tyrosines is necessary or sufficient for channel potentiation.

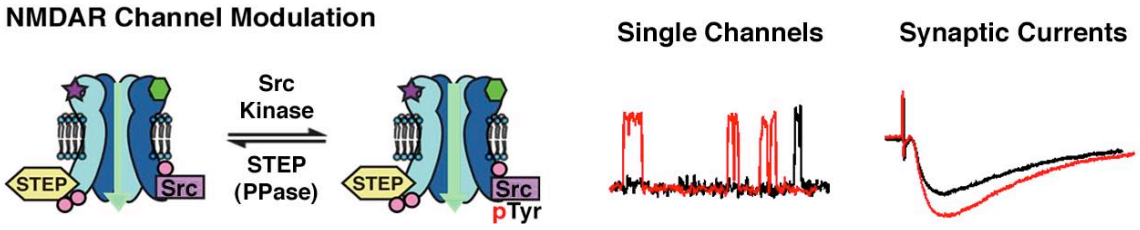

Figure 7. NMDAR Channel Modulation. Phosphorylation increases channel open times and whole-cell NMDA currents. Src phosphorylation and STEP dephosphorylation induced by application of recombinant protein to oocytes (Single Channels) or neuronal recordings (Synaptic Currents). Red indicates traces from phosphorylated NMDARs, black indicates unphosphorylated. Adapted from Salter *et al.*, 2004.[10]

So far we have thought of NMDARs as a trigger for LTP and LTD. However, NMDAR populations are not entirely static, they too are trafficked.[20] On the surface of living neurons there are mobile and immobile pools of NMDARs, at both synaptic and extrasynaptic sites. The mechanisms by which NMDARs can rapidly move between the intracellular and extracellular compartments of neurons are now being elucidated. Trafficking of NMDARs is regulated by the C terminus of NR1, and surface expression of NMDARs is facilitated by a PDZ protein interaction.[1] As this NMDAR domain is replete with Tyr phsophorylation sites, it is likely that Tyr phosphorylation plays an important role in NMDAR trafficking.

Summary

In studies of GluRs, proteins and mechanisms have been identified that directly regulate channel modification and synaptic surface expression that might be important to LTP and LTD. Receptors are commonly stabilized at the synaptic plasma membrane by interactions with scaffolding proteins that contain multiple protein–protein interaction domains. Similar interactions might be involved in concentrating receptors at intracellular sites. Phosphorylation is a dominant control mechanism for both trafficking of these receptors to the surface, and modification of individual channels. In short, this process is extremely complicated, and any biochemical control that can be asserted will be welcome in deconvoluting these processes. In the following two chapters, we describe our initial foray into controlling phosphorylation and studying glutamate receptors.

References

(1) Collingridge, G. L.; Isaac, J. T.; Wang, Y. T., *Nat. Rev. Neurosci.* **2004,** 5, 952-962.

(2) Winder, D. G.; Schramm, N. L., *Physiol. Behav.* **2001,** 73, 763-780.

(3) Lamprecht, R.; LeDoux, J., *Nat. Rev. Neurosci.* **2004,** 5, 45-54.

(4) Kullmann, D. M.; Asztely, F.; Walker, M. C., *Cell. Mol. Life Sci.* **2000,** 57, 1551-1561.

(5) Song, I.; Huganir, R. L., *Trends Neurosci.* **2002,** 25, 578-588.

(6) Manning, G.; Whyte, D. B.; Martinez, R.; Hunter, T.; Sudarsanam, S., *Science* **2002,** 298, 1912-+.

(7) Zhu, H. B.; Luo, J. H., *Prog. Biochem. Biophys.* **1999,** 26, 541-543 Malinow, R.; Mainen, Z. F.; Hayashi, Y., *Curr. Opin. Neurobiol.* **2000,** 10, 352-357.

(8) Review Dingledine, R.; Borges, K.; Bowie, D.; Traynelis, S. F., *Pharm. Revs.* **1999,** 51, 7-61.

(9) Ferrer-Montiel, A. V.; Sun, W.; Montal, M., *Biophys. J.* **1996,** 71, 749-758.

(10) Salter, M. W.; Kalia, L. V., *Nat. Rev. Neurosci.* **2004,** 5, 317-328.

(11) Armstrong, N.; Sun, Y.; Chen, G.-Q.; Gouaux, E., *Nature* **1998,** 395, 913-917 Hogner, A.; Kastrup, J. S.; Jin, R.; Liljefors, T.; Mayer, M. L.; Egebjerg, J.; Larsen, I. K.; Gouaux, E., *J. Mol. Biol.* **2002,** 322, 93-109 Jin, R. S.; Banke, T. G.; Mayer, M. L.; Traynelis, S. F.; Gouaux, E., *Nat. Neurosci.* **2003,** 6, 803-810.

(12) Furukawa, H.; Gouaux, E., *Embo J.* **2003,** 22, 2873-2885.

(13) Kennedy, M. B., *Science* **2000,** 290, 750-754.

(14) Mayer, M. L.; Westbrook, G. L.; Guthrie, P. B., *Nature* **1984,** 309, 261-263 Wollmuth, L. P.; Kuner, T.; Sakmann, B., *J. Physiol. (Lond)* **1998,** 506, 33-52 Wollmuth, L. P.; Kuner, T.; Sakmann, B., *J. Physiol. (Lond)* **1998,** 506, 13-32.

(15) Williams, K.; Pahk, A. J.; Kashiwagi, K.; Masuko, T.; Nguyen, N. D.; Igarashi, K., *Mol. Pharmacol.* **1998,** 53, 933-941.

(16) Lee, H. K.; Takamiya, K.; Han, J. S.; Man, H.; Kim, C. H.; Rumbaugh, G.; Yu, S.; Ding, L.; He, C.; Petralia, R. S.; Wenthold, R. J.; Gallagher, M.; Huganir, R. L., *Cell* **2003,** 112, 631-643.

(17) Monahan, S. L.; Lester, H. A.; Dougherty, D. A., *Chem. Biol.* **2003,** 10, 573-580.

(18) Lu, W.; Man, H.; Ju, W.; Trimble, W. S.; MacDonald, J. F.; Wang, Y. T., *Neuron* **2001,** 29, 243-254.

(19) Shi, S. H.; Hayashi, Y.; Petralia, R. S.; Zaman, S. H.; Wenthold, R. J.; Svoboda, K.; Malinow, R., *Science* **1999,** 284, 1811-1816.

(20) Carroll, R. C.; Zukin, R. S., *Trends Neurosci.* **2002,** 25, 571-577.

Section 2: Chapter 7

Biochemical Control of Protein Phosphorylation

Caging Amino Acids to Control Phosphorylation

The phosphorylation of serine, threonine, and tyrosine residues in proteins is a central mechanism of cellular regulation.[1] Phosphorylation can profoundly modulate the role of the protein in a biological system, by altering either the activity of the isolated protein or interactions with other proteins. The phosphorylation state of a protein is dynamic; it is determined by the interplay of kinases, which append the phosphate group, and phosphatases (PPases), which remove it.[2] (Fig. 1) Currently available biological experiments such as chemical inhibition, gene knockout, or point mutation studies do not allow real time studies of protein phosphorylation in biochemical signaling pathways.

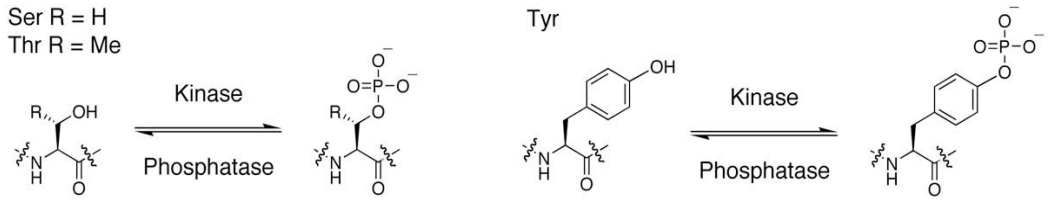

Figure 1. Phosphorylation is a Dynamic Modification.

Caged amino acids afford researchers spatial and temporal control over the effective phosphorylation state at a specific site in a target protein.[3] In general, the "cage" comprises a photocleavable protecting group (PG) that masks the essential functionality. Photolysis of the PG generates a bioactive protein. This can entail a caged, unmodified amino acid that can be photolyzed to reveal the natural amino acid which can then be phosphorylated by a kinase. Alternatively, a caged, phosphorylated amino acid can be incorporated, from which photolysis generates a protein that is phosphorylated at a single site. This achieves greater temporal and spatial (i.e. site specificity with 100% phosphorylation) resolution than is possible with the other techniques mentioned above.

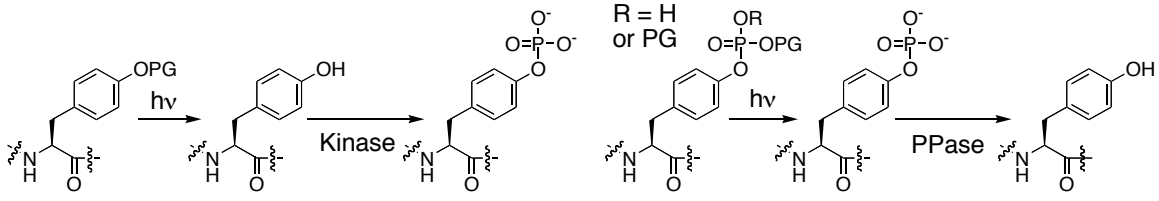

Figure 2. Control of Phosphorylation with Photocleavable Protecting Groups (PGs).

We employ nitrobenzyl–derived protecting groups in our work here: either 2-nitrobenzyl (Nb), 4,5-dimethoxy-2-nitrobenzyl (nitroveratryl, Nv), or *o*-nitrophenethyl (NPE). These have been shown to be effective in caging both hydroxyl and phosphate moieties in several previous small molecule studies.[4]

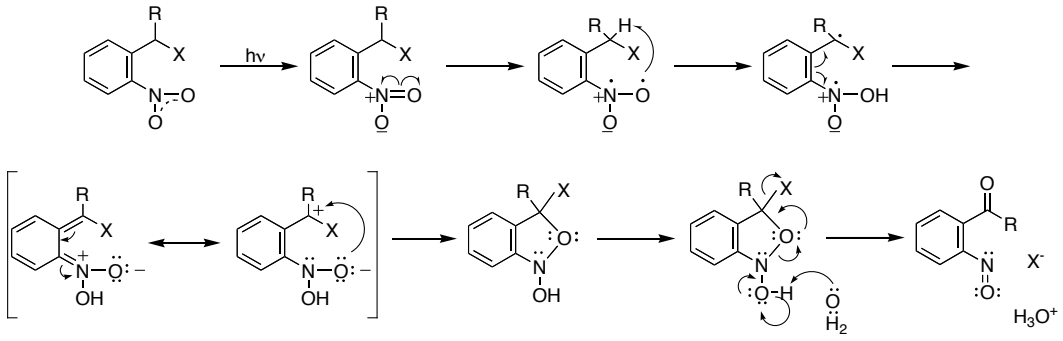

Scheme 1. Nitrobenzyl Photodeprotection Mechanism. Adapted from Adams, 1993.[5]

Previous Work: Caged Amino Acids

Caged amino acids have been available for incorporation into full-length proteins for some time.[6, 7] Previous to the work described here caged Ser (CSer, Ser(ONv), **1**), caged Thr (CThr, Thr(ONv), **2**), and caged Tyr ((CTyr(ONb), Tyr(ONb), **3**); have been synthesized in our labs.[8, 9] **1** and **3** have been successfully incorporated into ion channels *in vivo,* and the effects of decaging have been monitored in real time with electrophysiology.[8, 9]

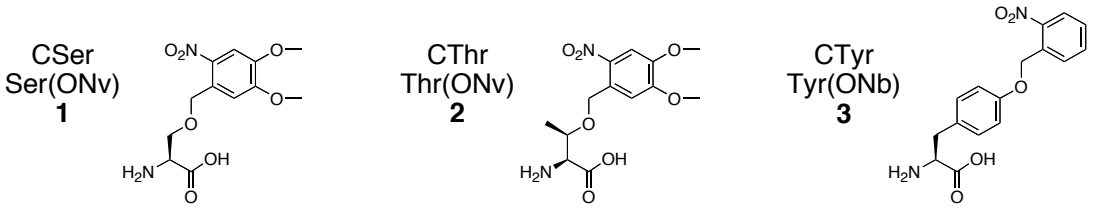

Figure 3. Caged Amino Acids.

A conventional rig set up for two electrode voltage clamp electrophysiology was modified to include a fiber optic cable which provided irradiation from a 400 W Hg arc lamp. A UG-11 filter was used to confine the wavelengths of irradiation to 300 to 350 nm. Residues **1** or **3** were incorporated in the pore of the nicotinic acetylcholine receptor so that no current was observed from receptors in which the residue was caged, but decaging permitted ion flux.[9] Thus, we were able to establish that complete decaging and activation of the channels with residues **1** and **3** could be observed in 0.5 s. One may expect more rapid decaging rates based on previous caged, small molecule studies[10], but it is important to keep in mind that we will be studying membrane proteins on the highly invaginated surface of an oocyte, and that solution studies of small molecules may not be applicable.

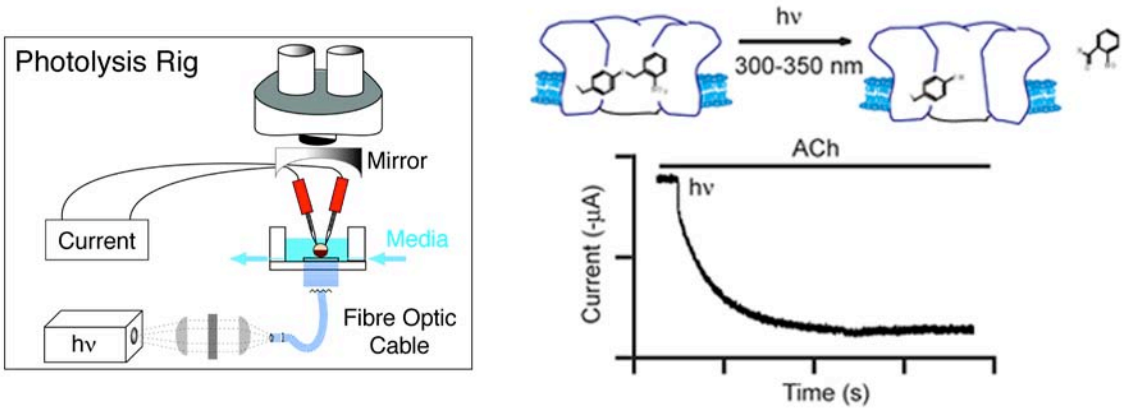

Figure 4. Photolysis Rig and Example Decaging of **3** in the pore of the nAChR. Adapted from Philipson *et al.*, 2001.[9]

In another study, it was established that we could control the onset of ion channel phosphorylation with the caged residue **3**.[11] It was believed that phosphorylation of Tyr 242 in the Kir 2.1 channel lead to its removal from the membrane. When **3** was incorporated at position 242, no change in channel current was observed in the absence of decaging. Likewise, no change was observed upon irradiation in the absence of Src kinase activity. Only when **3** was decaged to reveal a native Tyr and the Src kinase activity was stimulated did we observe the expected decreases in channel current and membrane capacitance with loss of Kir 2.1 (and associated lipid membrane) from the oocyte surface. As one can see from Figure 5, the timecourse of this removal is on the order of 25 minutes. Thus we have seen, that we can control decaging on the second time scale while, in at least one case, kinase phosphorylation occurs on the timescale of tens of minutes.

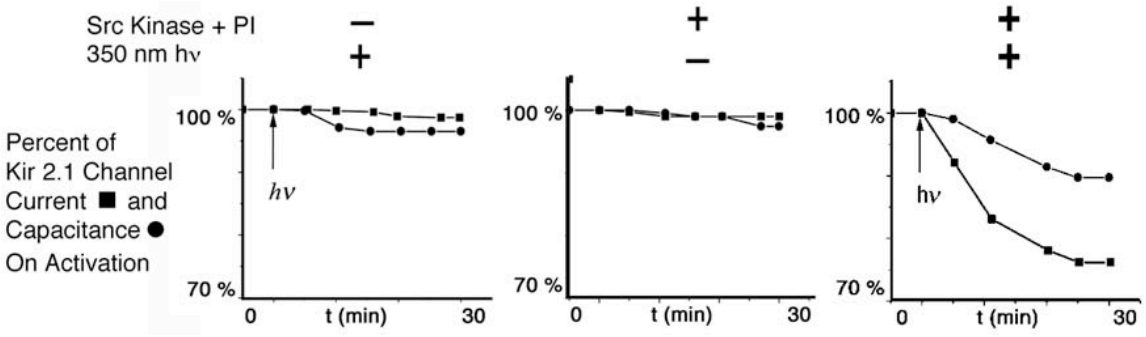

Figure 5. Photochemical control of phosphorylation onset. Adapted from Tong *et al.*, 2001.[11]

Initial Studies: Doubly-Caged Phosphoamino Acids

Once we had established that we could control half of the phosphorylation cycle with unnatural amino acids, we wished to design amino acids to control the other half, the onset of dephosphorylation by PPases. To this end, we sought to synthesize caged, phosphorylated amino acids.

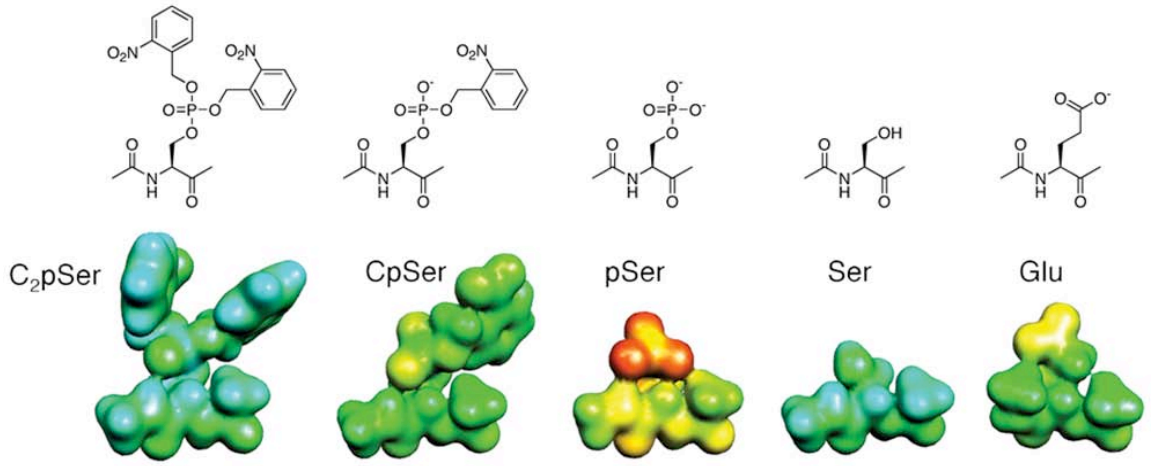

Figure 6. Amino acid analogs and their electrostatic potential surfaces (EPSs). EPSs shown from – 190 kcal/mol (red) to + 5 kcal/ mol (blue) mapped on electron densities with a 0.002 e/Å^3 cut-off.

Initially, we were forced to make a decision as to the number of caging groups on the amino acids. In molecular recognition, two essential characteristics of the molecule play a role: shape and charge distribution. Electrostatic potential surfaces of the sort shown in Figure 6 describe both of these characteristics. Thus, to disguise pSer, we alter both its shape and atomic charge when we cage it. Employing two Nb caging groups will clearly eliminate the negative charge observed on pSer, but C_2pSer may be too bulky to be incorporated by the ribosome (and cause other problems, as we will see below). A single caging group, while it alters the steric bulk of the sidechain, does not eliminate the negative charge. It has been shown that a Glu residue may function as a mimic of pSer in several phosphoprotein studies. Thus, it may be that CpSer appears sufficiently like pSer so as to be functionally uncaged in its application. It is for this reason that we chose to risk the potential ribosomal incompatibility of doubly caged residues like C_2pSer in our initial attempts at generating caged phosphoamino acids.

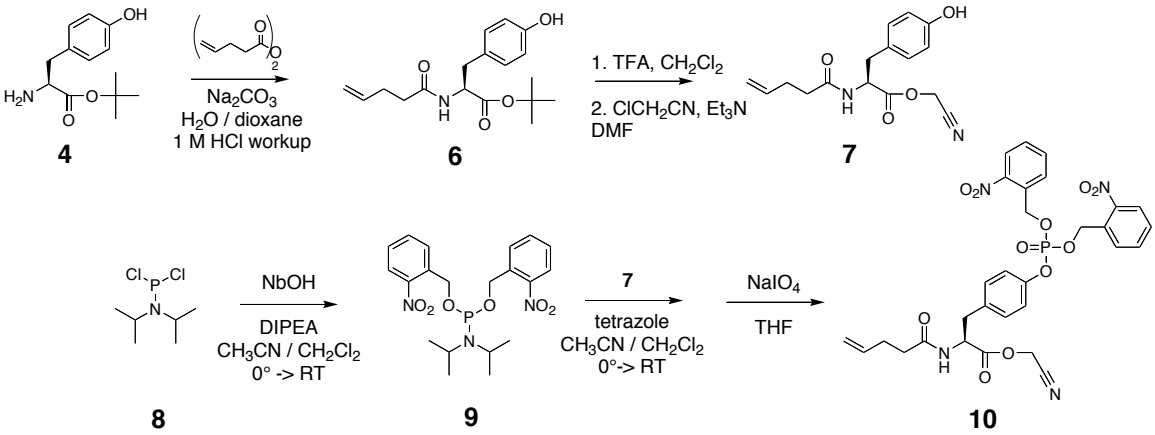

Scheme 2. Synthesis of C_2pTyr (pTyr(ONb)$_2$) cyanomethyl ester.

The syntheses of the doubly-caged phosphoamino acids were developed by Gabriel Brandt.[12] The route to the C_2pTyr (pTyr(ONb)$_2$) precursor **10** was straightforward, borrowing phosphoramidite techniques from nucleic acid syntheses for installing the caged phosphate moiety. (Scheme 1) These were protected on the α-amine with a 4-pentenoyl (4-PO) group which can be removed by iodolactonization, a chemistry orthogonal to photodeprotection of the Nb and Nv groups.

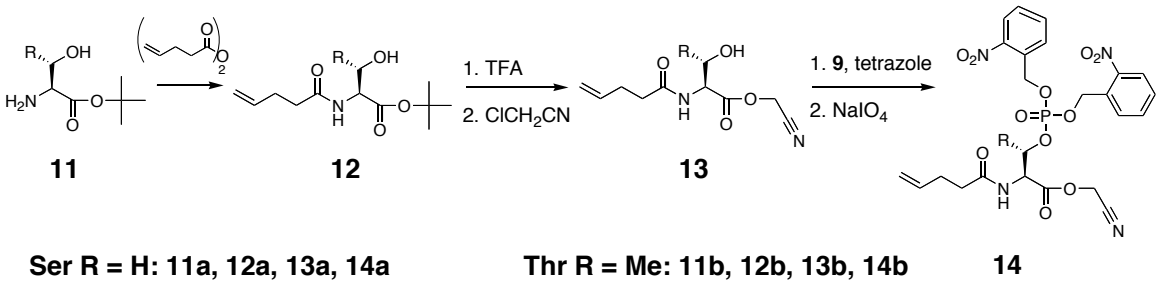

Scheme 3. Synthesis of C_2pSer (pSer(ONb)$_2$) and C_2pThr (pThr(ONb)$_2$) cyanomethyl esters.

The key intermediate, **9**, could also be used in the syntheses of the Ser and Thr compounds, **14a** and **14b**. (Scheme 2) The three cyanomethyl esters **10**, **14a**, and **14b** appeared ready for coupling to the dinucleotide dCA and subsequent ligation to 74-base $tRNA_{CUA}^{-CA}$. However, while the dCA coupling of **10** proceeded smoothly, coupling of the Ser derivative **14a** saw substantial decomposition of the starting material with no product formation.

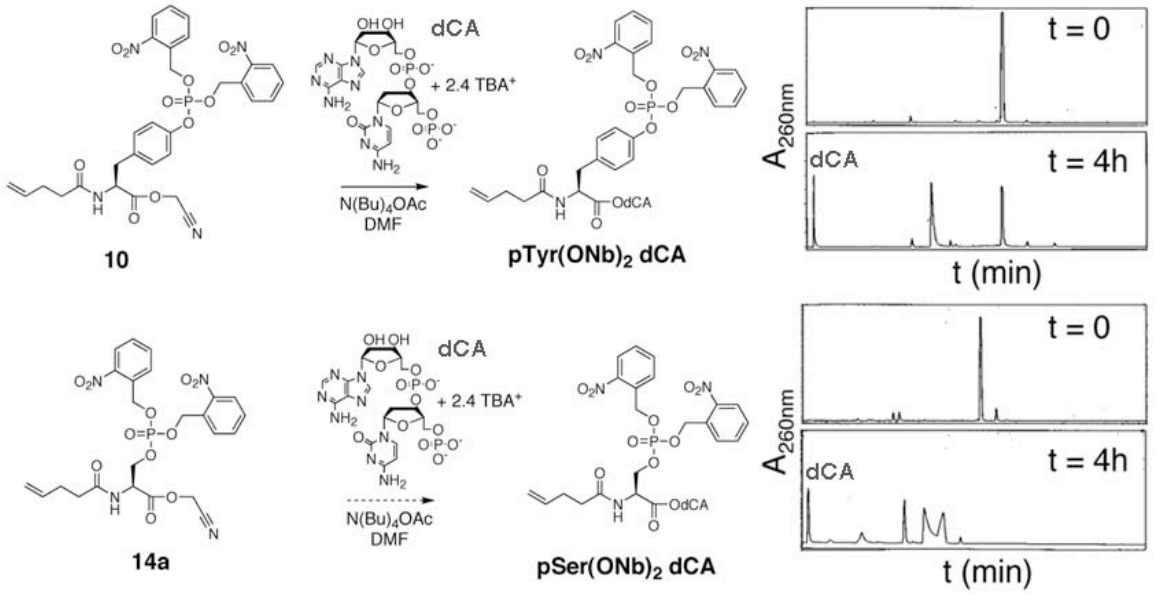

Figure 7. Coupling of Cyanomethyl Esters. HPLC traces show clean reaction of **10** with dCA and mixtures of products in the reaction of **14a** with dCA.

Several decomposition products were observed; some could be attributed to breakdown of the phosphotriester, but not all of them could be identified by MS or NMR. Several reaction conditions were considered, including the addition of a non-nucleophilic proton source (TfOH) or direct coupling of the trivalent phosphorous species (**15a**) followed by periodate oxidation of the dCA-coupled product. This led to some yield of product (by HPLC and MS), but these products were also labile to the same degradation reactions, such as β-elimination of the phosphate moiety to give an α,β- unsaturated ester.

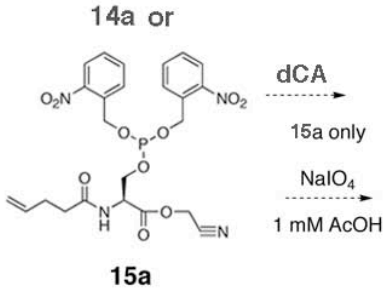

Ester	Eq. $N(Bu)_4^+$	Solvent	Yield (%)
14a	2.4	DMF	
	2.4	CH_3CN	
	2.4	CH_3CN + 0.05% TfOH	
	3.0	CH_3CN	
15a	2.4	CH_3CN	
	2.4	CH_3CN	
	2.4	DMF	1
	3.0	CH_3CN / DMF	2-5

Figure 8. Attempts to Couple Cyanomethyl Esters to generate $pSer(ONb)_2$.

The Thr derivative **14b** performed slightly better in dCA coupling, possibly due to an increased barrier to forming the *anti* geometry necessary for β-elimination. Before addressing the problems in coupling the Ser or Thr derivatives, we sought to assess the viability of C_2pTyr in suppression experiments. To do this, we ran *in vitro* translation reactions in which we suppressed the given amino acid at a highly tolerant position in the nAChR (All nAChR suppressions were performed at α70, α124, or α127).[13, 14] The efficiency of protein production was determined by the intensity of labeling with an antibody targeted to an 11 amino acid hemaglutanin (HA) epitope C-terminal to the suppression site. (Fig. 9) While CTyr (Tyr(ONb)) incorporates quite well, consistent with previous results, $C_2pTyr(ONb)_2$ incorporates only very weakly, barely above background.

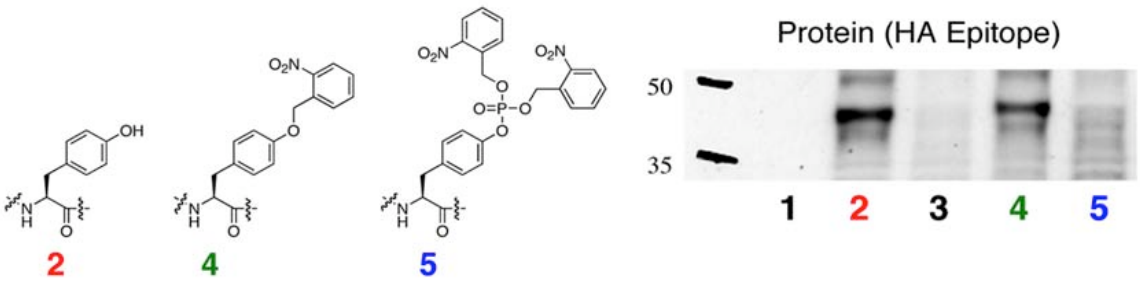

Figure 9. *in vitro* PAGE Gel Assessment of Suppression Efficiency. Translations run in rabbit reticulocyte mixtures with α70Z nAChR mRNA and the following: 1: No tRNA, 2: Tyr-tRNA, 3: tRNA with no amino acid, 4: CTyr-tRNA (Tyr(ONb)-tRNA), 5: C_2pTyr-tRNA ($pTyr(ONb)_2$-tRNA).

It may be that C_2pTyr is simply too large to be incorporated in ribosomal protein synthesis. Sisido and coworkers have attempted to map the steric permissivity of the ribosome by investigating the incorporation efficiencies of a series of rigid, benzene-derived unnatural amino acids like pyrenylAla.[15] They developed a map, reproduced in Figure 10, of the regions of sidechain space at which bulk was and was not tolerated. C_2pTyr (pTyr(ONb)$_2$) places significant bulk at the poorly-tolerated B positions.

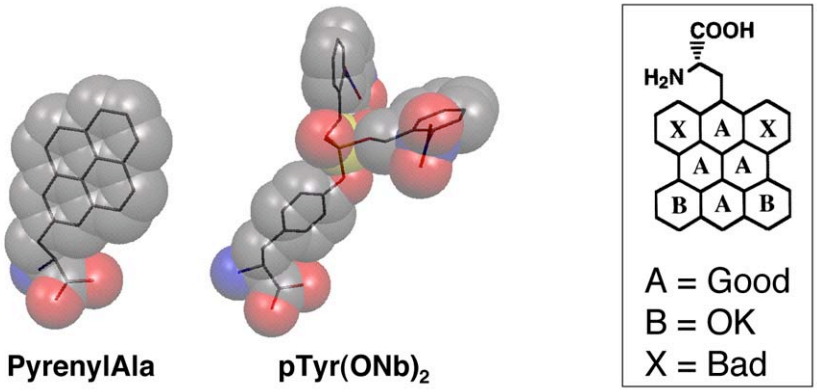

Figure 10. Steric Restrictions to Incorporation of C_2pTyr. Space-filling models of pyrenylAla and C_2pTyr (pTyr(ONb)$_2$. Map of ribosomal steric permissivity based on the data of Sisido and coworkers. PyrenylAla sidechain corresponds to the A positions.

Second Generation Studies: Singly-Caged Amino Acids

The difficulties in synthesizing the doubly caged Ser and Thr derivatives and the inefficient incorporation of the C_2pTyr led us to reconsider the use of singly caged phosphoamino acids. Since steric limitations appeared to be a problem, we began with the smallest conceivable caged phosphoamino acid, CpSer.

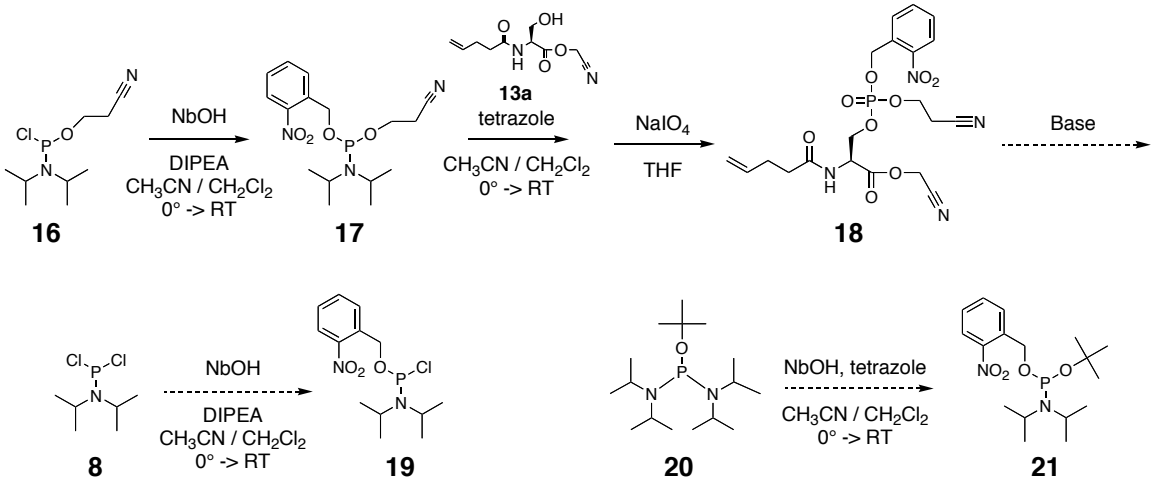

Scheme 4. Attempts to synthesize CpSer via differentially protected phosphoramidite reagents.

First, we attempted to synthesize CpSer using the differentially protected phosphoramidite reagent, **17**. However, we found that we could not cleave the cyanoethyl protecting group, common in nucleic acid syntheses, without causing β-elimination of the phospate ester. Transient, acid-labile *t*-butyl protection enables manipulation of the serine and threonine amino acid derivatives and avoids β-elimination reactions. Unfortunately, attempts to synthesize a differentially protected phosphoramidite with an acid-labile protecting group, such as **21**, were also frustrated. When monoadditions were desirable, we typically observed bis addition or none at all.

At this point, we began collaborations with the Imperiali group at MIT. They had recently developed peptides with singly caged phosphoamino acids as tools for studying cell signaling pathways.[16] Furthermore, they also wished to incorporate caged phosphoamino acids into full size proteins using suppression methods. To achieve our common goal, we combined our unnatural amino acid expertise with their experience in synthesizing these types of amino acids. In these studies, phosphoamino acid analogs with a single NPE caging moiety were strategically targeted. The Imperiali group had also experienced difficulties in selectively making mono additions to phosphoryl chlorides, but they were able to employ cyanoimidazole chemistry with phosphoramidites to achieve this. The phosphoramidite (**25**) can be synthesized from hexaethyl phosphorus triamide in a one-pot procedure, as shown in Scheme 4.

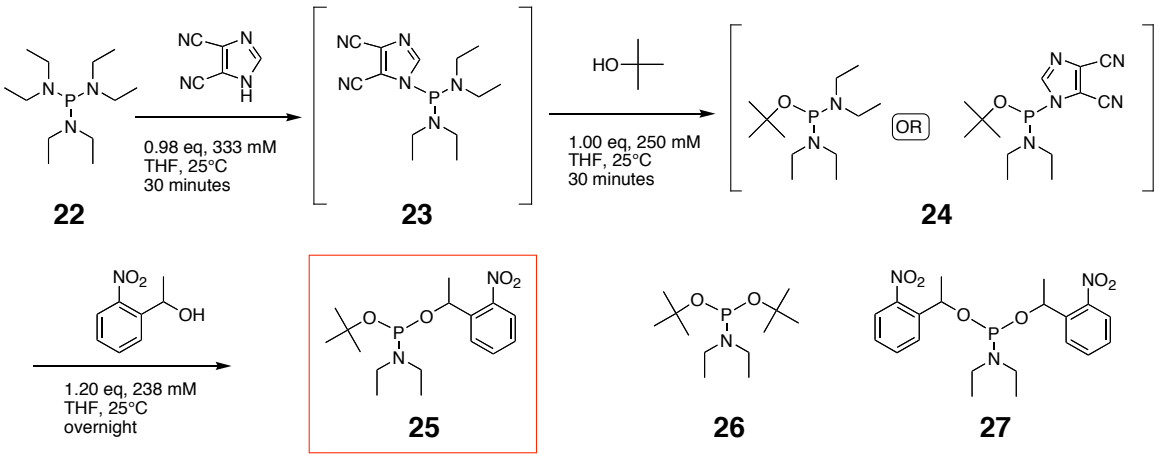

Scheme 5. Synthesis of phosphoramidite reagent for generation of singly caged phosphoamino acids.

The target amino acids such as Ser, shown as an example in Scheme 5, were synthesized as the corresponding N^{α}-4-PO-phospho(1-NPE)-cyanomethyl ester (**30**) for coupling to the dinucleotide, dCA. The CpThr cyanomethyl ester **31** was synthesized by the same route. The tyrosine derivative **32** was synthesized using a slightly modified version of the CpSer/CpThr route.

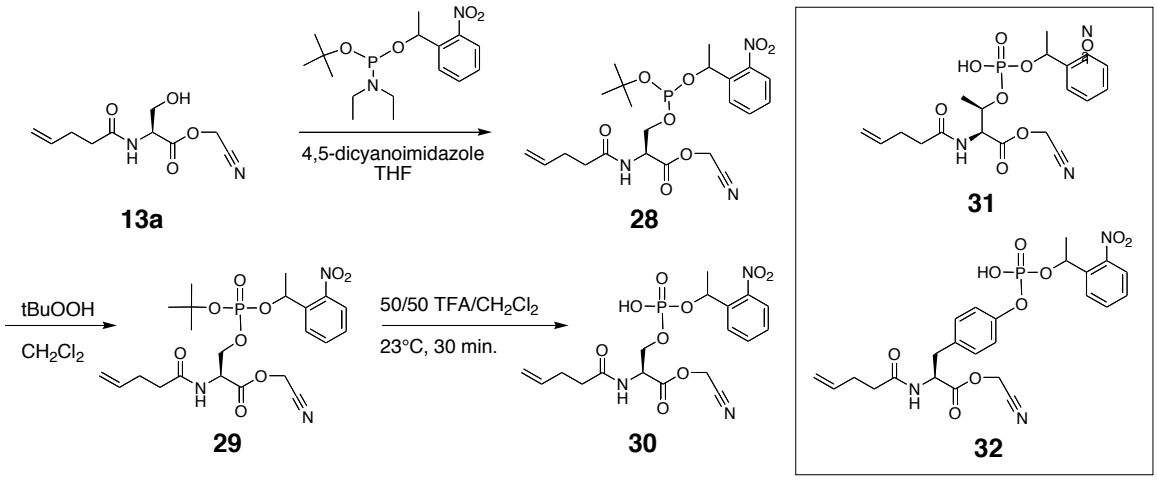

Scheme 6. Synthesis of singly caged phosphoamino acids. Serine derivative shown as an example.

30 was found to be far more stable to dCA coupling conditions than its doubly caged cousin, **14a**. In fact, **30** was too inert; although no degradation was observed after several hours, no reaction was observed, either. Solvent and salt conditions were varied, and we observed that tetrabutylammonium acetate (NBu_4OAc) salt beyond the typical 2.4 equivalents was required to achieve coupling. We believe that the additional salt aided in solubilizing the negatively charged amino acids in the presence of the negatively charged dCA. It was found that 250 mM NBu_4OAc optimally increased coupling efficiency with minimal β-elimination side reactions. These conditions were used in the dCA coupling of **31** and **32** as well.

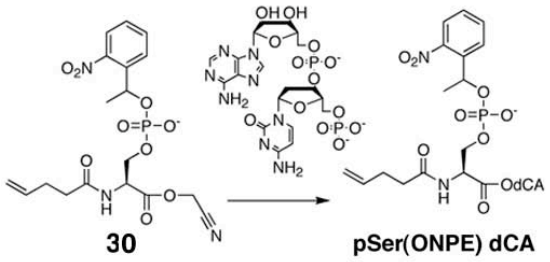

Temp (°C)	Salts (Equiv's)	Solvent	Yield (%)
25	$N(Bu)_4OAc$ (2.4)	DMF	
25	$N(Bu)_4OAc$ (2.4)	CH_3CN	
55	$N(Bu)_4OAc$ (2.4)	DMF	
25	$N(Bu)_4OAc$ (2.8)	DMF	5
25	**$N(Bu)_4OAc$ (3.2)**	**DMF**	**20**
25	$N(Bu)_4OAc$ (3.6)	DMF	10
25	LiCl	DMF	

Figure 11. Optimization of coupling of cyanomethyl ester **31** to dCA.

Next, the aminoacylated dCAs were ligated to truncated $tRNA_{CUA}$s using a slightly modified literature procedure. This gave full-length, aminoacylated tRNAs, designed to deliver the caged phosphoamino acid to a position specified by an amber (UAG) codon. Matrix-assisted laser desorption ionization mass spectrometry (MALDI MS) was used to assess, in a qualitative fashion, the success of the ligation reaction. The major peak in MALDI spectra of the ligated amino acids is the full-length, caged, phosphorylated product. Furthermore, we can observe the decaging event on the tRNA by a change in mass

consistent with the loss of a NPE upon irriation. (CpThr is shown as an example in Fig. 12) This gives us confidence that the aminoacyl tRNA species that we add to our translation mixture indeed contains the caged phosphoamino acid, and little degradation has occurred.

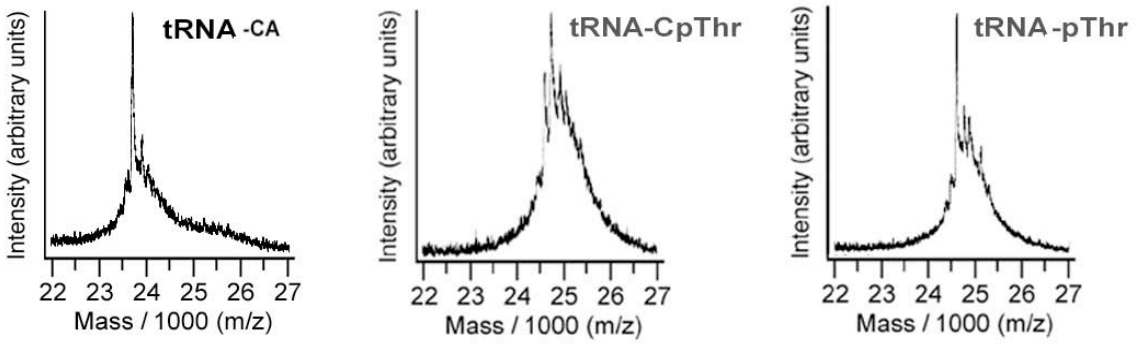

Figure 12. MALDI MS Spectra for CpThr Coupling. Truncated tRNA before ligation ($tRNA^{-CA}$), tRNA-CpThr, and irradiated tRNA-CpThr (tRNA-pThr).

With the caged, phosphoaminoacyl tRNAs in hand, the suppression efficiency of these bulky and negatively charged residues was tested in a system known to accept natural and non-natural amino acids using nonsense suppression: position 122 of the nicotinic acetylcholine receptor nAChR α-subunit.[14] The mRNA for nAChR α with an amber stop codon in position 122 was introduced into a rabbit reticulocyte lysate translation system, and the results were monitored by Western blot analysis. (Fig. 13) Uncaged, phosphorylated amino acids do incorporate, but with relatively low efficiency (Fig. 13, Lanes 4, 7, 10), consistent with earlier findings from Hecht.[7, 17] However, adding a single caging group does not further diminish suppression efficiency (Fig. 13, Lanes 3, 6, 9).

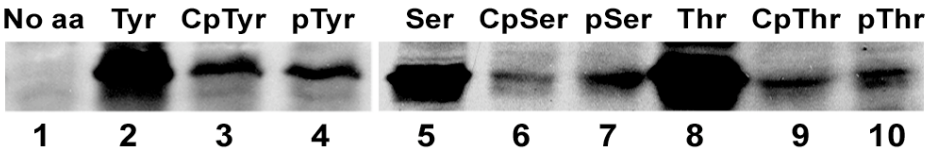

Figure 13. Test suppression in nAChR α subunit: A122TAG mRNA with $tRNA_{CUA}$ charged with amino acids listed above lanes.

The inefficient suppression may be attributable to low affinity binding of the aminoacyl tRNAs by elongation factors (i.e. EF-1A). Uhlenbeck has shown that elongation factor Tu (EF-Tu) binds tRNAs bearing negatively charged amino acids poorly, and that glutaminyl tRNAs (from which our $tRNA_{CUA}$ is derived) have a low inherent EF-Tu affinity.[18] Recall that masking this charge by doubly caging the phosphate moiety was not feasible. It resulted in far lower incorporation efficiency for tyrosine derivatives, and use of bis-caged phosphoserine and threonine was intractable due to β-elimination side reactions.

Functional Tests of Caged Phosphoamino Acids

Next, the suppression ability of the caged phosphoamino acids was needed tested in a biologically significant system relating to phospho-regulated signaling. Rather than moving directly to an ion channel study, we sought to find verify expression and functional decaging of the amino acids in a simpler, *in vitro* system. The vasodilator-stimulated phosphoprotein, VASP, is a protein of interest to the Imperiali group, one involved in cell migration processes.[19] Specifically, phosphorylation of serine 153 has been associated with cell leading edge protrusion and forward cell movement.[20] This is believed to occur by disruption of its interaction with profilin, so that while profilin is still bound to monomeric G-actin, it can no longer nucleate the formation of F-actin filaments which drive cell motility.[21] (Fig. 14) The mechanism of this is poorly understood, although phosphorylation occurs on Ser153, which lies in the EVH1 domain, profilin binds to the proline-rich domain (C-terminal to 153), and actin-polymerization occurs on the EVH2 domain.[22] VASP with CpSer153 would thus be a valuable tool for determining the precise role of this phosphoserine in the complex process of cell migration.

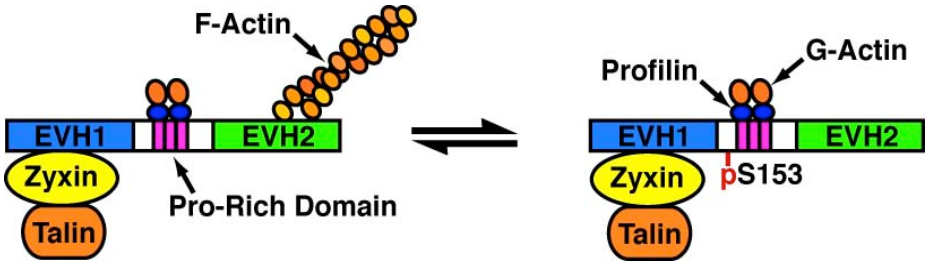

Figure 14. Schematic representation of the effect of VASP phosphorylation on actin polymerization. VASP EVH1 and 2 domains labeled, S153 phosphorylation shown, and Pro-rich domain shown in grey.

The rabbit reticulocyte mixture was highly reactive with the polyclonal anti-VASP antibody, so our VASP proteins had to be purified by His-tagging methods. For this reason, we inserted a His-tag sequence at the C-terminus of the protein, so that only full-length (suppressed) protein would be purified. Lanes 2, 5, and 8 of Figure 15 show the initial, unpurified translation mixture for wild type (unsuppressed) translation, CSer suppression, or CpSer suppression. We found that traditional imidazole purification methods were not compatible with our assays, because the imidazole was photoreactive at the wavelengths of irradiation used. A pH-based purification method was used instead in which acidification of the Ni-bead-bound proteins led to release of those proteins. Lanes 3, 6, and 9 of Figure 15 show the background proteins that were removed by washing with a buffer of intermediate pH. Lanes 4, 7, and 10, of Figure 15 show the results of our purification, after washing with low pH buffer and subsequent basification. One can see that the purification process is extremely effective in removing the background material.

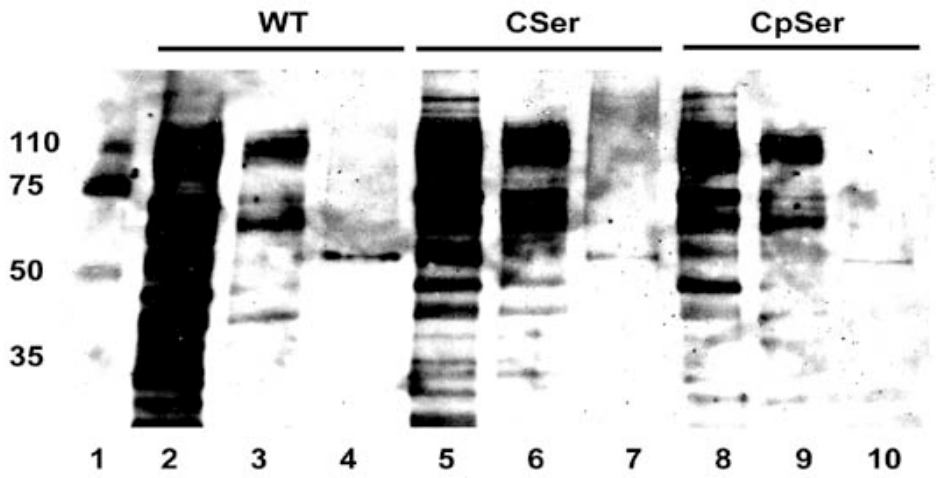

Figure 15. Suppression efficiency in VASP-S153TAG. Lanes (Left to Right): 1, Molecular Weight Markers; 2, WT translation mix, unpurified (2 μL); 3, WT Buffer C Wash (10 μL); 4, WT Buffer D elution (2 μL); 5, S153TAG mRNA and $tRNA_{CUA}$-CSer translation mix, unpurified (2 μL); 6, CSer Buffer C Wash (2 μL); 7, CSer Buffer D elution (10 μL); 8, S153TAG mRNA and $tRNA_{CUA}$-CpSer translation mix, unpurified (2 μL); 9, CpSer Buffer C Wash (2 μL); 10, CpSer Buffer D elution (10 μL).

Purified proteins (corresponding to lanes 4, 7, and 10 of Fig. 15) were used in *in vitro*, kinase, PPase, and decaging assays to test their function once suppressed in VASP. Figure 16A depicts the translation of the wild type (Ser) VASP in rabbit reticulocyte lysate (Lane A1). The VASP appears as two bands due to a gel shift caused by phosphorylation at serine 153; the shift is not caused by the increase in molecular weight, but rather by a conformational change and altered SDS binding capacity of VASP that results in decreased mobility in the SDS-PAGE analysis. This gel shift was anticipated, and was one of the reasons that VASP was chosen as a test system for our methodology; it makes it very easy to asses the results of phosphorylation or dephosphorylation.[20, 22]

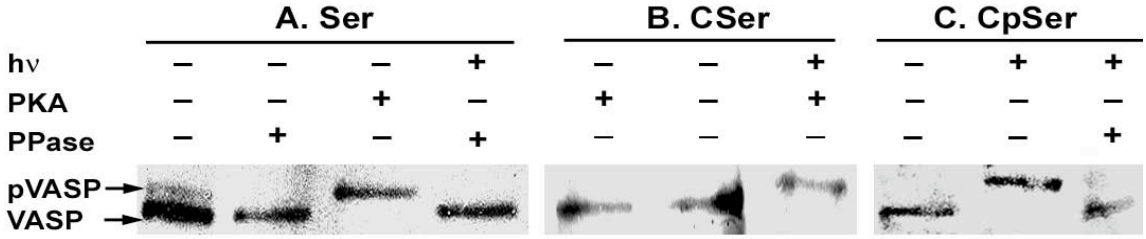

Figure 16. Suppression at VASP position 153 with CSer or CpSer. Lanes (Left to Right): A) 1, WT translation; 2, WT with λ-PPase; 3, WT with PKA; 4, WT with λ-PPase, then UV-irradiated. B) 1, CSer with PKA; 2, CSer; 3, CSer subjected to UV, then PKA. C) 1, CpSer; 2, CpSer subjected to UV; 3, CpSer subjected to UV, then λ-PPase.

In order to ascertain that the proteins produced by *in vitro* translation behave as expected, several experiments were performed. Phosphorylation of the wild type protein with protein kinase A (PKA) caused all the protein to migrate as the phospho-species (Fig.

16, Lane A3), and dephosphorylation by λ-phosphatase (λ-PPase) caused all the protein to migrate as the unphosphorylated species (Lane A2). Next, mRNA for VASP-S153TAG was suppressed with caged-serine (CSer) and the behavior of the protein product was examined (Fig. 16, B). With the caging group on the serine hydroxyl group, the full-length protein migrated as the unphosphorylated species in the presence or absence of PKA (Lanes B1 and B2, respectively). Upon uncaging with 350 nm light, the serine hydroxyl group was liberated, and subsequent phosphorylation by PKA caused the protein to migrate as the phosphorylated species (Lane B3). Next, the suppression of VASP-S153TAG mRNA with caged phosphoserine was evaluated (Figure 16, C). The full-length protein with the caged-phosphoserine migrated as the unphosphorylated species (Lane C1). The uncaged protein migrated with a shift characteristic of the phosphorylated species (Lane C2). Finally, upon uncaging and subsequent reaction with λ-PPase, the protein migrated as the unphosphorylated species (Lane C3). As a positive control, wild-type VASP (λ-PPase-treated) was irradiated under the uncaging conditions to show that this did not alter the gel mobility of the wild-type protein (Lane A4).

Conclusion

Herein is presented the chemical and biological synthesis of caged phosphoproteins using the *in vitro* nonsense suppression methodology. Although Hecht and Chamberlin have used this method for the incorporation of phosphonoserine and phosphotyrosine, this is the first report of caged phosphoamino acids (CpAAs) in proteins.[7, 17, 23] Caged phosphoproteins will allow the real time study of kinase targets with phosphorylated residues in any position of a native protein sequence. Several suppression reactions were performed in order to evaluate the ability of the native ribosomal machinery to incorporate these large and charged residues into full-length proteins. Additionally, the protein products were tested for native-like behavior in biochemical studies. Access to such caged phosphoproteins will enable studies of a large number of kinase targets in real-time. We hope to apply the set of caged amino acids and caged phosphoaminoacids to ion channels. The recent success in incorporating unnatural amino acids into an ionotropic glutamate receptor (Chapter 8) gives us hops that we may soon be able to use the tools developed here to study important phosphorylation events in learning and memory processes.

Materials and Methods

General Experimental Procedures

Many of the procedures described here were developed by Deborah Rothman and Barbara Imperiali at Massachusetts Institute of Technology. We present them here because almost all of them were repeated at Caltech as part of our collaborative effort to demonstrate incorporation of caged, phosphorylated amino acids. All starting amino acids and reagents used are commercially available, unless referenced to synthetic procedure. Dichloromethane was distilled from calcium hydride under nitrogen, and tetrahydrofuran was distilled from sodium under argon. Analytical thin-layer chromatography (TLC) was carried out on F_{254} 250-μm silica gel plates, and visualized by UV lamp. ^{1}H NMR spectra were acquired on a Bruker Avance (DPX) 400 MHz spectrometer or Varian Mercury 300 MHz spectrometer. ^{31}P NMR spectra were acquired on a Varian Mercury 300 MHz spectrometer. ^{13}C NMR spectra were acquired on a Varian Inova 500 MHz spectrometer or a Bruker Avance (DPX) 400 MHz spectrometer. Chemical shifts are reported in ppm from a standard (tetramethylsilane for ^{1}H, H_2PO_4 for ^{31}P, $CDCl_3$ for ^{13}C), and *J* values are in Hertz. High-resolution mass spectrometry was performed on a Fourier Transform Mass Spectrometer using an Electrospray Ion Source. High-performance liquid chromatography (HPLC) was performed using a Waters 600E HPLC fitted with a Waters 600 automated control module and a Waters 2487 dual wavelength absorbance detector recording at 228 and 280 nm. For analytical HPLC a Beckman Ultrasphere C_{18}, 5 μm, 4.6 x 150 mm reverse-phase column was used. For preparative separations a YMC-pack, C_{18}, 250 x 20 mm reversed phase column was used. The standard gradient for analytical and preparatory HPLC used was 93:7 to 0:100 over 35 minutes (water:acetonitrile, 0.1% TFA). Electrospray Ionization Mass Spectrometry (ESI-MS) was performed on a PerSeptive Biosystems *Mariner™ Biospectrometry Workstation* (Turbo Ion Source). All tRNAs were analyzed on a PerSeptive Biosystems (Framingham, MA) Voyager DE PRO MALDI-TOF mass spectrometer operating in linear and positive ion modes with settings as previously described.

Chemical Synthesis

The syntheses of compounds **1** to **14** were developed by Gabriel Brandt and are described in his doctoral thesis. **15a** is an intermediate in the synthesis of **14a**, which is taken on without the oxidation step described in Brandt's synthesis. Couplings of **10**, **14a**, **14b**, and **15a** to the dinucleotide pdCpA were performed according to literature precedent with the modifications to solvent and conditions shown in the table in Figure 8. The

synthesis of compound **17** has been described previously; coupling to **13a** to form **18** was analogous to the synthesis of **14a**.

***O*-1-(2-nitrophenyl)ethyl-*O'*-tertbutyl-*N,N*-diethyl phosphoramidite (25)**

To an oven dried flask with stir bar, hexaethyl phosphorus triamide (1.37 mL, 5.00 mmole) and 4,5-dicyanoimidazole (0.58 g, 4.90 mmole) are dissolved in anhydrous tetrahydrofuran (THF, 15 mL) under inert atmosphere. In an oven dried pear flask, *tert*-butyl alcohol (0.48 mL, 5.00 mmole) was dissolved in anhydrous THF (5.0 mL). In a separate oven dried pear flask, 1-2-(nitrophenyl)ethyl alcohol (1.00 g, 6.00 mmole) was dissolved in anhydrous THF (1 mL). The *t*BuOH solution was delivered to the phosphoramidite mixture via cannula, and the reaction allowed to stir at room temperature for 15 minutes, at which point, the nitrophenylethyl alcohol mixture was delivered to the reaction flask via cannula. The mixture was allowed to stir overnight, in the dark, at room temperature. The mixture was then concentrated under reduced pressure, and re-dissolved in ethyl acetate (EtOAc, 150 mL). The organic solution was washed with 20 % sodium bicarbonate ($NaHCO_3$, 2 x 150 mL) and brine (1 x 150 mL), then dried over magnesium sulfate ($MgSO_4$), filtered, and concentrated. The final product was purified by silica gel flash chromatography (98:2 Hexanes/triethylamine (NEt_3), R_f: 0.73,) to give **5** (1.27 g) in 74.0 % yield. ^{1}H NMR (300 MHz, $CDCl_3$) δ ppm: 7.92 (td, J_{HH} = 1.8 Hz, J_{HH} = 8.4 Hz, 2H), 7.65 (tt, J_{HH} = 1.5 Hz, J_{HH} = 7.5, 1H), 7.40, (tt, J_{HH} = 1.5 Hz, J_{HH} = 8.4 Hz, 1 H), 5.55 (m, 1 H), 3.06 (m, 4H), 1.57 (dd, J_{HH} = 4.5 Hz, J_{HH} = 6.3 Hz, 3H), 1.30 (d, J_{HH} = 19.5 Hz, 9H), 1.08 (dt, J_{HH} = 6.0 Hz, J_{HH} =43.5 Hz, 6 H). ^{31}P NMR (121.5 MHz, $CDCl_3$) δ ppm: 139.93, 139.16 (racemic mixture). ^{13}C NMR (125.8 MHz, $CDCl_3$) 147.9, 142.0, 133.8, 129.6, 128.2, 124.5, 75.5, 67.0, 38.3, 31.3, 25.9, 15.6. Product is not stable to MS measurements.

***N*$^{\alpha}$-4-pentenoyl-*O-tert*-butyl-L-Serine**

H-*O-tert*-butyl-L-Serine (**28**, 500 mg, 3.10 mmole) and *N,N*-diisopropylethylamine (DIPEA, 633 μL, 3.70 mmole) were dissolved in THF (30 mL) and water (30 mL). 4-pentenoic acid anhydride (676 μL, 3.70 mmole) was dissolved in THF (2 mL), and added to the serine solution. The reaction was monitored by TLC (1:1:0.01 hexanes/EtOAc/acetic acid (AcOH), R_f = 0.30), stained with iodine and ninhydrin. After the disappearance of starting material, the THF was removed under reduced pressure, and the water layer extracted with EtOAc (3 x 100 mL). The organic portions were dried over $MgSO_4$, filtered and concentrated under reduced pressure. The product was purified by silica gel flash chromatography (827 mg) in 93.7 % yield. ^{1}H NMR (300 MHz, $CDCl_3$) δ ppm: 6.99 (d, J_{HH} = 8.1 Hz, 1 H), 5.70 (m, 1 H), 4.94 (q, J_{HH} = 17.1, 10.2, 10.2 Hz, 2 H), 4.64 (m, 1 H), 3.71 (dd, J_{HH} = 9 Hz, J_{HH} = 3 Hz, 1 H), 3.46 (dd, J_{HH} = 9.3 Hz, J_{HH} =3 Hz, 1 H), 2.25 (s, 4

H), 0.99 (s, 9 H). ^{13}C NMR (125.8 MHz, $CDCl_3$) δ ppm: 176.0, 173.9, 136.7, 115.8, 73.7, 61.9, 53.0, 35.3, 29.7, 27.3. ESI-MS: $[M-H]^-$ 242.1401 (obsd), 242.1398 (calcd).

N^{α}-4-pentenoyl-*O*-*tert*-butyl-L-Serine cyanomethyl ester

N^{α}-4-pentenoyl-*O*-*tert*-butyl-L-Serine (825 mg, 3.39 mmole) was dissolved in chloroacetonitrile (644 μL, 10.20 mmole), and cooled to 0°C, stirring, under argon. Diazabicyclo[5.4.0]undec-7-ene (DBU, 507 μL, 3.39 mmole) was slowly added to the stirring mixture. The reaction was allowed to warm to room temperature, and stirred overnight under argon. The reaction mixture was diluted with EtOAc (150 mL), washed with water (2 x 150 mL), then brine (1 x 150 mL), dried over $MgSO_4$, filtered and concentrated (1:1 hexanes/EtOAc, R_f = 0.41) (765 mg, 79.9 %). ^{1}H NMR (300 MHz, $CDCl_3$) δ ppm: 6.81 (d, J_{HH} = 8.7 Hz, 1 H), 5.83 (m, 1 H), 5.11 (q, J_{HH} = 18.3, 6.6, 9.9 Hz, 2 H), 4.84 (m, 3 H), 3.86 (dd, J_{HH} = 9.3 Hz, J_{HH} = 3.3 Hz, 1 H), 3.58 (dd, J_{HH} = 9.3 Hz, J_{HH} = 3.3, 1 H), 2.38 (s, 4 H), 1.16 (s, 9 H). ^{13}C NMR (125.8 MHz, $CDCl_3$) δ ppm: 172.7, 169.6, 137.1, 115.7, 114.5, 73.8, 61.9, 52.7, 49.2, 35.2, 29.5, 27.3. ESI-MS: $[MNa]^+$ 305.1478 (obsd), 305.1472 (calcd).

N^{α}-4-pentenoyl-L-Serine cyanomethyl ester (29)

N^{α}-4-pentenoyl-*O*-*tert*-butyl-L-Serine cyanomethyl ester (750 mg, 2.69 mmole) was dissolved in an ice-cold solution of triflouroacetic acid (TFA) with 1 % (v/v) triisopropylsilane (TIS). The reaction was stirred at 0°C for 4 hours, and determined complete by TLC (EtOAc, R_f = 0.43). The reaction mixture was poured into ice-cold saturated $NaHCO_3$ (250 mL) and EtOAc (120 mL). The organic layer was washed with saturated $NaHCO_3$ (3 x 100 mL), then brine (1 x 100 mL), dried over $MgSO_4$, filtered, and concentrated under reduced pressure. The mixture was purified by silica gel flash chromatography to give the product (156 mg) in 25.6 % yield. ^{1}H NMR (300 MHz, $CDCl_3$) δ ppm: 6.90 (d, J_{HH} = 7.8 Hz, 1 H), 5.87 (m, 1 H), 5.10 (t, J_{HH} = 19.5, 10.8 Hz, 2 H), 4.80 (d, J_{HH} = 1.5 Hz, 3 H), 4.70 (m, 1 H), 4.06 (dd, J_{HH} = 11.7 Hz, J_{HH} = 3.6, 3.3 Hz, 1 H), 3.87 (dd, J_{HH} = 11.4 Hz, J_{HH} = 3.6, 3.6 Hz, 1 H), 2.38 (d, J_{HH} = 3.0 Hz, 4 H). ^{13}C NMR (125.8 MHz, $CDCl_3$) δ ppm: 173.5, 169.8, 137.0, 116.4, 114.5, 63.0, 54.6, 49.7, 35.8, 29.8. ESI-MS: $[MNa]^+$ 249.0847 (obsd), 249.0846 (calcd).

N^{α}-4-pentenoyl-phospho(1-nitrophenylethyl-2-*tert*-butyl)-L-Serine cyanomethyl ester (30)

N^{α}-4-pentenoyl-L-Serine cyanomethyl ester (**29**, 150 mg, 663 μmole) was dissolved in anhydrous THF (2.0 mL), in a round bottom flask fitted with an oven dried stir bar under argon. In a separate pear flask, *O*-1-(2-nitrophenyl)ethyl-*O'*-*tert*butyl-*N,N*-diethyl phosphoramidite (**25**, 340 mg, 995 μmole) and 4,5-dicyanoimidazole (157 mg, 1.33 mmole)

were dissolved in anhydrous THF (1.3 mL), and kept dark. The phosphoramidite solution was delivered to the serine solution via syringe, and the reaction was allowed to stir overnight, under argon, in the dark. The reaction was judged complete by loss of starting material by TLC. The mixture was concentrated under reduced pressure, and redissolved in EtOAc (50 mL). The organic layer was washed with 10 % $NaHCO_3$ (2 x 80 mL), brine (1 x 80 mL), then dried over sodium sulfate (Na_2SO_4), decanted and concentrated. The phosphite mixture was then oxidized with *tert*-butyl hydroperoxide (*t*BuOOH, 266 μL of 5 M solution in decane, 1.33 mmole) in dichloromethane (CH_2Cl_2, 10 mL) for one hour, in the dark. The mixture was diluted with CH_2Cl_2 (50 mL), and washed with 10 % $NaHCO_3$ (2 x 80 mL) and brine (1 x 80 mL), then dried over $MgSO_4$, filtered and concentrated. The product was partially purified by silica gel flash chromatography (1:2 hex/EtOAc, R_f = 0.26), and carried on to the next step before final purification (68.2 %).

N^{α}-4-pentenoyl-phospho(1-nitrophenylethyl)-L-Serine cyanomethyl ester (31)

N^{α}-4-pentenoyl-phospho(1-nitrophenylethyl-2-*tert*-butyl)-L-Serine cyanomethyl ester (**30**, 69 mg, 135 μmole) was dissolved in acetonitrile (MeCN, 4.0 mL) at room temperature, stirred, and kept dark. A solution of TFA (1.0 mL) with Triisopropyl silane (50 μL) was added to the solution, and stirred for 10 minutes at room temperature. The mixture was then poured into ice-cold saturated $NaHCO_3$ (4.0 mL). The product mixture was purified by reversed phase HPLC. (93:7 to 0:100 water/MeCN/0.1 % TFA, over 35 minutes, R_t = 22.68 min) in 99 % yield (61.0 mg). ^{1}H NMR (300 MHz, $CDCl_3$) δ ppm: 8.00 (ddd, J_{HH} = 8.1 Hz, J_{HH} = 3.6, 3.6 Hz, J_{HH} = 1.5, 1.2, 1.2, 1.5 Hz, 1 H), 7.79 (m, 2 H), 7.53 (m, 1 H), 6.04 (m, 1 H), 5.86 (m, 1 H), 5.11 (m, 2 H), 4.88 (m, 3 H), 4.40 (m, 3 H), 2.40 (d, J_{HH} = 7.5 Hz, 4 H), 1.71 (dd, J_{HH} = 6.3 Hz, J_{HH} = 1.2, 1.2 Hz, 3 H). ^{13}C NMR (125.8 MHz, $CDCl_3$) δ ppm: 173.7, 168.3, 147.3, 137.5, 137.0, 134.6, 129.5, 128.2, 125.0, 116.3, 114.2, 73.3, 67.2, 52.8, 50.1, 35.5, 29.7, 24.7. ^{31}P (121.5 MHz, $CDCl_3$): -1.382. ESI-MS: $[M-H]^-$ 454.1017 (obsd), 454.1021 (calcd).

N^{α}-4-pentenoyl-*O*-*tert*-butyl-L-Threonine

H-*O*-*tert*-butyl-L-Threonine (500 mg, 2.85 mmole) and DIPEA (683 μL, 3.99 mmole) were dissolved in THF (40 mL) and water (10 mL). 4-pentenoic acid anhydride (730 μL, 3.99 mmole) was dissolved in THF (5 mL), and added to the threonine solution. The reaction was monitored by TLC (1:1:0.01 hexanes/EtOAc/AcOH, R_f = 0.31), stained with iodine and ninhydrin. After the disappearance of starting material, the mixture was concentrated under reduced pressure, and the product was purified by silica gel flash chromatography (625 mg, 85.3 %). ^{1}H NMR (300 MHz, $CDCl_3$) δ ppm: 6.74 (d, J_{HH} = 8.4 Hz, 1 H), 5.88 (m, 1 H), 5.12 (q, J_{HH} = 17.4, 8.1, 10.2 Hz, 2 H), 4.60 (dd, J_{HH} = 8.7 Hz, J_{HH} = 2.7, 2.4 Hz, 1 H), 4.32

(m, 1 H), 2.43 (m, 4 H), 1.20 (s, 9 H), 1.71 (d, J_{HH} = 6.6 Hz, 3 H). ^{13}C NMR (125.8 MHz, $CDCl_3$) δ ppm: 174.3, 174.0, 136.9, 116.0, 75.2, 67.2, 57.7, 35.6, 29.7, 28.4, 20.1. ESI-MS: $[M-H]^-$ 256.1551 (obsd), 256.1554 (calcd).

N^{α}-4-pentenoyl-*O-tert*-butyl-L-Threonine cyanomethyl ester

N^{α}-4-pentenoyl-*O-tert*-butyl-L-Threonine (390 mg, 1.51 mmole) was dissolved in chloroacetonitrile (478 μL, 7.55 mmole) and cooled to 0°C, stirring, under argon. DBU (226 μL, 1.51 mmole) was slowly added to the stirring mixture. The reaction was allowed to warm to room temperature, and stirred overnight under argon. The reaction mixture was diluted with EtOAc (100 mL), washed with water (2 x 100 mL) and brine (1 x 100 mL), then dried over $MgSO_4$, filtered and concentrated (1:1 hexanes/EtOAc, R_f = 0.43) (321 mg, 71.7 %). ^{1}H NMR (300 MHz, $CDCl_3$) δ ppm: 6.39 (d, J_{HH} = 9.0 Hz, 1 H), 5.91 (m, 1 H), 5.14 (q, J_{HH} = 17.1, 7.5, 10.2 Hz, 2 H), 4.78 (d, J_{HH} = 3.0 Hz, 2 H), 4.61 (dd, J_{HH} = 9.3 Hz, J_{HH} = 2.1, 1.8 Hz, 1 H), 4.27 (m, 1 H), 2.42 (d, J_{HH} = 2.7 Hz, 4 H), 1.21 (d, J_{HH} = 6.3 Hz, 3 H), 1.14 (s, 9H). ^{13}C NMR (125.8 MHz, $CDCl_3$) δ ppm: 173.1, 169.9, 137.1, 115.9, 114.3, 74.5, 67.2, 57.7, 49.1, 35.5, 29.5, 28.6, 21.0. ESI-MS: $[MNa]^+$ 319.1617 (obsd), 319.1628 (calcd).

N^{α}-4-pentenoyl-L-Threonine cyanomethyl ester

N^{α}-4-pentenoyl-*O-tert*-butyl-L-Threonine cyanomethyl ester (315 mg, 1.06 mmole) was dissolved in an ice-cold solution of TFA with 1 % (v/v) TIS. The reaction was stirred at 0°C for two hours, and determined complete by TLC (1:1 hex/EtOAc, R_f = 0.15). The reaction mixture was poured into ice-cold saturated $NaHCO_3$ (80 mL) and EtOAc (80 mL). The organic layer was washed with saturated $NaHCO_3$ (2 x 80 mL) and brine (1 x 80 mL), then dried over $MgSO_4$, filtered, and concentrated under reduced pressure. The mixture was purified by silica gel flash chromatography to give the product (150 mg) in 59.0 % yield. ^{1}H NMR (300 MHz, $CDCl_3$) δ ppm: 6.39 (d, J_{HH} = 8.4 Hz, 1 H), 5.90 (m, 1 H), 5.14 (t, J_{HH} = 17.4, 13.8 Hz, 2 H), 4.87 (q, J_{HH} = 15.6, 7.5, 15.6 Hz, 2 H), 4.69 (dd, J_{HH} = 9.0 Hz, J_{HH} = 2.7, 2.4 Hz, 1 H), 4.46 (qd, J_{HH} = 6.3, 6.3, 6.3 Hz, J_{HH} = 2.4, 2.4, 2.4, 2.4 Hz, 1 H), 2.43 (d, J_{HH} = 2.7 Hz, 4 H), 1.27 (t, J_{HH} = 4.2, 2.1 Hz, 3 H). ^{13}C NMR (125.8 MHz, $CDCl_3$) δ ppm: 173.7, 170.2, 137.1, 116.4, 114.5, 68.0, 57.5, 49.6, 36.0, 29.8, 20.6. ESI-MS: $[MNa]^+$ 263.1005 (obsd), 263.1002 (calcd).

N^{α}-4-pentenoyl-phospho(1-nitrophenylethyl-2-*tert*-butyl)-L-Threonine cyanomethyl ester

N^{α}-4-pentenoyl-L-Threonine cyanomethyl ester (140 mg, 582 μmole) was dissolved in anhydrous THF (2 mL), in a round bottom flask fitted with an oven dried stir bar under argon. In a separate pear flask, *O*-1-(2-nitrophenyl)ethyl-*O'-tert*butyl-*N,N*-diethyl

phosphoramidite (**25**, 299 mg, 874 μmole) and 4,5-dicyanoimidazole (137 mg, 1.16 mmole) were dissolved in anhydrous THF (1 mL), and kept dark. The phosphoramidite solution was delivered to the threonine solution via syringe, and the reaction was allowed to stir overnight, under argon, in the dark. The reaction was judged complete by loss of starting material by TLC. The mixture was concentrated under reduced pressure, and re-dissolved in EtOAc (80 mL). The organic layer was washed with 10 % $NaHCO_3$ (2 x 80 mL), brine (1 x 80 mL), then dried over Na_2SO_4, decanted and concentrated. The phosphite mixture was then oxidized with *t*BuOOH (232 μL of 5 M solution in decane, 1.16 mmole) in dichloromethane (CH_2Cl_2, 10 mL) for one hour, in the dark. The mixture was diluted with CH_2Cl_2 (70 mL), and washed with 10 % $NaHCO_3$ (2 x 80 mL), brine (1 x 80 mL), then dried over $MgSO_4$, filtered and concentrated The product was partially purified by silica gel flash chromatography (R_f = 0.19, 1:1 hex/EtOAc) and carried on to the next step before final purification (70.1 %).

N^{α}-4-pentenoyl-phospho(1-nitrophenylethyl)-L-Threonine cyanomethyl ester

N^{α}-4-pentenoyl-phospho(1-nitrophenylethyl-2-*tert*-butyl)-L-Threonine cyanomethyl ester (250 mg, 476 μmole) was dissolved in MeCN (3.5 mL) at room temperature, stirring, and kept dark. A solution of TFA (3.5 mL) with TIS (70 μL) was added to the solution, and stirred for 15 minutes at room temperature. The mixture was then poured into ice-cold saturated $NaHCO_3$ (10 mL). The mixture was purified by reversed phase HPLC (93:7 to 0:100 water/acetonitrile/0.1 % TFA over 35 minutes, R_t = 23.86 min) in 41.0 % yield (92.0 mg). ^{1}H NMR (300 MHz, $CDCl_3$) δ ppm: 8.00 (d, J_{HH} = 7,=.8 Hz, 1 H), 7.79 (m, 2 H), 7.55 (m, 1 H), 6.89 (t, J_{HH} = 7.2, 9.0 Hz, 1 H), 6.53 (bs, 1 H), 6.05 (m, 1 H), 5.87 (m, 1 H), 5.13 (m, 2 H), 4.92 (m, 6 H), 2.42 (d, J_{HH} = 2.1 Hz, 4 H), 1.74 (d, J_{HH} = 6.3 Hz, 3 H), 1.35 (dd, J_{HH} = 24.0 Hz, J_{HH} = 6.3, 6.6 Hz, 3 H). ^{13}C NMR (125.8 MHz, $CDCl_3$) δ ppm: 174.8, 169.1, 147.8, 137.6, 137.0, 134.7, 129.8, 128.5, 125.2, 116.8, 114.5, 75.8, 73.7, 56.6, 50.5, 35.9, 30.1, 24.9, 19.2. ^{31}P (121.5 MHz, $CDCl_3$): -1.13, -1.17. ESI-MS: $[M-H]^-$ 468.1168 (obsd), 468.1177 (calcd).

N^{α}-4-pentenoyl-L-Tyrosine *tert*-butyl ester

H-L-Tyrosine-*tert*-butyl ester (475 mg, 2.0 mmol) was dissolved in anhydrous THF (15 mL) and anhydrous CH_2Cl_2 (5 mL). DIPEA (975 μL, 6.0 mmol) was added, and pentenoic acid anhydride (440 μL, 2.4 mmol) was added dropwise to the resulting mixture. The reaction mixture was stirred at room temperature for 45 minutes and then concentrated under reduced pressure. The clear oil was purified by silica gel flash chromatography (R_f = 0.70, 2:3 hex/EtOAc) to give the desired product as a clear oil (568 mg, 89%). ^{1}H-NMR (400 MHz, $CDCl_3$, δ): 1.42 (s, 9H), 2.0-2.3 (m, 4H), 2.9-3.0 (m, 2H), 4.71 (dd, 1H, J_1 = 7.6

Hz, J_{HH} = 6.2 Hz), 4.94-5.01 (m, 2H), 5.67-5.77 (m, 1H), 6.42 (d, 1H, J_{HH} = 7.9 Hz), 6.77 (d, 2H, J_{HH} = 8.3 Hz), 6.97 (d, 2H, J_{HH} = 8.3 Hz), 8.28 (s, 1H). ^{13}C-NMR (100.6 MHz, $CDCl_3$, δ): 172.9, 171.8, 155.8, 136.5, 130.4, 126.8, 115.9, 115.5, 82.6, 53.9, 37.2, 35.6, 29.4, 27.8. ESI-MS: $[M+H]^+$ 320.1855 (obsd), 320.1862 (calcd).

N^{α}-4-pentenoyl-phospho(1-nitrophenylethyl-2-cyanoethyl)-L-Tyrosine *tert*-butyl ester

N^{α}-4-pentenoyl-L-Tyrosine *tert*-butyl ester (1.13 g, 3.55 mmol) was placed in an oven dried round bottom flask with molecular sieves and dissolved in anhydrous THF (10 mL). In a separate flask, *N,N*-Diisopropyl-1-nitrophenylethyl-2-cyanoethyl phosphoramidite (1.95 g, 5.32 mmol) was dissolved in anhydrous THF (12 mL) and activated with *1H*-tetrazole (373 mg, 5.32 mmol) for 10 minutes. The resulting mixture was then added dropwise to the tyrosine solution. The reaction was stirred overnight at room temperature in the dark. The mixture was filtered over celite and concentrated under reduced pressure, then re-dissolved in CH_2Cl_2 (75 mL), washed with 1% aqueous $NaHCO_3$ (2 x 40 mL), dried over Na_2SO_4, decanted and concentrated. The phosphite resdiue was then dissolved in anhydrous CH_2Cl_2 (20 mL) and *tBu*OOH (800 μL, 6M solution in decane) was added dropwise. After 35 minutes, the reaction mixture was diluted with 30 mL CH_2Cl_2, washed with 1% aqueous $NaHCO_3$ (2 x 30 mL), then dried with Na_2SO_4, decanted and concentrated. The resulting pale yellow oil was purified by silica gel flash chromatography (R_f = 0.50, 2:3 hex/EtOAc) to give the product as a clear oil (1.64 g, 77.0 %). ^{1}H-NMR (400 MHz, $CDCl_3$, δ): 1.32 (s, 9H), 1.64 (dd, 3H, J_{HH} = 6.3 Hz, J_{HH} = 13.6 Hz), 2.16-2.26 (m, 4H), 2.54-2.59 (m, 2H), 2.90-3.00 (m, 2H), 4.11-4.20 (m, 2H), 4.51-4.66 (m, 1H), 4.86-4.95 (m, 2H), 5.20-5.40 (m, 1H), 6.2-6.3 (m, 1H), 6.5-6.65 (m, 1H), 6.90-7.07 (m, 4H), 7.36-7.45 (m, 1H), 7.55-7.73 (m, 2H), 7.89 (d, 1H, J_{HH} = 8.2 Hz). ^{13}C-NMR (100.6 MHz, $CDCl_3$, δ): 171.9, 170.5, 148.8, 146.6, 136.8, 133.9, 130.8, 128.9, 127.5, 124.4, 119.6, 119.5, 115.4, 82.2, 77.4, 73.6, 62.5, 53.3, 37.1, 35.2, 29.3, 27.8, 24.1, 24.0, 19.4. ESI-MS: $[M+H]^+$ 602.1304 (obsd), 602.2267 (calcd).

N^{α}-4-pentenoyl-phospho(1-nitrophenylethyl)-L-Tyrosine *tert*-butyl ester

N^{α}-4-pentenoyl-phospho(1-nitrophenylethyl-2-cyanoethyl)-L-Tyrosine *tert*-butyl ester (400 mg, 0.66 mmol) was dissolved in methanol (MeOH, 15 mL) and potassium hydroxide (KOH, 1.3 mL of stock solution 34 mg/mL in water, 0.79 mmol) was added. After 10 minutes, TLC (R_f = 0.30, 1:10:90 Et_3N/MeOH/CH_2Cl_2) shows that the starting material has been consumed. The reaction mixture was poured into water (150 mL) with brine (50 mL) and acidified with HCl to pH ~ 1. The product was extracted with EtOAc (2 x 50 mL). The combined organic layers were dried over Na_2SO_4, decanted, and concentrated

under reduced pressure to give the desired product as a white solid in quantitative yield. No further purification was necessary. ^{1}H-NMR (400 MHz, $CDCl_3$, δ): 1.38 (s, 9H), 1.63 (dd, 3H, J_{HH} = 2.7 Hz, J_{HH} = 3.5 Hz), 2.24-2.32 (m, 4H), 2.95-3.03 (m, 2H), 4.68 (br s, 1H), 4.96 (dd, J_{HH} = 1.4 Hz, J_2 = 10.2 Hz),), 4.99 (dd, J_{HH} = 1.5 Hz, J_{HH} = 17.1 Hz), 5.70-5.78 (m, 1H), 6.08 (q, 1H, J_{HH} = 6.3 Hz), 6.27 (br s, 1H), 6.94-7.01 (m, 4H), 7.40 (t, 1H, J_{HH} = 8.1 Hz), 7.59 (t, 1H, J_{HH} = 7.5 Hz), 7.74 (dd, 1H, J_{HH} = 1.0 Hz, J_{HH} = 7.9 Hz), 7.93 (td, 1H, J_{HH} = 1.5 Hz, J_{HH} = 8.2 Hz), 10.85 (br s, 1H). ^{13}C-NMR (100.6 MHz, $CDCl_3$, δ): 172.5, 170.7, 149.6, 146.6, 137.9, 136.9, 134.1, 133.1, 130.8, 128.7, 128.0, 124.5, 120.0, 115.9, 82.8, 73.1, 53.7, 37.5, 35.5, 29.5, 28.1, 24.5. ESI-MS: $[M+H]^+$ 549.1981 (obsd), 549.1996 (calcd).

N^{α}-4-pentenoyl-phospho(1-nitrophenylethyl)-L-Tyrosine cyanomethyl ester

N^{α}-4-pentenoyl-phospho(1-nitrophenylethyl)-L-Tyrosine *tert*-butyl ester (400 mg, 0.81 mmol) was dissolved in anhydrous CH_2Cl_2 (10 mL) and the resulting solution was cooled to 0 °C. TFA (10 mL) was slowly added to the reaction mixture, and the solution was stirred in the dark at 0 °C for 30 minutes, and then at room temperature for another 30 minutes. The reaction mixture was concentrated under reduced pressure, then re-dissolved in CH_2Cl_2 and concentrated three times to remove the TFA. The resulting residue was dissolved in chloroacetonitrile (1 mL, 15.8 mmol), and DBU (607 μL, 4.06 mmol) was added dropwise over the mixture; the reaction was allowed to stir in the dark overnight. The reaction mixture was then diluted with EtOAc (50 mL) and washed with a mixture of water (50 mL), brine (150 mL) and 6M HCl (2 mL). The combined organic layers were dried over Na_2SO_4, decanted, and concentrated under reduced pressure to give a dark brown oil that was purified by reversed phase HPLC to give the desired product as a sticky solid in 47.0 % yield (201 mg, 95:5 to 5:95 water/acetonitrile/0.1%TFA over 30 minutes, R_t = 22.50 min). ^{1}H-NMR (400 MHz, $CDCl_3$, δ): 1.65 (dd, 3H, J_{HH} = 5.2 Hz, J_{HH} = 0.86 Hz), 2.29 (s, 4H), 2.96, 3.12 (m, 2H), 4.97 (d, 2H, J_{HH} = 1.1 Hz), 4.98 (dd, 2H, J_{HH} = 26 Hz, J_{HH} = 1.0 Hz), 5.64-5.79 (m, 1H), 6.06 (q, 1H, J_{HH} = 6.6), 6.72 (br s, 1H), 6.96-6.99 (m, 4H), 7.42 (td, 1H, J_{HH} = 7.7 Hz, J_{HH} = 1.3 Hz), 7.61 (td, 1H, 7.6 Hz, J_{HH} = 0.95 Hz), 7.76 (dd, 1H, J_{HH} = 7.8, J_{HH} = 0.97), 7.92 (d, 1H, J_{HH} = 8.2 Hz), 10.4 (br s, 1H). ^{13}C-NMR (100.6 MHz, $CDCl_3$, δ): 174.1, 170.1, 150.0, 146.7, 137.8, 136.4, 134.2, 132.1, 130.6, 128.9, 128.1, 124.5, 120.5, 116.2, 114.1, 73.0, 53.4, 49.2, 36.7, 35.1, 29.4, 24.5. ESI-MS: $[M+H]^+$ 532.1477 (obsd), 532.1485 (calcd).

Coupling to pdCpA

pdCpA was synthesized as previously reported. In general, the coupling reactions were performed on a 20 to 50 μmole scale; additionally, the pdCpA (1.2 equivalents), N^{α}-4-

pentenoyl-phospho(1-nitrophenylethyl)-L-Serine, -Threonine, or -Tyrosine cyanomethyl ester (1.0 equivalents), and tetrabutylammonium acetate (NBu_4OAc) were dried under vacuum before use. A 250 mM solution of NBu_4OAc was made in anhydrous *N,N*-dimethylformamide (DMF). The pdCpA was dissolved to 130 mM concentration with the NBu_4OAc solution, and kept under inert atmosphere. This mixture was then added to the amino acid ester, and kept dark under inert atmosphere. The reaction was monitored by analytical reversed phase HPLC. When the amino acid ester was consumed, the reaction was quenched with 2:1 water/MeCN with 0.1 % TFA (1.5 to 2.0 mL, or ~12 mM final concentration of product). The product was purified by reversed phase HPLC (93:7 to 0:100 water/MeCN/0.1 % TFA over 35 minutes) and confirmed by ESI-TOF MS. pdCpA-4PO-cpSer, R_t = 23.23 min, $[MNa]^+$ 1059.0, $[MNaH]^{2+}$ 530.0 (obsd), 1057.7, 529.3 (calcd); pdCpA-4PO-cpThr, R_t = 23.40 min, $[MNa]^+$ 1072.9, $[MH]^+$ 1049.0 (obsd), 1072.7, 1049.7 (calcd). pdCpA-4PO-cpTyr, R_t = 25.80 min, $[MH]^+$ 1111.2, $[M+2H]^{2+}$ 556.1 (obsd), 1111.0, 556.0 (calcd).

Biochemical Synthesis and Molecular Biology

Ligation to $tRNA_{CUA}^{-CA}$

$tRNA_{CUA}^{-CA}$ was transcribed from linearized DNA as previously reported and stored in diethyl pyrocarbonate (DEPC) treated water at – 80 °C. Ligations were performed as published with two changes: the ligation scale was increased 1.5-fold, and the following desalting step was added. After redissolution in 20 μL 1mM NaOAc, pH 4.5, aminoacyl-$tRNA_{CUA}$ samples were desalted using BD Biosciences CHROMA SPIN-30 DEPC H2O columns (following manufacturer's instructions). The desalted samples were quantified using UV A_{260}, confirmed by MALDI-TOF MS on 3-hyroxypicolinic acid (3-HPA) matrix, and stored at – 80 °C.

$tRNA_{CUA}$CpSer: $[MH]^+$ 24, 732 (obsd), 24, 734 (calcd).
$tRNA_{CUA}$CpThr: $[MH]^+$ 24, 755 (obsd), 24, 748 (calcd).
$tRNA_{CUA}$CpTyr: $[MH]^+$ 24, 807 (obsd), 24, 810 (calcd).

Calculated masses based on external BSA calibration, and internal referencing to 74 base $tRNA_{CUA}^{-CA}$ (23, 716) and 76 base $tRNA_{CUA}$ (24, 334). Other tRNAs produced as previously described.

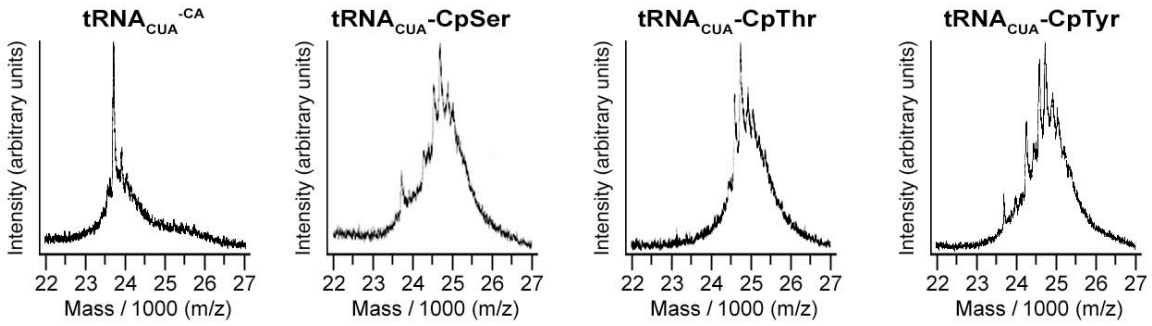

Figure 17. MALDI-TOF MS of $tRNA_{CUA}$.

VASP-WT and –S153TAG constructs

The VASP gene was received from the Gertler Lab (Massachusetts Institute of Technology) in a pBS-KSII vector with an upstream T5 promoter. The site-specific mutagenesis was performed following the Stratagene QuikChange protocol and the following primers: sense 5'-GAG CGC CGG GTC TAG AAT GCA GGA GGC CC; antisense 5'-GGG CCT CCT GCA TTC TAG ACC CGG CGC TC. Several colonies were selected, DNA was purified the by standard procedure, and submitted for sequencing; one sample with the correct sequence was kept for further use.

Both the WT and S153TAG VASP genes were amplified from the pBS-KSII vectors using PCR with *Pfu* Turbo Polymerase and the following primers: forward 5'-C ACC ATG ACG GAG ACG GTC; reverse 5'-AGG AGA ACC CCG CTT CCT CAG. The products were purified by agarose gel electrophoresis and stored at -20 °C. The PCR products were then used in the TOPO directional cloning reaction as described by the manufacturer (Invitrogen, TOPO Directional Cloning: pcDNA3.1/V5-His). Several colonies were selected and plasmid DNA purified by standard procedure. The DNA was screened by a single restriction enzyme digest: Sal I will cut the empty vector into two pieces, 2.3 and 3.2 kb in length, while it will cut the pcDNA/VASP vectors into two pieces, 2.1 and 4.4 kb in length. Several samples with the insert were submitted for sequencing, and one of each plasmid sample with the correct sequence was stored at –20 °C for future use.

mRNA run-off transcription

Plasmid DNA of WT and S153TAG VASP was amplified in DH5α cells using standard protocol. Approximately 100 μg of each plasmid were linearized with PmeI (cuts immediately downstream of the C-terminal His-tag). Linearized DNA was purified by agarose gel electrophoresis followed by PCI extraction, ethanol preceipitation, and re-dissolving in DEPC water. Run-off transcription of the genes was performed using the T7 mMessage mMachine Kit (Ambion) and following manufacturer protocol. The mRNA was

purified by PCI extraction and stored at –80 °C. Analysis by gloxal/agaorse gel confirmed the correct size of the transcripts. nAChR transcripts were run off as previously described.

Aminoacyl-tRNA$_{CUA}$ Deprotection

6-nitroveratryloxycarbonyl- (NVOC) protected aminoacyl-tRNA$_{CUA}$s (1 μg/μL) were deprotected by 5 minutes of irradiation with a 1000 W Hg/Xe arc lamp (Oriel, Stratford, CT) operating at 400 W equipped with WG-335 and UG-11 filters (Schott, Elmsford, NY). 4-pentenoyl- (4PO) protected aminoacyl-tRNA$_{CUA}$s were deprotected by a 10 minute incubation with 1 equivalent fresh saturated I_2 in H_2O. 4PO-protected aminoacyl-tRNA$_{CUA}$s are stored at 2 μg/μL; the final concentration is 1 μg/μL after I_2 treatment.

***In Vitro* Translation**

In vitro protein synthesis was carried out using the Promega (Madison, WI) rabbit reticulocyte lysate translation kit according to the manufacturer's instructions. For nAChR translations, the following reagents were combined and incubated for 1 hour at 30 °C: 1.5 μL DEPC H_2O, 0.75 μL complete amino acids (1mM), 0.5 μL Roche (Basel, Switzerland) RNAse inhibitor, 4 μL deprotected aminoacyl-tRNA$_{CUA}$ (suppression: 1 μg/μL) or DEPC H_2O (unsuppressed), 1 μL mRNA (nAChR-HA-WT: 1.0 μg/μL, nAChR-HA-122TAG: 0.1 μg/μL), and 16.25 μL lysate. For VASP translations, the following reagents were combined and incubated for 3 hours at 30 °C: 10 μL DEPC H_2O, 6 μL complete amino acids (1mM), 4 μL Roche (Basel, Switzerland) RNAse inhibitor, 32 μL deprotected aminoacyl-tRNA$_{CUA}$ (suppression: 1 μg/μL) or DEPC H_2O (unsuppressed), 8 μL mRNA (VASP-WT: 1.0 μg/μL, VASP-S153TAG: 0.1 μg/μL), and 140 μL lysate.

Ni-NTA Purification of His-Tagged Proteins

The following buffers were used in the purification and concentration of His-tagged VASP proteins:

Buffer A: 100 mM NaH_2PO_4, 2% SDS, 2 mM β-mercaptoethanol, pH 8.0
Buffer B: 50 mM NaH_2PO_4, 150 mM NaCl, 2 mM β-mercaptoethanol, pH 8.0
Buffer C: 50 mM NaH_2PO_4, 150 mM NaCl, 2 mM β-mercaptoethanol, pH 7.0
Buffer D: 50 mM NaH_2PO_4, 150 mM NaCl, 2 mM β-mercaptoethanol, pH 4.5
Buffer E: 50 mM NaH_2PO_4, 150 mM NaCl, 2 mM β-mercaptoethanol, 1X BSA, pH 7.0.

400 μL Qiagen Ni-NTA Superflow (Valencia, CA) were washed three times with 400 μL Buffer B. 200 μL translation mix was combined with 400 μL Buffer A, added to the beads, and rocked at room temperature for two hours. The beads were washed four times with 400 μL Buffer C. 400 μL Buffer D was added to beads, which were rocked for

two hours at room temperature. Buffer D was removed from the beads, another 400 μL Buffer D was added, and the beads were rocked at room temperature for two hours. Buffer D elutions were combined.

Three Millipore (Billerica, MA) Ultrafree MC Biomax (30 kDa NMWL) centricon columns were used per translation for concentrating solutions, one for loading Buffer A, one for Buffer C washes, and one for Buffer D elutions. Columns were blocked for 2 hours at room temperature with Buffer E, which was removed by pipetting. 2 X 400 μL Buffer B were added to each column and removed by pipetting (removes excess BSA). Loading Buffer A, Buffer C washes, and Buffer D elutions were added to the columns and concentrated by centrifuging the columns at 4000 x *g* until their respective volumes were reduced to 40 μL. Buffer B was used to dilute the concentrated Buffer A, Buffer C, and Buffer D solutions to 100 μL (final pH ~6.6). Samples stored at –80 °C. Concentrated Buffer D solutions are hereafter referred to as VASP-WT (unsuppressed) or Suppressed VASP.

λ–PPase Treatment

λ-PPase dephosphorylation of murine VASP Ser153 is well-precedented. Dephosphorylation was performed with New England Biolabs (Beverley, MA) Lambda Protein Phosphatase (λ-PPase), according to the manufacturer's instructions. VASP samples (WT: 2 μL, Suppressed: 10 μL) were dissolved in sterile H_2O to a total volume of 15.5 μL. 2 μL 20 mM $MnCl_2$, 2 μL λ-PPase Buffer, and 0.5 μL λ-PPase enzyme were added to a total volume of 20 μL. This mixture was incubated 0.5 hours at 30°C and stored at -80°C.

PKA treatment

PKA phosphorylation of murine VASP Ser153 is well-precedented. Phosphorylation was performed with New England Biolabs cAMP-dependent Protein Kinase (PKA), according to the manufacturer's instructions. VASP samples (WT: 2 μL, Suppressed: 10 μL) were dissolved in sterile H_2O to a total volume of 15.5 μL. 2 μL 10 mM ATP, 2 μL PKA Buffer, and 0.5 μL PKA enzyme were added to a total volume of 20 μL. This mixture was incubated 0.5 hours at 30°C and stored at -80°C.

Caging Group Photolysis

Irradiation of the His-Tag purified VASP samples was performed with the arc lamp assembly described above (Aminoacyl-$tRNA_{CUA}$ Deprotection). WT samples were treated with λ-PPase as described above; after dephosphorylation the 20 μL sample was irradiated for 5 minutes at room temperature. CSer and CpSer samples were diluted with sterile H_2O to a total volume of 15.5 μL, irradiated for 5 minutes at room temperature, and then treated with PKA or λ-PPase (respectively) as described above.

nAChR PAGE Analysis

PAGE samples were prepared by mixing 10 μL of unpurified rabbit reticulocyte translation mix with 4 μL 6X SDS gel loading buffer and diluting to a total volume of 24 μL. Samples were run at 150 V on a 10% polyacrylamide Readygel (BioRad, Hercules, CA) in 1X Tris/Glycine/SDS buffer (10X stock from BioRad). Protein was transferred to nitrocellulose membrane, which was blocked with 5% milk in 1 X PBS (Irvine Scientific, Santa Ana, CA) with 0.1 % (v/v) Tween 20 (Sigma-Aldrich) for 1 hour. The blot was labeled with mouse anti-HA epitope primary antibody (Covance Research Products, Grand Rapids, MI) for 1 hour at a 1:3000 dilution in the 5% milk solution. After washing 3 times 1 X PBS + 0.1 % (v/v) Tween 20, the membrane was labeled for 1 hour with horse radish peroxidase-conjugated goat anti-mouse secondary antibody (Jackson Immunoresearch Laboratories, West Grove, PA). The blot was washed 3 times 1 X PBS + 0.1 % (v/v) Tween 20 and developed with Supersignal West Pico chemiluminescence reagents from Pierce (Rockford, IL) on Amersham (Buckinghamshire, England) Hyperfilm.

VASP PAGE Analysis

PAGE samples were prepared by mixing 4 μL 6X SDS gel loading buffer with one of the following: 2 μL of unpurified rabbit reticulocyte translation mix; 10 μL concentrated loading Buffer A, wash Buffer C, or elution Buffer D; 20 μL enzymatically-treated VASP. The final samples were diluted to 24 µL. Samples were run at 150 V on a 12% polyacrylamide Readygel (BioRad) in Tris/Glycine/SDS. Protein was transferred to nitrocellulose membrane, which was blocked with 5% BSA (minimum 96%, Sigma-Aldrich, St. Louis, MO) in 1 X PBS with 0.1 % (v/v) Tween 20 for 1 hour. The blot was labeled with rabbit anti-VASP primary antibody (a gift from the Gertler lab, Massachusetts Institute of Technology) for 1 hour at a 1:3000 dilution in the 5% BSA solution. After washing 3 times 1 X PBS + 0.1 % (v/v) Tween 20, the membrane was labeled for 1 hour with horse radish peroxidase-conjugated goat anti-rabbit secondary antibody (Upstate, Charlottesville, VA). The blot was washed 3 times 1 X PBS + 0.1 % (v/v) Tween 20 and developed as above.

Primary Data

The original PAGE gels that are summarized in Figure 16 are presented below. These were produced according to the VASP PAGE gel protocol above. The regions included in Figure 16 are boxed.

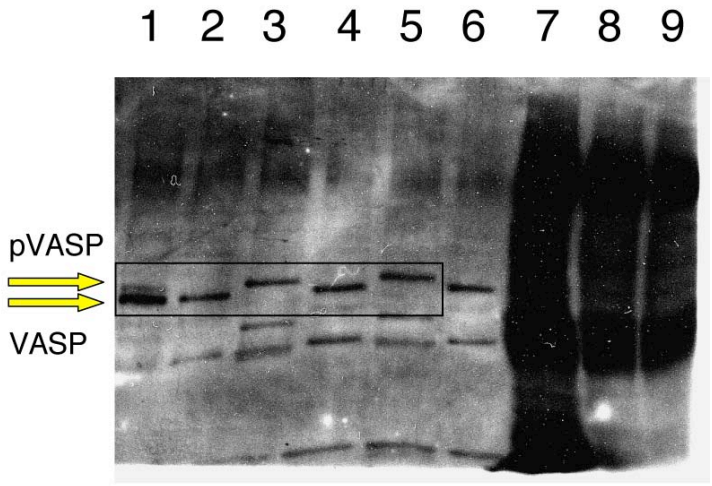

Figure 18. Test of Irradiation Effects on WT VASP. Lanes (Left to Right): 1, WT translation; 2, WT with λ-PPase; 3, WT with PKA; 4, WT with λ-PPase, then UV-irradiated; 5, WT with PKA, then UV-irradiated; 6, WT with λ-PPase, then UV-irradiated; 7-9 Unpurified translation mixes.

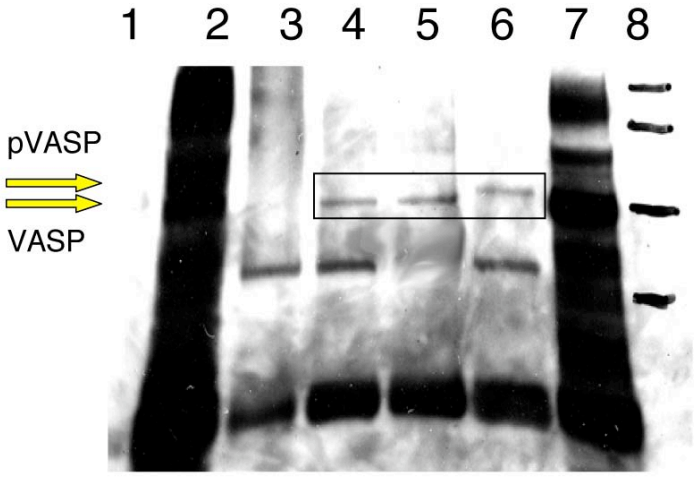

Figure 19. Test of CSer Decaging and Phosphorylation. Suppression at VASP position 153 with CSer. 1, Blank; 2, Unpurified translation mix; 3, PKA in Buffer D, irradiated; 4, CSer with PKA; 5, CSer; 6, CSer subjected to UV, then PKA. 7, Unpurified translation mix, 8, Molecular Weight Markers.

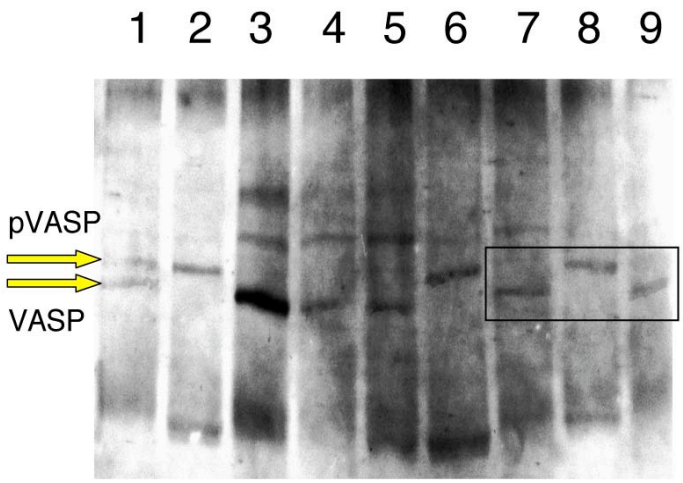

Figure 20. Suppression at VASP position 153 with CSer or CpSer. Lanes (Left to Right): 1, WT translation; 2, WT with λ-PPase; 3, WT with PKA; 4, CSer 5, CSer with PKA; 6, CSer subjected to UV, then PKA. 7, CpSer; 8, CpSer subjected to UV; 9, CpSer subjected to UV, then λ-PPase.

References

(1) Manning, G.; Whyte, D. B.; Martinez, R.; Hunter, T.; Sudarsanam, S., *Science* **2002,** 298, 1912-1916.

(2) Woodgett, J. R., *Protein Kinase Functions*. 2nd ed.; Oxford, 2000.

(3) Marriott, G.; Ottl, J.; Heidecker, M.; Gabriel, D., *Methods Enzymol*. **1998,** 291, 95-116.

(4) Marriott, G., Ed.; "Caged Compounds." *Methods Enzymol*.; Academic Press, San Diego, CA, 1998; Vol. 291.

(5) Adams, S. R.; Tsien, R. Y., *Annu. Rev. Physiol*. **1993,** 55, 755-784.

(6) Petersson, E. J.; Brandt, G. S.; Zacharias, N. M.; Dougherty, D. A.; Lester, H. A., *Methods Enzymol*. **2003,** 360, 258-273.

(7) Short, G. F.; Laikhter, A. L.; Lodder, M.; Shayo, Y.; Arslan, T.; Hecht, S. M., *Biochem*. **2000,** 39, 8768-8781.

(8) Miller, J. C.; Silverman, S. K.; England, P. M.; Dougherty, D. A.; Lester, H. A., *Neuron* **1998,** 20, 619-624.

(9) Philipson, K. P.; Gallivan, J. P.; Brandt, G. S.; Dougherty, D. A.; Lester, H. A., *Am. J. Physiol.: Cell Physiol*. **2001,** 281, C195.

(10) Holmes, C. P., *J. Org. Chem*. **1997,** 1997, 2370-2380.

(11) Tong, Y.; Brandt, G. S.; Li, M.; Shapovalov, G.; Slimko, E.; Karschin, A.; Dougherty, D. A.; Lester, H. A., *J. Gen. Physiol*. **2001,** 117, 103-118.

(12) Brandt, G. S. Ph.D. Thesis. California Institute of Technology, 2002.

(13) Gallivan, J. P., Lester, H. A., Dougherty, D. A., *Chem. Biol*. **1997,** 4, 739-749.

(14) England, P. M.; Lester, H. A.; Dougherty, D. A., *Biochem*. **1999,** 38, 14409-14415.

(15) Hohsaka, T.; Kajihara, D.; Ashizuka, Y.; Murakami, H.; Sisido, M., *J. Am. Chem. Soc*. **1999,** 121, 34-40.

(16) Nguyen, A., Rothman, D. M., Stehn, J., Yaffe, M. B., Imperiali, B., *Nat. Biotechnol*. **2004,** 22, 993-1000 Rothman, D. M., Vazquez, M.E., Vogel, E.M., Imperiali, B., *Org. Lett*. **2002,** 4, 2865-2868 Rothman, D. M., Vazquez, M.E., Vogel, E.M., Imperiali, B., *J. Org. Chem*. **2003,** 68, 6795-6798.

(17) Arslan, T.; Mamaev, S. V.; Mamaeva, N. V.; Hecht, S. M., *J. Am. Chem. Soc*. **1997,** 119, 10877-10887.

(18) Dale, T.; Sanderson, L. E.; Uhlenbeck, O. C., *Biochem*. **2004,** 43, 6159-6166.

(19) Krause, M., Bear, J. E., Loureiro, J. J., Gertler, F. B., *J. Cell Sci*. **2002,** 115, 4721-4726 Krause, M., Dent, E. W., Bear, J. E., Loureiro, J. J., Gertler, F. B., *Ann. Rev. Cell Develop. Biol*. **2003,** 19, 541-564.

(20) Butt, E., Abel, K., Krieger, M., Palm, D., Hoppe, V., Hoppe, J., Walter, U., *J. Biol. Chem*. **1994,** 269, 14509-14517.

(21) Harbeck, B.; Huttelmaier, S.; Schluter, K.; Jockusch, B. M.; Illenberger, S., *J. Biol. Chem*. **2000,** 275, 30817-30825.

(22) Lambrechts, A.; Kwiatkowski, A. V.; Lanier, L. M.; Bear, J. E.; Vandekerckhove, J.; Ampe, C.; Gertler, F. B., *J. Biol. Chem.* **2000,** 275, 36143-36151.

(23) Bain, J. D.; Wacker, D. A.; Kuo, E. E.; Chamberlin, A. R., *Tetrahedron* **1991,** 47, 2389-2400.

Supporting Information

We present the following supporting information to help describe elctrophysiological experiments done in combination with caging group photolysis in this chapter and in Chapter 10. It is adapted from an invited review in *Methods in Enzymology*, written with Gabriel Brandt and Niki Zacharias.[1]

Incorporating caged unnatural amino acids makes it possible to photochemically control a broad range of processes, from protein folding to protein-protein interactions, to ligand binding. We have expressed several receptors containing photodeprotectable unnatural amino acids in *Xenopus* oocytes, permitting *in vivo* electrophysiological studies. Caged tyrosine was incorporated in place of an endogenous tyrosine to cage the binding site of the mouse muscle nicotinic acetylcholine receptor (nAChR).[2] Flash photolysis permitted recovery of the nAChR's response to acetylcholine. The pore of the same ion channel has been caged by incorporating *o*-nitrobenzyl (Nb) cysteine and tyrosine in pore-lining segments of the receptor.[3] Photochemical initiation of protein trafficking was demonstrated by decaging a *o*-Nb tyrosine on the inward rectifier potassium channel Kir2.1.[4] Revealing the tyrosine hydroxyl group permitted recognition by endocytotic machinery.

The above examples are provided to give an idea of the scope of experiments that are possible with caged unnatural amino acids in conjunction with electrophysiology. We will focus here on receptor-based expression methodology and assays. Once one has chosen a protein of interest and a residue within that protein, one must pick a photolabile protecting group for the side-chain (Figure 1A) and an orthogonal (i.e. non-photochemical) protecting group for the a-amine of the amino acid (Figure 1B). This is necessary for coupling the amino acid to the pdCpA dinucleotide prior to enzymatic ligation to form the full length suppressor tRNA. Following expression of the protein in *Xenopus* oocytes, the decaging can be done in a variety of manners; we will describe two, one of which permits real-time electrophysiological monitoring. Thorough descriptions of *in vivo* nonsense suppression methodology are available elsewhere,[5, 6] therefore we will focus on the techniques that apply specifically to using caged unnatural amino acids in this context.

Figure 1. Protecting Groups for Use with Unnatural Amino Acids. A. Photolytic side-chain caging groups: **1a** Nitrobenzyl (Nb),[7,] **1b** Nitroveratryl (Nv),[7] **2a** Nitroveratryloxycarbonyl (NVOC),[7, 8] **2b** Nitromandelyloxycarbonyl(NMOC),[7, 9] **3** Dinitrobenzyl,[10, 11] **4** 3-Nitrobenzyl,[12] **5** Phenacyl,[13, 14] **6** Desyl,[10, 13, 15] **7** Cinnamoyl,[16] **8** Coumarinyl.[17] B. Non-photolytic a-amino protecting groups: **9a** 4-Pentenoyl (4-PO),[18, 19] **9b** 2,2-Dimethyl-4-pentenoyl,[18] **10** Allyloxycarbonyl (Alloc),[20] **11** N-Benzyl-N-phenylfluorenyl-2-amino-4-pentenoyl,[21] **12** Pyroglutamoyl,[22] **13** Biphenylisopropoxycarbonyl (Bpoc),[23,24] **14** (9-Fluorenylmethyloxy)carbonyl (Fmoc),[23] **15***t*-Butyloxycarbonyl (Boc),[23] **16** Benzyloxycarbonyl (Cbz).[23]

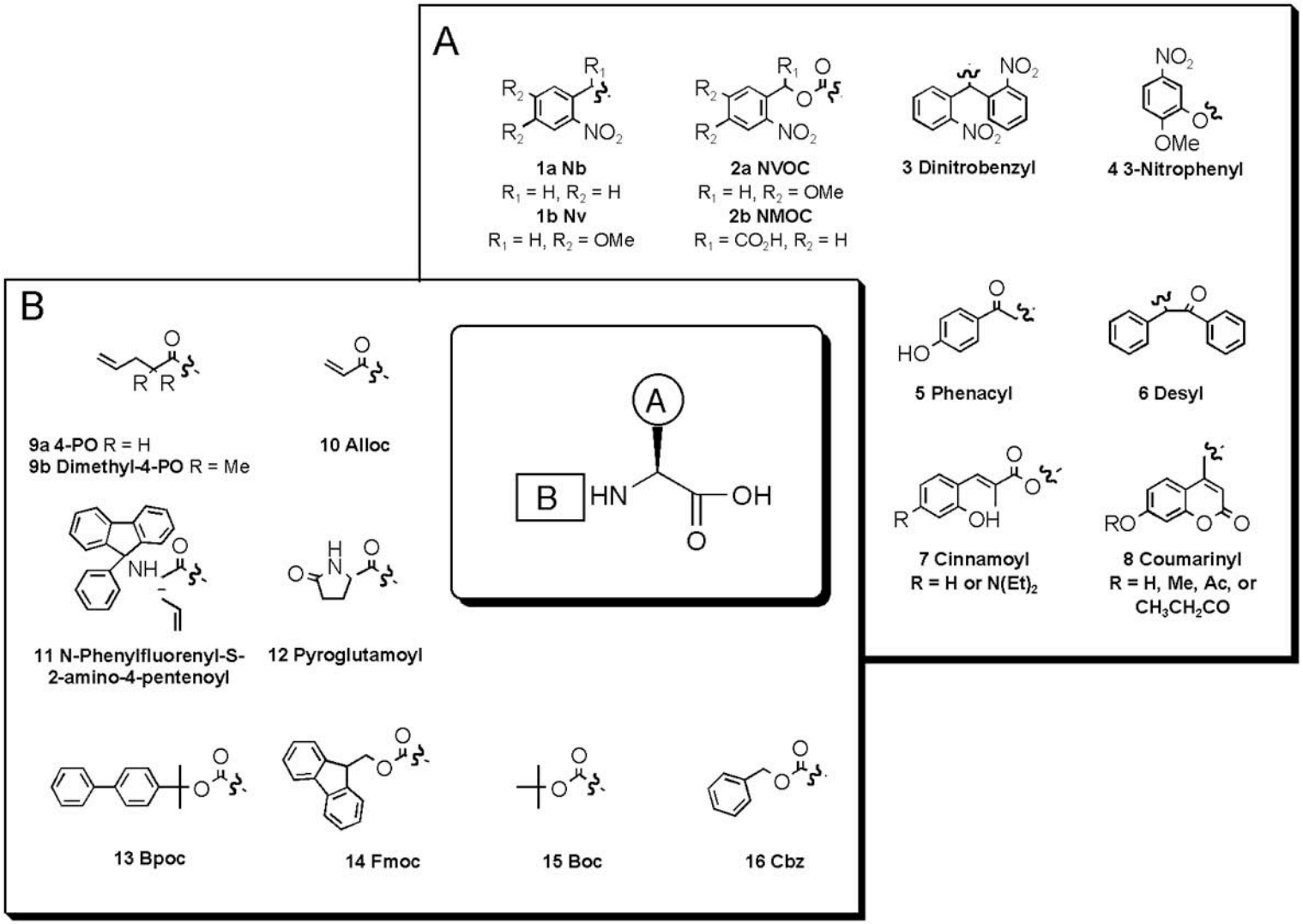

Figure 1. Protecting Groups. **A.** Photolytic side-chain caging groups **B.** Non-photolytic α-amine protecting groups.

Experimental Protocols

We describe here minimal protocols relevant to nonsense suppression. The following section then deals with aspects of the suppression methodology that are specific to introducing photolabile amino acids. The reader should consult the earlier methods papers for guidelines on implementing unnatural amino acid mutagenesis in general.[25 5, 26, 27] Here we outline a procedure for suppression of *amber* codons in ion channels expressed in *Xenopus* oocytes.

Injection of $tRNA_{CUA}$ and mRNA Into Oocytes

Oocytes are co-injected with *N*-deprotected aminoacyl $tRNA_{CUA}$ plus mRNA as follows. Typically, tRNA charged with an enantiomerically pure amino acid protected with the iodine-labile 4PO group is resuspended at 2 μg/μL. Immediately prior to injection, it is combined for ten minutes with an equal volume (typically 0.5 μL) of saturated aqueous iodine. The 1 μL of de-protected aminoacyl tRNA is then mixed with an equal volume (1 μL) of mRNA in water. For a multi-subunit receptor, such as the nAChR, the suppressed subunit is usually present in some excess over the wild-type subunits. For instance, suppression in the a subunit is often carried out at a subunit ratio of 10:1:1:1 (α:β:γ:δ) and a total mRNA concentration of 4.0 ng in 25 nL. Given a 50 nL oocyte injection, each cell thus receives 25 ng tRNA and 25 ng mRNA. Positive and negative control oocytes from the same batch are also injected. Negative controls include injection of mRNA without $tRNA_{CUA}$ and injection of mRNA with $tRNA_{CUA}$ that has not been synthetically aminoacylated. As a positive control, tRNA aminoacylated with the wild-type residue is injected along with the mRNA. The oocytes are incubated at 18 °C with shaking in ND96 medium supplemented with sodium pyruvate, theophylline, Gentamycin sulfate, and 5% heat-inactivated horse serum. Typically, expression may be observed after 24 hours and is maximal by 48 hours post-injection.

Electrophysiology

Oocytes are assayed in an electrophysiological apparatus designed for simultaneous irradiation and recording (Fig. 2).[2] In a typical experiment, the oocyte is held at the desired membrane potential in a standard two-electrode voltage clamp setup and assayed for expression of the receptor.[4] The pre-photolysis record is used to determine the effect, if any, of the presence of the unnatural amino acid and its caging group on receptor function. Optimally, recording continues during the irradiation, so that rate-limiting steps can be monitored. In favorable cases, the decaging proceeds so efficiently that the light is delivered as a flash, briefer than activation of the channels (Miller *et al.*, 1998; Philipson *et al.*, 2001).[2, 3] In other cases, the rate-limiting step is delivery of the light itself (several s to several hrs.). It is not practical to record voltage-clamp currents from an oocyte for periods

longer than tens of min. Therefore, for longer irradiations, photocleavage of the caging group is not done on the electrophysiology rig. Naturally, the control oocytes injected above are subject to the identical procedure.

Where desired, oocytes may be utilized in biochemical assays subsequent to or in addition to electrophysiologial recording. Oocytes have been subjected to a full range of modern physiological measurements, such as simultaneous fluroescence and voltage-clamp, modification by cysteine reagents, and electrochemistry; and these techniques are also available for oocytes expressing proteins with caged side chains.

Experimental Considerations

Receptor

Suppression has been demonstrated in the major classes of neuroreceptors and ion channels. Unnatural amino acids have been incorporated into a number of ligand-gated channels, such as the nAChR (numerous subunits) and 5-HT_3 receptors, a G-protein-coupled receptor (NK1), GIRKs, and several potassium channels including Kir2.1 and Shaker.[2, 4, 28-30] In unpublished work from our lab, we have incorporated unnatural amino acids into CFTR, a P2X receptor, a neurotransmitter transporter, and the NMDA receptor (Chapter 8). Among these are monomeric and multimeric receptors, both homomeric and heteromeric versions of the latter. We emphasize that heterologous expression of any novel protein is by no means guaranteed, since it is uncertain whether the protein will be folded, assembled, or transported properly. However, our experience suggests that any protein that can be expressed effectively in *Xenopus* oocytes will be amenable to incorporation of unnatural amino acids by nonsense suppression.

Site of Incorporation

Based on our experience to date, there is considerable freedom in choosing a suppression site. Unnatural amino acids have been incorporated in extracellular domains,[2, 30, 31] in transmembrane regions,[3, 32] and in intracellular loops.[4, 29] Sites have been suppressed successfully near both the N- and C-termini and in regions with a variety of secondary structures. However, suppression efficiency is variable, and clear rules have yet to be established for predicting whether suppression will work well at any given site.

Caging groups

The choice of caged sidechain depends, of course, on the exact nature of the information to be gained from the experiment. The literature contains precedents for caged sidechain hydroxyls (Tyr[2-4] and Ser[33]), thiols (Cys[3]), acids (Asp[19, 34]), amines (β-aminoalanine[24]) and amides,[29] in which backbone cleavage can be seen as photolytic "decaging" of the peptide bond). As mentioned above, the suppression efficiency of an

unnatural amino acid is related to the nature of its sidechain, but in a complex fashion. Most investigators have employed relatively small caging groups, because the charged tRNA must pass through the ribosome in order for the amino acid to be incorporated into the receptor. As will be discussed further below, it is difficult to predict whether one will encounter problems in incorporating a particular amino acid. Workers in the field have generally reported that steric and especially charge conservation of the native sidechain help promote efficient expression. In practice, there is no substitute for simply attempting the suppression at the desired position with the desired unnatural amino acid.

The only caging groups precedented for unnatural amino acid suppression prior to the work described in Chapter 7 are nitrobenzyl (Nb, **1a**)[2-4, 19, 24, 29, 33, 34] and nitroveratryl (Nv, **1b**).[19] Other groups also have very attractive photochemical properties (Fig. 1A). It remains to be seen whether or not these groups can be incorporated by nonsense suppression. There are several considerations in choosing a caging group: 1) synthetic characteristics: the degree to which it is synthetically accessible and compatible with coupling to pdCpA; 2) photochemical characteristics: its action spectrum, quantum yield for photolysis, and speed of the dark reactions that complete photolysis; and 3) reactivity in the system of interest: its stability in water, and the possible reactivity of its photoproducts.

The α-amino group of the unnatural amino acid must also be protected for the coupling to pdCpA. Conventionally, this is done with a nitroveratryloxycarbonyl (NVOC (**2a**, Fig. 2A) group. However, since this group requires photochemical deprotection, NVOC is not compatible with the introduction of caged side chains. While it is theoretically possible to use photocleavable protecting groups with non-overlapping action spectra, this is not recommended as several a-amino protecting groups that are cleavable chemically or enzymatically (pyroglutamoyl, **12**)[22] are available. These are illustrated in Figure 1B. We have primarily used the 4-PO (**9a**)[3, 4, 18, 21, 29, 35] group. but all of the others have been used successfully in suppression experiments. 4-PO is removed by mixing the aminoacyl-tRNA with 25% (v/v) saturated I_2 in water prior to oocyte injection.

Figure 2. Real Time Electrophysiological Monitoring of Protein Decaging. Apparatus for simultaneous irradiation and electrophysiological recording from *Xenopus* oocytes The output of the arc lamp (in this case, a flashlamp) is passed through a 300 - 350 nm bandpass filter and focused onto a fiber optic liquid light guide. When continuous illumination is used, the beam is also passed through a water filter to eliminate IR. The light guide directs the beam onto the oocyte, which is clamped in a standard two-electrode configuration. A concave mirror can be moved into position above the bath, reflecting some of the beam that has passed around the oocyte back to the shadowed upper surface. The mirror increases the overall flash intensity by ~55%. The inset depicts the photolytic decaging of a Tyr(NB) incorporated into the pore-lining M2 region of the mouse nAChR g subunit. The electrophysiological trace below shows that removal of the caging group increases acetylcholine (ACh) -induced current in the ion channel. Electrophysiological data reproduced from Philipson *et al.*, 2001.[3]

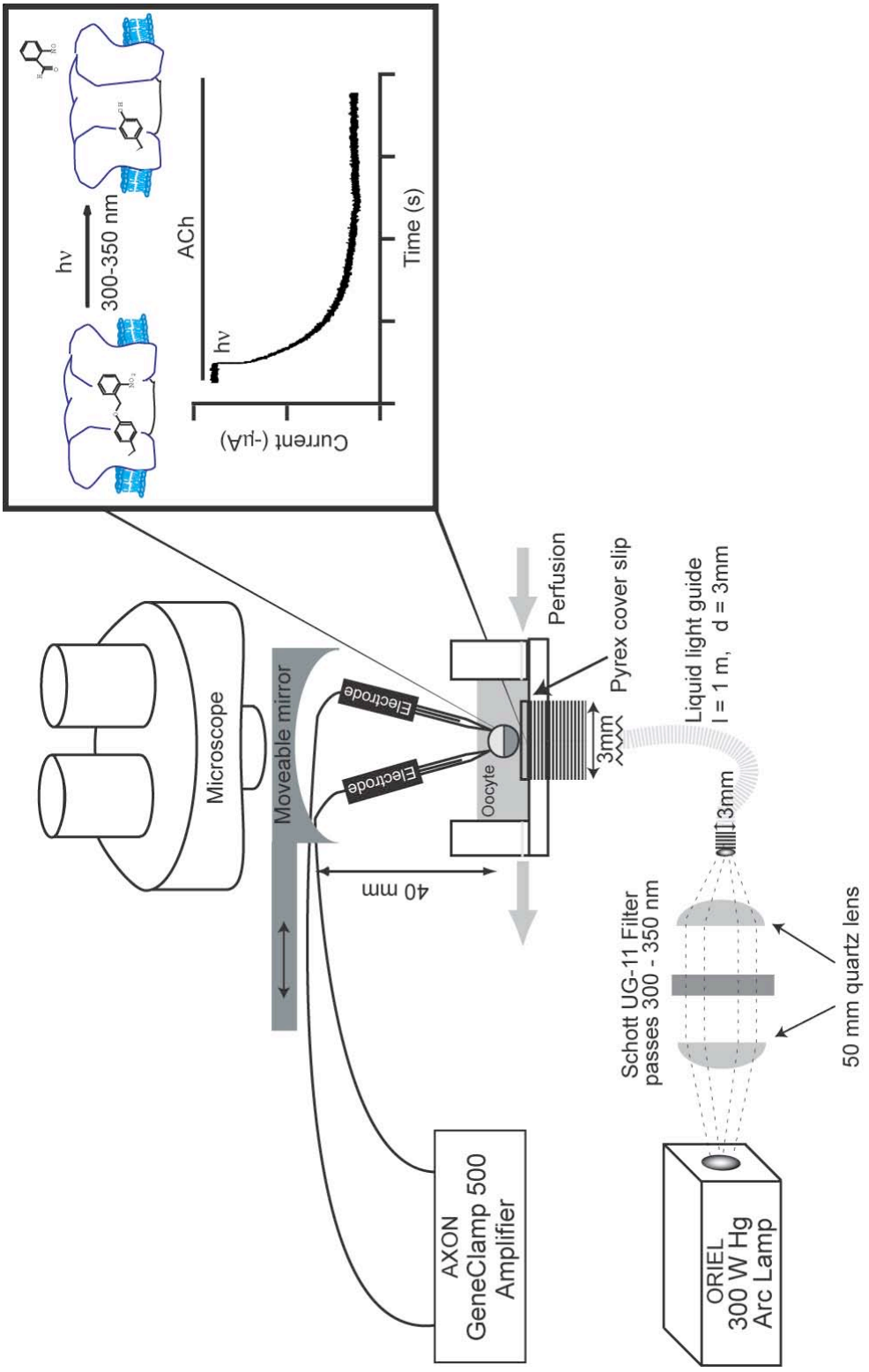

Figure 2. Real Time Electrophysiological Monitoring of Protein Decaging.

Photolysis apparatus

Various types of photolysis apparatus have been employed for sidechain decaging. Experiments involving photoreactive unnatural amino acids such as diazirine, aryl azides, and benzophenone[20, 26, 36] are also relevant here, as are experiments with caged small molecules in *Xenopus* oocytes.[37 38] In general, methods of photolysis can be divided into those performed on single oocytes and those performed on batches of oocytes.

An apparatus for real-time decaging in single oocytes (Fig. 2)[2-4, 39] is designed for the particular needs of these unusually large cells (~ 1 mm diameter). In most cases, inexpensive arc lamps (either continuous irradiation or pulsed) are preferred over the much more costly lasers if one wishes to illuminate the entire oocyte.[38] A "point-source" arc has a diameter (2-3 mm) on the order as the oocyte; therefore one loses relatively little light in focusing onto the oocyte. The coherence of the laser becomes an advantage only when one wishes to focus the laser down to a spot < 100 mm in diameter, e. g. for patch recording. The briefer pulse of the laser can rarely be exploited, because voltage-clamp circuits typically have time resolution on the order of the flashlamp (~ 1 ms).

The voltage-clamp electronics must be carefully shielded from the 14-kV trigger pulse of the flashlamp circuit. Also, metal surfaces in the microelectrodes must be shielded from the flash itself, to avoid photoelectric effects. Although the flash lamps in our laboratory are custom-built,[39] excellent devices can be bought from Rapp OptoElectronic (http://www.rapp-opto.com/) and Till Photonic (http://www.till-photonics.de/). Our setup employs an Oriel 66011 lamp housing with a high pressure Hg/Xe lamp run at 300 W by an Oriel 68810 power supply. The output is filtered by a Schott UG-11 filter (and a water IR filter (Oriel) if the lamp is run in continuous irradiation mode) and focussed with 50 mm quartz lenses (Oriel). An Ealing 22-8411 electronic shutter is employed to run the lamp in flash mode. The focused beam is directed onto the oocyte with a liquid light guide (1 m long, 3 mm diameter, Oriel 77554) aimed through a Pyrex coverslip. Finally, a concave first-surface mirror (Rolyn, 20 mm focal length, 50 mm diameter) is positioned ~ 40 mm above the oocyte.

Summary

The caging of specific residues of proteins is a powerful tool. This discussion attempts to alert the reader to the considerations one must make in preparing and analyzing a caged protein through nonsense suppression. While the suppression methodology is conceptually straightforward, it not possible to provide a fail safe, "cookbook" method for using caged unnaturals. We have emphasized the preparation of caged receptors expressed in *Xenopus* oocytes here, but these approaches be adapted to many other systems.

References

(1) Petersson, E. J.; Brandt, G. S.; Zacharias, N. M.; Dougherty, D. A.; Lester, H. A., *Methods Enzymol.* **2003,** 360, 258-273.

(2) Miller, J. C.; Silverman, S. K.; England, P. M.; Dougherty, D. A.; Lester, H. A., *Neuron* **1998,** 20, 619-624.

(3) Philipson, K. P.; Gallivan, J. P.; Brandt, G. S.; Dougherty, D. A.; Lester, H. A., *Am. J. Physiol. Cell Physiol.* **2001,** 281, C195.

(4) Tong, Y.; Brandt, G.; Li, M.; Shapovalov, G.; Slimko, E.; Karschin, A.; Dougherty, D. A.; Lester, H., *J. Gen. Physiol.* **2001,** 117, 103-118.

(5) Nowak, M. W.; Gallivan, J. P.; Silverman, S. K.; Labarca, C. G.; Dougherty, D. A.; Lester, H. A., *Methods Enzymol.* **1998,** 293, 504-529.

(6) Saks, M. E.; Sampson, J. R.; Nowak, M. W.; Kearney, P. C.; Du, F.; Abelson, J. N.; Lester, H. A.; Dougherty, D. A., *J. Biol. Chem.* **1996,** 271, 23169-23175.

(7) Holmes, C. P., *J. Org. Chem.* **1997,** 1997, 2370-2380.

(8) Ellman, J. A.; Mendel, D.; Anthony-Cahill, S. J.; Noren, C. J.; Schultz, P. G., *Methods Enzymol.* **1991,** 202, 301-336.

(9) Rossi, F. M.; Margulis, M.; Hoesch, R. E.; Tang, C. M.; Kao, J. P., *Methods Enzymol.* **1998,** 291, 431-443.

(10) Gee, K. R.; Carpenter, B. K.; Hess, G. P., *Methods Enzymol.* **1998,** 291, 30-50.

(11) Gee, K. R.; Niu, L.; Schaper, K.; Jayaraman, V.; Hess, G. P., *Biochem.* **1999,** 38, 3140-3147.

(12) Hess, G. P.; Grewer, C., *Methods Enzymol.* **1998,** 291, 443-473 Kuzmic, P.; Pavlickova, L.; Soucek, M., *Coll. Czech. Chem. Commun.* **1986,** 51, 1293-1300.

(13) Givens, R. S.; Weber, J. F.; Jung, A. H.; Park, C. H., *Methods Enzymol.* **1998,** 291, 1-29.

(14) Sheehan, J. C.; Umezawa, K., *J. Am. Chem. Soc.* **1973,** 38, 3771-3774.

(15) Sheehan, J. C.; Wilson, R. M.; Oxford, A. W., *J. Am. Chem. Soc.* **1971,** 93, 7222-7228.

(16) Stoddard, B. L.; Koenigs, P.; Porter, N.; Petratos, K.; Petsko, G. A.; Ringe, D., *Proc. Natl. Acad. Sci. USA* **1991,** 88, 5503-5507 Turner, A. D.; Pizzo, S. V.; Rozakis, G.; Porter, N. A., *J. Am. Chem. Soc.* **1998,** 110, 244-250.

(17) Furuta, T.; Iwamura, M., *Methods Enzymol.* **1998,** 291, 50-63 Givens, R. S.; Matuszewski, B., *J. Am. Chem. Soc.* **1984,** 106, 6860-6861.

(18) Lodder, M.; Golovine, S.; Laikhter, A. L.; Karginov, V. A.; Hecht, S. M., *J. Org. Chem.* **1998,** 63, 794-803.

(19) Short, G. F.; Lodder, M.; Laikhter, A. L.; Arslan, T.; Hecht, S. M., *Journal of the American Chemical Society* **1999,** 121, 478-479.

(20) Kanamori, T.; Nishikawa, S.; Nakai, M.; Shin, I.; Schultz, P. G.; Endo, T., *Proc. Natl. Acad. Sci. USA* **1999,** 96, 3634-3639 Kanamori, T.; Nishikawa, S.; Shin, I.; Schultz, P. G.; Endo, T., *Proc. Natl. Acad. Sci. USA* **1997,** 94, 485-490.

(21) Lodder, M.; Wang, B.; Hecht, S. M., *Tetrahedron* **2000,** 56, 9421-9429.

(22) Roesser, J. R.; Xu, C.; Payne, R. C.; Surratt, C. K.; Hecht, S. M., *Biochem.* **1989,** 28, 5185-5195.

(23) Bain, J. D.; Wacker, D. A.; Kuo, E. E.; Lyttle, M. H.; Chamberlin, A. R., *J. Org. Chem.* **1991,** 56, 4615-4625 Bain, J. D.; Wacker, D. A.; Kuo, E. E.; Chamberlin, A. R., *Tetrahedron* **1991,** 47, 2389-2400.

(24) Cornish, V. W.; Mendel, D.; Schultz, P. G., *Angew. Chem. Int. Ed.* **1995,** 34, 621-633.

(25) Gilmore, M. A.; Steward, L. E.; Chamberlin, A. R., *Topics Curr. Chem.* **1999,** 202, 77-99.

(26) Sisido, M.; Hohsaka, T., *Bull. Chem. Soc. Japan* **1999,** 72, 1409-1425.

(27) Steward, L. E.; Chamberlin, A. R., *Methods Mol. Biol.* **1998,** 77, 325-354 Thorson, J. S.; Cornish, V. W.; Barrett, J. E.; Cload, S. T.; Yano, T.; Schultz, P. G., *Methods Mol. Biol.* **1998,** 77, 43-73.

(28) Chollet, A.; Turcatti, G., *Lett. Pept. Sci.* **1998,** 5, 79-82 Dang, H.; England, P. M.; Farivar, S. S.; Dougherty, D. A.; Lester, H. A., *Mol. Pharmacol.* **2000,** 57, 1114-1122 Lu, T.; Ting, A. Y.; Mainland, J.; Jan, L. Y.; Schultz, P. G.; Yang, J., *Nat. Neurosci.* **2001,** 4, 239-246 Silverman, S. K. Ph.D. Thesis, California Institute of Technology, Pasadena, CA, 1998.

(29) England, P. M.; Lester, H. A.; Davidson, N.; Dougherty, D. A., *Proc. Natl. Acad. Sci. USA* **1997,** 94, 11025-11030.

(30) Turcatti, G.; Nemeth, K.; Edgerton, M. D.; Knowles, J.; Vogel, H.; Chollet, A., *Receptors Channels* **1997,** 5, 201-207.

(31) Turcatti, G.; Nemeth, K.; Edgerton, M. D.; Meseth, U.; Talabot, F.; Peitsch, M.; Knowles, J.; Vogel, H.; Chollet, A., *J. Biol. Chem.* **1996,** 271, 19991-19998.

(32) England, P. M.; Lester, H. A.; Dougherty, D. A., *Tetrahedron Lett.* **1999,** 40, 6189-6192.

(33) Cook, S. N.; Jack, W. E.; Xiong, X.; Danley, L. E.; Ellman, J. A.; Schultz, P. G.; Noren, C. J., *Angew. Chem. Int. Ed.* **1995,** 34, 1629-1630.

(34) Mendel, D.; Ellman, J. A.; Schultz, P. G., *J. Am. Chem. Soc.* **1991,** 113, 2758-2760.

(35) Lodder, M.; Golovine, S.; Hecht, S. M., *J. Org. Chem.* **1997,** 62, 778-779.

(36) Hohsaka, T.; Kajihara, D.; Ashizuka, Y.; Murakami, H.; Sisido, M., *J. Am. Chem. Soc.* **1999,** 121, 34-40 Martoglio, B.; Hofmann, M. W.; Brunner, J.; Dobberstein, B., *Cell* **1995,** 81, 207-214 Mothes, W.; Heinrich, S. U.; Graf, R.; Nilsson, I.; von Heijne, G.; Brunner, J.; Rapoport, T. A., *Cell* **1997,** 89, 523-533.

(37) Niu, L.; Vazquez, R. W.; Nagel, G.; Friedrich, T.; Bamberg, E.; Oswald, R. E.; Hess, G. P., *Proc. Natl. Acad. Sci. USA* **1996,** 93, 12964-12968.

(38) Parker, I.; Callamaras, N.; Wier, W. G., *Cell Calcium* **1997,** 21, 441-452.

(39) Nargeot, J.; Lester, H. A.; Birdsall, N. J.; Stockton, J.; Wassermann, N. H.; Erlanger, B. F., *J. Gen. Physiol.* **1982,** 79, 657-678.

Section 2: Chapter 8

Investigating the Magnesium Blockade of the *N*-Methyl-D-Aspartate Receptor

The *N*-Methyl-D-Aspartate Receptor

The *N*-methyl-D-aspartate receptor (NMDAR) is the switch that lies at the heart of the molecular processes of learning and memory.[1] This ion channel opens in the presence of glutamate (Glu) and glycine (Gly) to allow the influx of Ca^{2+}. However, at resting membrane potentials, the channel is blocked by Mg^{2+}. Depolarization of the neuron by other nearby ion channels removes the blockade. The need for both synaptic glutamate release and a change in membrane voltage makes the receptor a coincidence detector. The calcium flow that results from this coincidence detection initiates a strengthening of the synapse (termed long-term potentiation, LTP) which is generally considered to be a key step in memory formation.[2] (See Chapter 6) This is a simplistic treatment of the downstream events, but there is no doubt that the lynchpin that triggers LTP is the removal of the Mg^{2+} ion from the pore of the NMDAR. We wish to study the precise chemical nature of the Mg^{2+} blockade in order to understand this crucial ion channel.

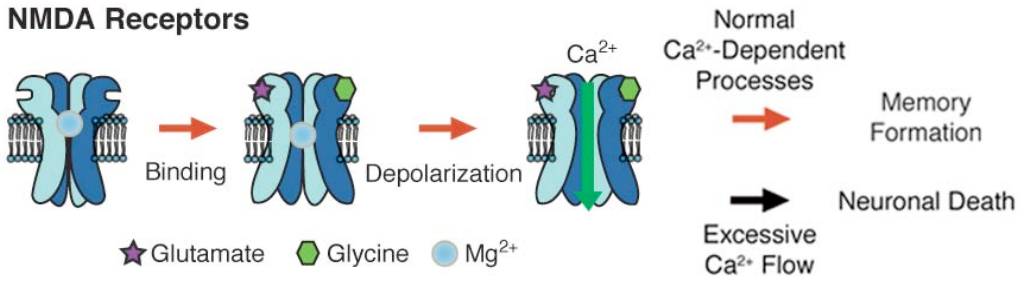

Figure 1. NMDA receptor opening requires the presence of the ligands glutamate and glycine and membrane depolarization to alleviate the Mg^{2+} block.

Overstimulation of NMDA receptors causes a large increase in intracellular calcium, which can lead to neuronal death in a process referred to as "excitotoxicity."[3] This is the accepted mechanism by which ischaemia and stroke cause neurodegeneration, and it is speculated that excitotoxicity underlies neurodegeneration in Alzheimer's disease, Parkinson's disease, and amyotrophic lateral sclerosis (ALS).[4] Since these diseases are disorders of endogenous proteins, drugs that completely disable these proteins like mechanism-based inhibitor antibiotics are not going to be effective treatments. Neurological disorders require drugs that can subtly tweak a protein's function back to normal. The development of such drugs requires a detailed understanding of the subtleties of neuronal protein function. In fact, some NMDAR open-channel blockers have already shown

neuroprotective effects.[5, 6] The pore of the NMDAR is also the target of several drugs of abuse such as phenylcyclidine (PCP) and ketamine, which appear to act by blocking the receptor under certain conditions.[6, 7] As one can see, understanding block of this receptor is important to both basic neuroscience and to many fields of medicine.

Since we are chemists, it is important that the Mg^{2+} blockade site is also very chemically interesting. Most Mg^{2+}-binding sites in proteins have a highly negatively-charged character, with Asp or Glu residues that chelate the metal. In fact, *all* Protein Data Bank (PDB) structures of Mg^{2+}-binding sites contain at least one Asp or Glu.[8] The NMDAR blockade site is very different. It is in the middle of a transmembrane region, and previous biochemical studies have concluded that it is composed of Phe, Asp, Gly, and Trp residues.[9] This divalent metal cation binding site in the middle of a hydrophobic, membrane-spanning region is extremely unusual and intriguing from the perspective of basic physical organic chemistry. Nature has arranged to solvate this metal cation with grease in a subtly tweakable way, so that it can be ejected from the pore by a change in voltage. An understanding of the structural features involved will not only be of biochemical value, but should aid the process of molecular design as well.

Our studies with the ACh receptor (Chapters 2-4) have demonstrated that we can gain precise atomic-scale information through unnatural amino acid incorporation. We turn these techniques to the study of the NMDAR for a number of related reasons. Firstly, we wish to add glutamate receptors to the repertoire of receptors studied in our labs in order to study the phenomenon of LTP with unnatural amino acids like those described in Chapter 7. Study of the NMDAR magnesium binding site is a good starting point for us. It is a well-defined problem, with a wealth of conventional mutagenesis data to use as a benchmark for our initial unnatural amino acid incorporation trials. (See below) Most important, despite all of the previous study of this interaction, it is still not understood on a chemical level. Raymond Dingledine, an acknowledged expert in the field, said in a recent review article: "The chemical nature of the intrapore Mg^{2+}-binding site is impossible to ascertain from any of the standard approaches presently used to study channel block."[9] We are in a position to obtain this information by assaying the functional consequences of the subtle changes to protein structure that unnatural amino acids allow.

NMDA Receptor Structure

Glutamate is the major excitatory neurotransmitter in the brain, and the large and diverse family of glutamate receptors plays a central role in learning and memory. The NMDAR and its cousins, the AMPA and kainite receptors (these receptors respond to Glu but lack the Mg^{2+} block site), constitute the family of ionotropic glutamate receptors. Less is known about the detailed structure of the glutamate receptors than the ACh receptor, but

the presently accepted model is as follows. The receptors are tetramers, with a novel subunit topology (Fig. 2) involving a re-entrant P loop that is reminiscent of the P loop of K^+ channels.[10] Our research will focus on the NMDA receptor and the magnesium blockade site (Fig. 3).

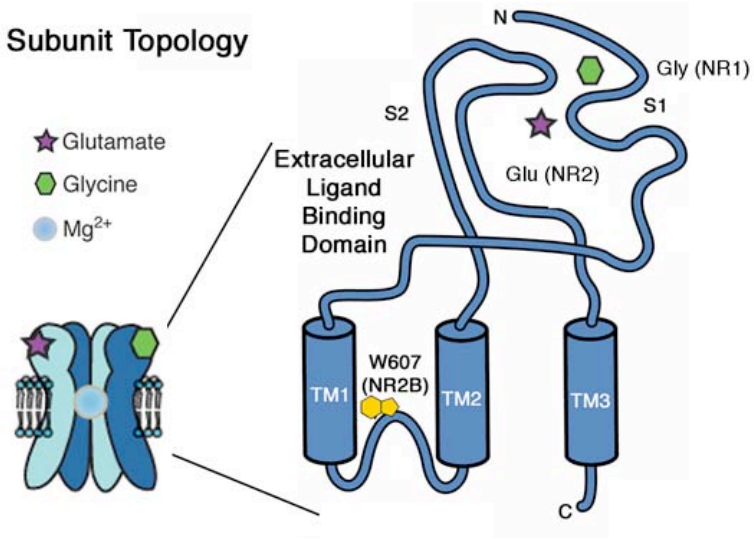

Figure 2. Topology of an Individual Subunit of the NMDAR. The S1 and S2 domains form the ligand binding region. The Mg^{2+} site is located in a reentrant transmembrane region.

Glutamate and glycine (or D-serine) must bind to the NMDAR extracellular domain (Glu to NR2 and Gly to NR1) to initiate a conformational change that opens the gate to the ion channel's pore.[11] This is merely the key that unlocks the door, the "doorstop" of Mg^{2+} block must be removed for the door to open and Ca^{2+} to flow. (Fig. 1) Mg^{2+} block is only removed by membrane depolarization. (By convention, the outside of the cell is assigned a potential of 0 V; the inside resting potential is negative, typically –50 to –100mV. Depolarization involves moving the resting potential toward zero, and it facilitates the firing of an action potential.) Although there is some direct structural information on glutamate receptors available, there is little that is relevant to the Mg^{2+} binding site. Much is known about the glutamate and glycine binding sites through the work of Gouaux and coworkers.[12] They have expressed a soluble protein in which the S1 and S2 domains (Fig. 2) of the NR1 or related glutamate receptors are linked together, and crystallography of this species has produced detailed insights into the extracellular ligand binding domain. Very recently Sheng has obtained electron microscopy images of functional tetrameric glutamate receptors showing a few different conformations of the extracellular domains corresponding to various states of ligand occupancy.[13] Although this work feeds our understanding of the binding domains, the magnesium binding site is in the transmembrane region, and as we

noted in Chapter 1, transmembrane proteins are notoriously difficult to crystallize. Therefore there is no direct structural information about this important site.

Previous Studies of the Magnesium Binding Site

Electrophysiological studies have provided important clues as to the location and character of the Mg^{2+} blockade. Measurement of the voltage dependence of the block has lead to the proposal that Mg^{2+} binds to a site deep within the pore.[14] Mg^{2+} can be driven through the channel at hyperpolarized (highly negative) potentials, probably in a dehydrated state. Both the fact that divalent cation permeabilites correlate inversely with dehydration energies and that hydrated Mg^{2+} (0.64 nm) is larger than the pore (< 0.6 nm) support this.[15] Thus, it must be possible to strip magnesium's solvation shell on the way through the pore. Models of ion conduction in K^+ channels suggest that this hydration shell would be replaced by ion-protein interactions on the ion's trip through the pore.[16]

Studies of the NMDAR residues involved in Mg^{2+} interactions point to two types, both located on the P loop: asparagines at the apex of the turn (on both subunits) and a nearby hydrophobic site containing Trp 607. (Fig. 3) Williams *et al.* have demonstrated the importance of this tryptophan and implicated a cation-π binding interaction with the metal ion.[17] Substitutions of non-aromatic hydrophobic residues at NR2B W607 increased Mg^{2+} IC_{50} (similar to EC_{50}, the concentration of half-maximal inhibition) from 19 μM to greater than 300 μM at -70 mV. Analogous mutations of the other Trp residues shown in Figure 3 changed the IC_{50} little. (See Fig. 3, Table for IC_{50} data.) In contrast to the large changes seen when W607 was exchanged for non-aromatic residues, when it was replaced with the aromatic residues Phe and Tyr, IC_{50} increased only slightly. These channels all show responses to pH, glutamate, and glycine similar to those of wild-type channels, implying that they are otherwise unaffected. It is noted that W607F and W607Y mutants are more permeable to Mg^{2+} than wild-type channels, which fits with their relative cation-π binding abilities, but may simply be a result of their smaller size.

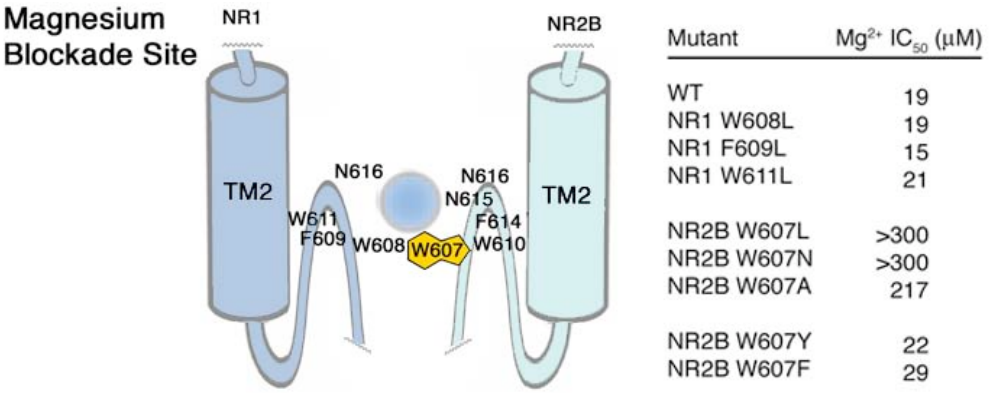

Mutant	Mg^{2+} IC_{50} (μM)
WT	19
NR1 W608L	19
NR1 F609L	15
NR1 W611L	21
NR2B W607L	>300
NR2B W607N	>300
NR2B W607A	217
NR2B W607Y	22
NR2B W607F	29

Figure 3. View of the Mg^{2+} Blockade Site. The amino acids relevant to this study are highlighted. Changes in IC_{50} for some mutations are shown.[17]

The asparagines at the top of the P loop have also been explored. Substitutions by Gly, Gln, Ser, and Asp at NR2B 615 and 616 have shown that they interact with the cation through an electrostatic interaction rather than merely a steric block.[18, 19] NR1 N615G substitutions have little effect on Mg^{2+} block, supporting the idea that the block is not determined solely by pore size. Wollmuth *et al*. propose that Mg^{2+} loses some of its hydration sphere in the pore and attempts to form its preferred six-coordinate geometry *via* interactions with the NR2B Asn residues.[18]

The work described above provides a starting point for our dissection of the Mg^{2+} binding site. We began by evaluating Williams' hypothesis of a cation-π interaction at W607 by incorporating a series of fluorinated Trp residues, which should reduce Mg^{2+} block in a step-wise manner. In previous studies, we were able to use these unnatural amino acids to conclusively identify a cation-π interaction between acetylcholine (ACh) and Trp 149 of the muscle acetylcholine receptor.[20] (Chapters 2-4) The fluorinated Trp analog is an especially elegant perturbation of this interaction, as it is nearly isosteric with the Trp but a much weaker cation-binder. For a Trp that we suspect is involved in a cation-π interaction, we progressively replace the Trp with monofluoro-, difluoro-, trifluoro-, and terafluoro-Trp. We then compare the calculated, innate cation-π binding ability of the aromatic ring (kcal/mol) to the EC_{50} of the agonist when that ring is present (using log EC_{50} to put all on an energy scale). In the case of ACh, an excellent correlation was seen. We interpret such straight lines as unambiguous evidence of a cation-π interaction between the ligand and the receptor at the Trp of interest.

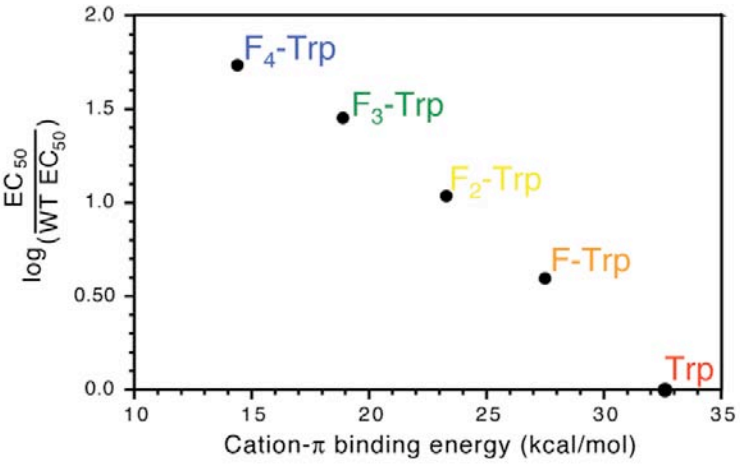

Figure 4. Fluorination Plot for ACh at Trp 149 of the nAChR α subunit. A linear correlation is seen between calculations of cation-π binding in a model system and the measured ACh EC_{50}, indicating a cation-π interaction.

Since the NR2B Trp 607 site has been the primary site implied in Mg^{2+} binding by mutagenesis, it was the first to be explored with fluorinated Trps. Incorporation of

sequentially fluorinated tryptophan residues should lead to a step-wise decrease in the Mg^{2+} block if the cation-π interaction is a modulator of the Mg^{2+} blockade. A linear relationship would be seen between calculated cation-π binding energies and measured IC_{50} (concentration of drug needed to inhibit 50% of the current) values. The experiments that follow represent our initial foray into study of the NMDA receptor; they were conducted side-by-side with Katie McMenimen, who will continue to study the receptor.

Wild Type NMDA Receptor Expression

Before we began incorporation of unnatural amino acids, we had to verify that we could obtain robust expression of wild type NMDA receptors in accordance with literature precedent. NMDA NR1 and NR2B constructs were obtained from the Williams lab. These constructs were originally assembled in an outdated pBluescript vector. In order to increase the expression levels of the NMDA subunits in *Xenopus laevis* oocytes, the constructs were subcloned into a vector expression system designed for use with *Xenopus* oocytes, pAMV, which is a derivation of pBluescript that incorporates a 5' untranslated region from the alfalfa mosaic virus that aids ribosomal binding.[21]

The wildtype NR1a/NR2B mRNA subunits were injected into *Xenopus* oocytes. In order to confirm expression, we obtained a dose response curve for magnesium block of this wild type receptor. Our electrophysiological protocols mirror those of Williams and coworkers.[17] (See Fig. 5, Left) A series of applications of 100 μM Glu and 10 μM Gly is delivered to the oocyte. (Fig. 5 A, duration indicated by thin green and purple lines) EC_{50} concentrations of glutamate and glycine are reported at 1.4 and 0.14 μM, respectively. It is important to use glutamate and glycine concentrations larger than EC_{50} to promote full receptor activation. In each application, once the inward current has plateaued, we apply a dose of blocking Mg^{2+}. (Fig. 5 B, duration indicated by thick blue line) The magnesium is then washed out to demonstrate the reversibility of the block. (Fig. 5 C)

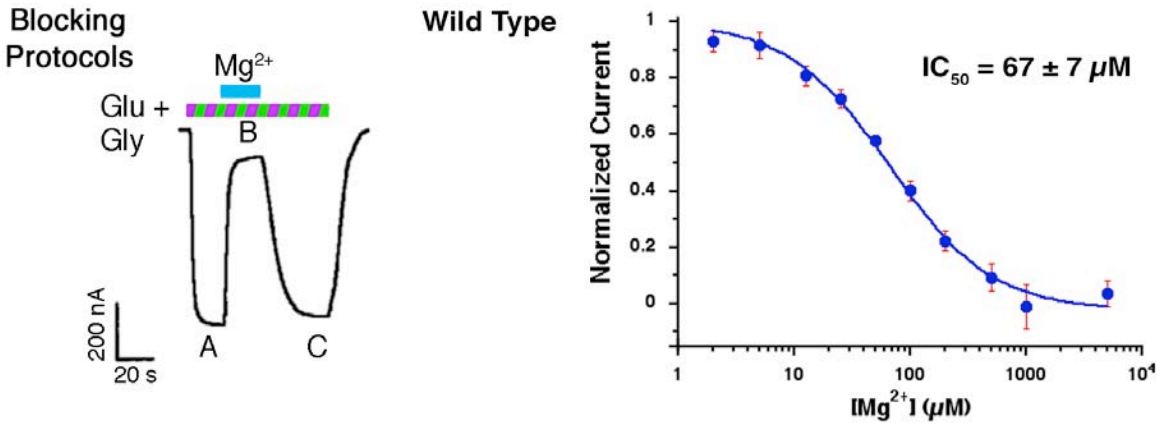

Figure 5. Wild Type NMDAR Expression. Left: Mg^{2+} blocking protocol. Right: Wild type (NR1a/NR2B mRNA injected) IC_{50} data.

We plot the ratio of response in the presence and absence of Mg^{2+} against the Mg^{2+} concentration to obtain an IC_{50}. (see Fig. 5, Right) Previous work has reported the Mg^{2+} IC_{50} value for the wildtype NR1a/2B receptor at 19μM.[17] In our hands, wildtype NR1/2B Mg^{2+} IC_{50} was recorded at 66.7μM. The fact that this is different from the numbers from Williams' lab is not shocking; we have previously seen that acetylcholine receptor EC50s recorded on the OpusXpress™ were higher than those recorded with conventional rigs.

There are reports that NR1a subunits form homomeric channels in *Xenopus* oocytes.[22] In order to confirm correct assembly of the heteromeric NR1a/2B channels in oocytes, NR1a subunit mRNA alone was injected into the oocyte. Then, applications of 100μM glutamate and 10μM glycine were given, along with increasing concentrations of Mg^{2+}. After application of glutamate and glycine, no current was recorded, indicating that the previous recordings measured just the NR1a/2B receptors, not a mixture of NR1a homomers and NR1a/2B heteromers.

The muscle nAChR mRNA typically incubates in an oocyte for 1-2 days. In order to increase the amount of NMDAR expression, injected oocytes were recorded from between 2 and 4 days after injection. After 4 days of incubation, the oocytes injected with wild type NR1a/2B mRNA were unhealthy and not amenable to electrophysiological recordings. Two days was determined sufficient incubation time for wild type receptors.

Unnatural Amino Acid Incorporation Controls

Once we had assured ourselves that we could express wild type receptors, the next logical experiment to do was to demonstrate that we could recover the wild type receptor phenotype by incorporating Trp at position 607 through nonsense suppression. Several experiments were performed to optimize conditions for unnatural amino acid incorporation in the NMDAR. A TAG mutation was made in the NR2B gene at position 607. Wild type recovery experiments were made by injecting NR1a/2B607UAG mRNA and $tRNA_{CUA}$-Trp. Again, incubation trials were performed from 2-4 days after initial injection and it was determined that 2 days of incubation were sufficient for expression. Additionally, a "booster" injection of $tRNA_{CUA}$-Trp was given on the second day of incubation to improve expression of the receptors. As noted in Chapter 1, the nonsense suppression method is not catalytic; the limiting factor is the amount of aminoacyl tRNA injected into the oocyte. However, after the amino acid from the injected tRNA is removed from the tRNA, aminoacyl tRNA synthetases in the cell can re-acylate the tRNA. This will lead to incorporation of an unwanted amino acid at the site of interest. To test the amount of misincorporation current produced, NR1a/2B607TAG mRNA was injected into oocytes without any tRNA. No current was recorded during glutamate and glycine application.

However, when unaminoacylated $tRNA_{CUA}$ (76mer) was co-injected with mRNA in order to identify substantial background currents were recorded. The receptors produced in these experiments showed no noticeable magnesium block, and in fact appeared to be permeable to Mg^{2+} at concentrations greater than ~ 1mM. The logarithmic relationship between the NMDAR currents and the magnesium concentration shown in Figure 6 is consistent with Mg^{2+} functioning as a charge carrier.[23]

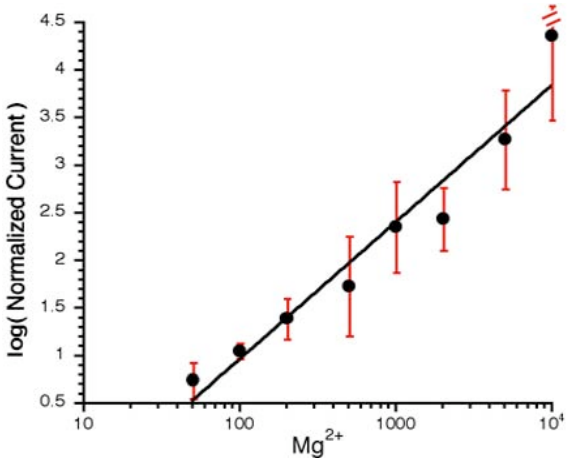

Figure 6. Misincorporation Phenotype. Currents recorded from oocytes expressing receptors generated from NR1a/2B607TAG mRNA with unaminoacylated $tRNA_{CUA}$.

Our observations agree with work by Williams that identified magnesium permeability in poorly blocking mutants such as the 607 Leu mutation.[17] Fortunately, incubation studies showed that the amount of misincorporation current is decreased if suppression experiments are recorded after two days of incubation instead of three days. This background seemed sufficiently low to allow us to carry on our unnatural amino acid mutagenesis experiments. We found that dose-response curves with Trp suppression at the 607 site gave an IC_{50} that was within error identical to the wild type IC_{50}.

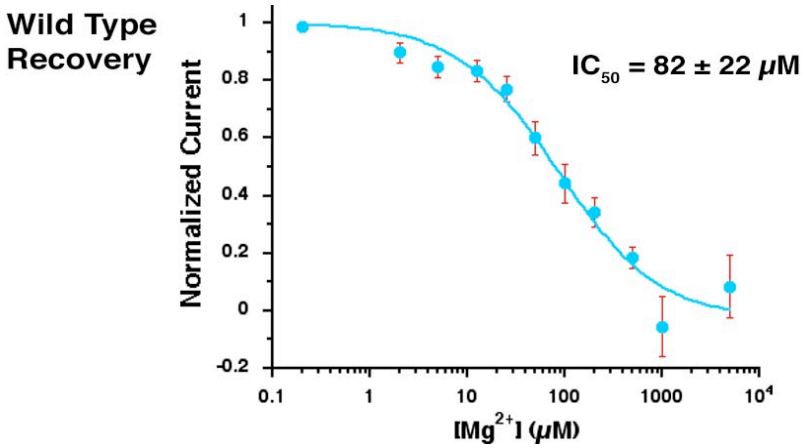

Figure 7. Wild Type Recovery. Currents recorded from oocytes expressing receptors generated from NR1a/2B607TAG mRNA with $tRNA_{CUA}$-Trp.

F_n-Trp Incorporation

Using the protocol above, $tRNA_{CUA}$-F-Trp and NR1a/2B mRNA were injected into oocytes to determine the importance of the cation-π interaction between W607 and Mg^{2+}. These gave roughly 20% smaller than Trp incorporation, and expression was more sporadic, but we were able to record dose-response curves from these cells as well. Example electrophysiology traces from wild type, Trp suppression, and F-Trp suppression experiments are shown in Figure 8.

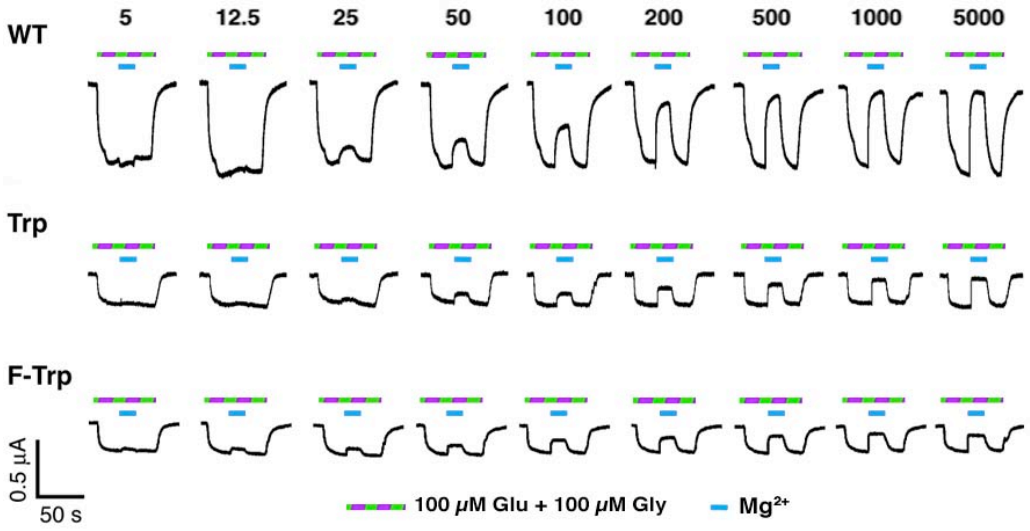

Figure 8. Primary Electrophysiological Data for NMDAR Recordings.

The traces recorded in the F-Trp experiment differ somewhat from the wild type recovery experiments in that we do not seem to be able to fully block the agonist-induced currents, even at high Mg^{2+} concentrations. This may be due to some currents from "misincorporation" receptors. In spite of this, we felt that the data was sufficiently sound to plot a dose-reponse curve and compare the IC_{50} to the wild type receptor.

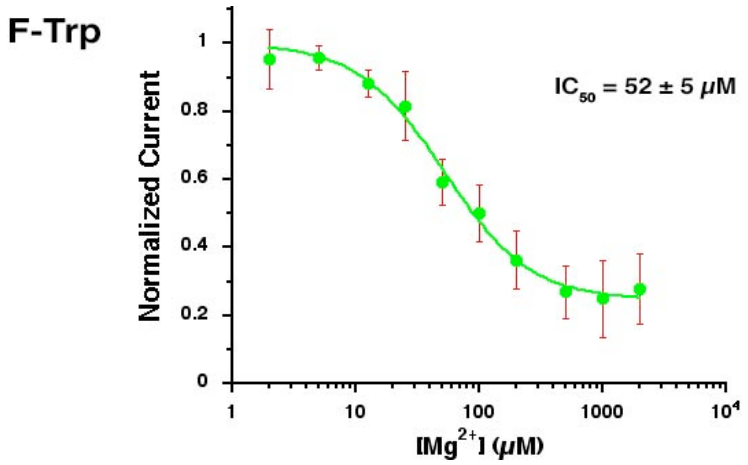

Figure 9. F-Trp Dose Response Curve. (NR1a/2B607TAG mRNA with $tRNA_{CUA}$-F-Trp).

F-Trp incorporation at NR2B607 did not result in a rightward IC_{50} shift, with a value of 52 μM Mg^{2+}. (Figure 9) Since there was no rightward shift in IC_{50} for NR2BW607FTrp (if anything, a slight leftward shift), a cation-π interaction is not likely. To rule out any possibility of a cation-π interaction, we attempted to incorporate F_2-Trp at NR2B607. However, the currents resulting from these experiments were too small to accurately measure a dose-response curve.

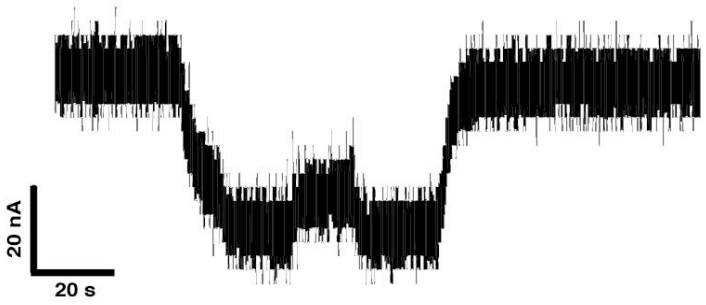

Figure 10. F_2-Trp Preliminary Electrophysiology Data.

Calculated Magnesium Binding Energies

Although we are left with only the F-Trp data in examining Mg^{2+} cation-π binding to Trp 607, this should be sufficient. As decribed in Chapter 2, fluorination reduces the negative electrostatic potential at the center of the 6-membered ring of indole, weakening its cation-π binding ability. (Fig. 11, Left) High level *ab initio* calculations of the binding of Mg^{2+} to indole and 5-F-indole predict a shift of Mg^{2+} binding affinity of many orders of magnitude upon fluorination. (Fig. 11, Right) This is seen regardless of the character of the medium, as indicated by calculations in THF, EtOH, and water (represented by changes in dielectric in an implicit solvation model). Therefore, we should certainly see some effect on the magnesium IC_{50} in our experiments.

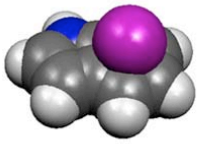

	Mg^{2+} Binding Energy (kcal/mol)		
	Trp	5-F-Trp	5-F-Trp - Trp
Gas	-142.3	-131.0	11.3
THF	-24.2	-14.8	9.4
EtOH	4.0	11.3	7.3
H_2O	6.7	15.1	8.4

Figure 11. Calculated Mg^{2+} Cation-π Binding. Counterpoise-corrected Mg^{2+} binding energies with Trp sidechains. All calculations performed at the B3LYP/6-31++G (d,p) lvel of theory and basis set.

Conclusions and Future Work

We can therefore conclude that Mg^{2+} does not interact with NR2B Trp 607 through a cation-π interaction. All previous studies of this site using conventional mutagenesis had concluded that the interaction was dependent on the aromaticity of the 607 residue because the block phenotype was unique to Trp, Tyr, and Phe.[9, 17] This lead them to hypothesize that the magnesium ion bound through a cation-π interaction. Our studies, employing the subtle unnatural mutations permitted by nonsense suppression, have conclusively shown that the interaction is not cation-π in nature. It may simply be that a large, flat residue is required. Leucine has been incorporated at this site indicating that residue bulk does not regulate the block.[17] However, rigid bulk might be necessary for the Mg^{2+} blockade. Future experiments will include the incorporation of a phenylalanine residue at NR2B607 followed by the incorporation of cyclohexylalanine. These are reasonably isosteric sidechains, yet the cyclohexyl sidechain is unequivocably not aromatic. If the Mg^{2+} IC_{50} for the cyclohexylalanine mutant is near that of Phe, this will establish the mechanism of block as a simple steric interaction with a large, flat residue.

These experiments demonstrate that unnatural amino acids can be utilized to study the NMDA receptor. Future experiments will explore the interactions between NR2B607 and organic cationic blockers of the NMDARs, such as drugs of abuse, like PCP, and drugs of therapy, like MK-801. Although Mg^{2+} does not, these NMDAR blockers could interact with W607 through a cation-π interaction. It will also be interesting to investigate the other Mg^{2+} binding determinants. A role has been shown for NR1 Asn 616 and NR2A/B Asn 615 and Asn 616 in Mg^{2+} binding. We will probe these presumed side-chain carbonyl interactions by introducing a series of fluorinated-ketone Asn analogs that should be capable of modulating this carbonyl-chelation interaction in a manner similar to the F-Trp series modulation of the cation-π interaction.

NMDARs play important roles in neuronal signaling cascades because of their high Ca^{2+} permeability. Now that methodology is in place to study the NMDARs, we will be able to use unnatural amino acids to study the role of the NMDARs in signaling cascades. Using the amino acids developed in Chapter 7, we will be able to study the subtle effects of phosphorylation on these receptors with unprecedented precision. These experiments would begin to unlock chemical scale information about the structure and function of the NMDARs, which influence learning, memory, and many neurodegenerative diseases.

Materials and Methods

Molecular Biology

The NR1a/NR2B genes were obtained in a pBluescript plasmid and subcloned into a pAMV plasmid. In order to subclone NR1a, primers complimentary to the 5' and 3' ends of the gene were produced, the gene was amplified by PCR, and then, using the *NcoI* and *BamHI* restriction enzymes, the gene was ligated into the pAMV vector. For NR2B, the first 1.5 kb of the NR2B subunit (5' end) were amplified using PCR and subcloned into pAMV utilizing overlapping PCR primers. The overlapping primers were constructed using 12 amino acids from the AMV sequence that directly preceded the start codon of the plasmid and the first 12 amino acids of the NR2B gene. The second 3.0 kb were subcloned into this modified pAMV by restriction digestion between the plasmid and the fragment with *BamH1* and *AflII* and ligating with T4 DNA ligase. All of the genes were linearized using the *NotI* enzyme and mRNA was transcribed with the Ambion T7 mMESSAGE MACHINE kits (Austin, TX). Aminoacyl tRNA was prepared as described previously.[24]

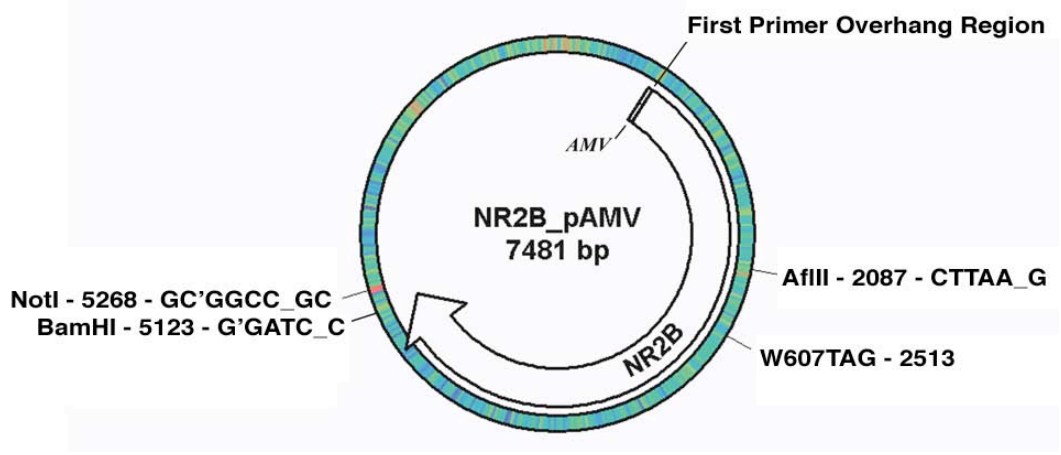

Figure 12. Vector map of NR2B in pAMV with the TAG (stop) codon inserted at the 607 site.

Electrophysiology

Stage V-VI *Xenopus laevis* oocytes were injected with 50nL of mRNA/tRNA mixtures per injection. Oocytes were recorded in a Ca^{2+} and Mg^{2+}-free saline solution and activated by a Ca^{2+} and Mg^{2+} free solution containing 100 μM glutamate and 10 μM glycine (96 mM NaCl, 5 mM HEPES, 2 mM KCl, 1 mM $BaCl_2$). All of the electrophysiological recordings were performed on the OpusXpress™ (Axon Instruments, San Jose CA). Eight oocytes were simultaneously voltage clamped at -60 mV and dose-response relationships were obtained by application of 1mL of various concentrations of Mg^{2+} in the above buffer. The data was analyzed using the Clampfit 9.0 software (Axon Instruments). The Hill equation was used to fit data where $I/I_{max} = 1-(1/(1+(IC_{50}/[A]^n)))$.

Computational Modeling

Mg^{2+}, indole, 5-F-indole, the complex shown in Fig. 11 and the analogous 5-F-indole complex were optimized at the B3LYP/6-31++G (d,p) level of theory. The optimized geometries were fully characterized as minima by frequency analysis. Energies were calculated at the B3LYP/6-31++G (d,p) level. Basis set superposition error (BSSE) corrections were determined in the gas phase at the B3LYP/6-31++G (d,p) level, using the counterpoise correction method of Boys and Bernardi.[25] All calculations were carried out with the Gaussian 98 program.[26] Binding energies were determined by comparing the BSSE- and ZPE-corrected energies of the separately optimized Mg^{2+} and indole to the energy of the complex. Solvent effects were added to the gas phase structures using the polarizable continuum model (PCM) self-consistent reaction field with ε(THF) = 7.6, ε(EtOH) = 24.3, and ε(H2O) = 78.5.[27]

References

(1) Zhu, H. B.; Luo, J. H., *Prog. Biochem. Biophys.* **1999,** 26, 541-543 Kullmann, D. M.; Asztely, F.; Walker, M. C., *Cell. Mol. Life Sci.* **2000,** 57, 1551-1561 Malinow, R.; Mainen, Z. F.; Hayashi, Y., *Curr. Opin. Neurobiol.* **2000,** 10, 352-357 Winder, D. G.; Schramm, N. L., *Physiol. Behav.* **2001,** 73, 763-780.

(2) Gnegy, M. E., *Crit. Rev. Neurobiol.* **2000,** 14, 91-129 Martin, S. J.; Grimwood, P. D.; Morris, R. G. M., *Annu. Rev. Neurosci.* **2000,** 23, 649-711 Lisman, J.; Schulman, H.; Cline, H., *Nat. Rev. Neurosci.* **2002,** 3, 175-190 Isaac, J. T. R., *Neuropharmacology* **2003,** 45, 450-460.

(3) Ashcroft, A. M., *Ion Channels and Disease*; Academic Press: San Diego, 2000 Arundine, M.; Tymianski, M., *Cell Calcium* **2003,** 34, 325-337.

(4) Raymond, L. A., *Clin. Neurosci. Res.* **2003,** 3, 121-128 Mattson, M. P.; Chan, S. L., *Cell Calcium* **2003,** 34, 385-397 Brown, G. C.; Bal-Price, A., *Mol. Neurobiol.* **2003,** 27, 325-355.

(5) Valera, E.; Fernandez-Salguero, P. M.; Planells-Cases, R.; Messeguer, A.; Van Den Nest, W.; Carreno, C.; Ferrer-Montiel, A.; Merino, J. M., *Neuromol. Med.* **2002,** 2, 271-280 Planells-Cases, R.; Montoliu, C.; Humet, M.; Fernandez, A. M.; Garcia-Martinez, C.; Valera, E.; Merino, J. M.; Perez-Paya, E.; Messeguer, A.; Felipo, V.; Ferrer-Montiel, A., *J. Pharmacol. Exp. Ther.* **2002,** 302, 163-173 Tai, K. K.; Blondelle, S. E.; Ostresh, J. M.; Houghten, R. A.; Montal, M., *Proc. Natl. Acad. Sci. U. S. A.* **2001,** 98, 3519-3524 Berger, M. L., *Neurosci. Lett.* **2000,** 296, 29-32 Sobolevsky, A. I., *Biophys. J.* **2000,** 79, 1324-1335.

(6) Dilmore, J. G.; Johnson, J. W., *Biophys. J.* **1998,** 75, 1801-1816.

(7) Buck, D. P.; Howitt, S. M.; Clements, J. D., *Biophys. J.* **2000,** 79, 2454-2462.

(8) Dudev, T.; Lim, C., *Chem. Rev.* **2003,** 103, 773-787.

(9) Review Dingledine, R.; Borges, K.; Bowie, D.; Traynelis, S. F., *Pharm. Revs.* **1999,** 51, 7-61.

(10) Wood, M. W.; VanDongen, H. M.; VanDongen, A. M., *Proc. Natl. Acad. Sci. USA* **1995,** 92, 4882-4886 Rosenmund, C.; Stern-Bach, Y.; Stevens, C. F., *Science* **1998,** 280, 1596-1599 Bennett, J. A.; Dingledine, R., *Neuron* **1995,** 14, 373-384.

(11) Ivanovic, A.; Reilander, H.; Laube, B.; Kuhse, J., *J. Biol. Chem.* **1998,** 273, 19933-19937 Anson, L. C.; Chen, P. E.; Wyllie, D. J. A.; Colquhoun, D.; Schoepfer, R., *J. Neurosci.* **1998,** 18, 581-589.

(12) Armstrong, N.; Sun, Y.; Chen, G. Q.; Gouaux, E., *Nature* **1998,** 395, 913-917 Furukawa, H.; Gouaux, E., *Embo J.* **2003,** 22, 2873-2885 Jin, R. S.; Banke, T. G.; Mayer, M. L.; Traynelis, S. F.; Gouaux, E., *Nat. Neurosci.* **2003,** 6, 803-810 Hogner, A.; Kastrup, J. S.; Jin, R.; Liljefors, T.; Mayer, M. L.; Egebjerg, J.; Larsen, I. K.; Gouaux, E., *J. Mol. Biol.* **2002,** 322, 93-109.

(13) Nakagawa, T.; Cheng, Y.; Ramm, E.; Sheng, M.; Walz, T., *Nature* **2005,** 433, 545-549.

(14) Nowak, L.; Bregestovski, P.; Ascher, P.; Herbet, A.; Prochiantz, A., *Nature* **1984,** 307, 462-465 Mayer, M. L.; Westbrook, G. L.; Guthrie, P. B., *Nature* **1984,** 309, 261-263 LiSmerin, Y.; Johnson, J. W., *J. Physiol. (Lond)* **1996,** 491, 137-150 98142670 Wollmuth, L. P.; Kuner, T.; Sakmann, B., *J. Physiol. (Lond)* **1998,** 506, 33-52.

(15) Ascher, P.; Nowak, L., *J. Physiol. (Lond)* **1988,** 399, 247-266.

(16) Zhou, Y. F.; Morais-Cabral, J. H.; Kaufman, A.; MacKinnon, R., *Nature* **2001,** 414, 43-48.

(17) 98252894 Williams, K.; Pahk, A. J.; Kashiwagi, K.; Masuko, T.; Nguyen, N. D.; Igarashi, K., *Mol. Pharmacol.* **1998,** 53, 933-941.

(18) 98142669 Wollmuth, L. P.; Kuner, T.; Sakmann, B., *J. Physiol. (Lond)* **1998,** 506, 13-32.

(19) 96259900 Wollmuth, L. P.; Kuner, T.; Seeburg, P. H.; Sakmann, B., *J. Physiol. (Lond)* **1996,** 491, 779-797.

(20) Zhong, W. G.; Gallivan, J. P.; Zhang, Y. O.; Li, L. T.; Lester, H. A.; Dougherty, D. A., *Proc. Natl. Acad. Sci. USA* **1998,** 95, 12088-12093.

(21) Petersson, E. J.; Brandt, G. S.; Zacharias, N. M.; Dougherty, D. A.; Lester, H. A., *Methods Enzymol.* **2003**, 360, 258-273.

(22) Williams, K.; Russell, S. L.; Shen, Y. M.; Molinoff, P. B., *Neuron* **1993,** 10, 267-278.

(23) Hille, B., *Ionic Channels of Excitable Membranes*; Sinauer Associates, Inc.: Sunderland, MA, 1992.

(24) Petersson, E. J.; Shahgholi, M.; Lester, H. A.; Dougherty, D. A., *RNA* **2002,** 8, 542-547.

(25) Boys, S. F.; Bernardi, F., *Mol. Phys.* **1970,** 19, 553-557.

(26) Frisch, M. J.; Trucks, G. W.; Schlegel, H. B.; Scuseria, G. E.; Robb, M. A.; Cheeseman, J. R.; Zakrzewski, V. G.; J. A. Montgomery, J.; Stratmann, R. E.; Burant, J. C.; Dapprich, S.; Millam, J. M.; Daniels, A. D.; Kudin, K. N.; Strain, M. C.; Farkas, O.; Tomasi, J.; Barone, V.; Cossi, M.; Cammi, R.; Mennucci, B.; Pomelli, C.; Adamo, C.; Clifford, S.; Ochterski, J.; Petersson, G. A.; Ayala, P. Y.; *et. al. Gaussian 98 (Revision A.9)*, Gaussian, Inc.: Pittsburgh PA, 1998.

(27) Cossi, M.; Barone, V.; Cammi, R.; Tomasi, J., *Chem. Phys. Lett.* **1996,** 255, 327-335.